المهندس

مجلة علمية محكمة تصدرها جمعية المهندسين العراقية

عدد خاص لبحوث مؤتمر الطاقة المستدامة والمتجددة الاول

- الجزء الثالث -

المجلد ١٥٣ - العدد ٣

ISSN 2413 - 0230

ايلول _ ٢٠١٦

البريد الالكتروني : jmise@ise-iq.org

السنة الواحد والستون
العدد الثالث
ايلول ٢٠١٦
تكون جميع المراسلات على البريد
الالكتروني للمجلة
jmise@ise-iq.org
حي النضال م/١٠٣ ش/٣٠ مبنى/٥

مجلة المهندس

تصدرها
جمعية المهندسين العراقية
الاشتراكات السنوية
للمؤسسات ١٠٠,٠٠٠ دينار
للجامعات والكليات وا لمهندسين ٦٠,٠٠٠ دينار
لأعضاء الجمعية ٤٠,٠٠٠ دينار
لطلبة الجامعات ٤٠,٠٠٠ دينار

مجلة فصلية رقم الايداع في المكتبة الوطنية بغداد ٥١٠, ١٩٨٣ مسجلة بدائرة البريد رقم ٥٦

كلمة العدد

ان العلاقة المباشرة بين عدد السكان والتحضر والعلوم الهندسية تتفاعل باستمرار. وخلال ال ١٠٠ سنة الماضية، نمت اعداد سكان العالم من مليار ونصف الى ستة مليارات (ربما اكثر) وبسبب ذلك فان الاحتياجات البشرية تتزايد باستمرار وينبغي على علوم الهندسة وبمختلف اختصاصاتها ان تجد حلولا للمشاكل المرافقة لهذه الاحتياجات.

صممت هذه المجلة لكي تعكس التطور والتقدم الذي يتم احرازه في المجالات العامة لعلوم الهندسة والتكنولوجيا الهندسية. وان كلمة الهندسة هنا تعني كل ما يتصل بها بالمعنى الواسع، بما في ذلك (لكن لا يقتصر على) الهندسة المعمارية، المدنية، الكهربائية، الميكانيكية، الإنتاج والتصنيع، انظمة التحكم، الميكاترونكس، الكيميائية، النفط، المعادن.

تهدف المجلة في هذا السياق الى تحقيق فهم أفضل للقضايا الهندسية، توفير اطار لحلول غير عادية او تقليدية، وتطوير أنظمة لتوفير الطاقة منخفضة التكلفة وتجسير الفجوة بين علوم المواد، والأداء والهندسة، والآثار البيئية، والسلوك الميداني، التصميم، والعمر الخدمي للمنتجات الهندسية.

نحن نعلم أن هذه المواضيع لن تتوقف عن التطور ولذلك نرحب بكل الأعمال البحثية الجديدة والمبتكرة والبحوث التي تجد لها صدى عملي في التطبيق الصناعي.

هيئة تحرير مجلة المهندس

جمعية المهندسين العراقية

تاسست عام ١٩٣٨

الهيئة الادراية ـ ٢٠١٦

الـــرئـيـس: المهندس الاستشاري فالح كاظم زاير
نائب الرئيس: المهندس الاستشاري وهاب رزوقي المرعب
اميـن السر: المهندس الاستشاري صباح عبد الرضا الجزائري
اميـن المـال: المهندس محمد فاروق عبد الخالق
الاعـضـــاء: أ.د. مظفر علي الجابري
المهندس الاستشاري عبد الله ضاري العامري
المهندس الاستشاري منعم صالح السبع
المهندس الاستشاري فالح خضر الجوفي
المهندس الاستشاري فلاح حسن المعروف
المهندس الاستشاري عبد الامير صبري القريشي
المهندس الاستشاري رياض كتاب حسين
المهندس حسنين محمد حسن

هيئة تحرير المجلة

رئيس التحـريـر: أ.د. مظفر علي الجابري
مديـــر التحـريـر: أ.م.د. معن سلمان حسن
سكرتير التحرير: م.د. زينب بهاء محمد
الاعـــضـــــاء: أ.د. نجدت نشأت عبد الله
أ. ماهر خضير محمود العزاوي
أ.د. محمد زكي الفائز
أ.د. رسول مجبل خلف
أ.م.د. سميرة محمد حمد الله
أ.م.د. نصير عبود الحبوبي
م.د. فرات ابراهيم حسن

هواتف جمعية المهندسين العراقية

٠٧٩٠١٤٧١٦٢١ ـ ٠٧٧٠٢٥٢٦٧٢١ ـ الادارة
٠٧٩٠١١٥١٠٩٢ ـ المجلة
P.O Box - ١٨٤٢٩
Email: Jmise@ise-iq.org
info@ise-iq.org
www.ise-iq.org

تعليمات النشر

١ - نوع الحرف المستعمل باللغه الانكليزية Times New Roman وباللغة العربية Arabic Transparent.
٢ - حاشية الصفحة من الاعلى والاسفل والايمن والايسر ٤سم.
٣ - هوامش الصفحة من اعلى والاسفل ٣سم.
٤ - يطبع عنوان البحث بحجم (١٤) اسود غامق اعلى الخلاصة وباللغتين العربية والانكليزية. اما العناوين داخل البحث فهي بدون ترقيم او خط اسفل العناوين وتكتب بحجم (١١) اسود غامق باللغة الانكليزية وبحجم (١٢) اسود غامق باللغة العربية.
٥ - يكتب متن البحث بحجم (١١) باللغة الانكليزية وبحجم ١٢ باللغة العربية.
٦ - يكتب اسم الباحث بحجم (١٢) وتوضع نجمة على اخر اسم الباحث الثلاثي. واذا شارك اكثر من باحث فتكتب اسماؤهم في سطر واحد وتترك مسافة كافية بين الاسماء وتوضع نجمة على اول اسم في الجانب الايسر. اذا كان الباحثون يعملون في جهة واحدة وتوضع نجمة اخر اسم من الاسم الثلاثي لكل بحث اذا كان الباحثون يعملون في اماكن مختلفة
٧ - يكتب البحث بعمودين عرض كل عمود ٦سم وتفصل لبينهما ١سم، ولا يقل عدد الاسطر في العمود الواحد عن ٤٢ سطر. (لا تشمل هذه النقطة الخلاصة باللغتين وكذلك الجداول والاشكال).
٨ - اذا كان البحث باللغة العربية توضع نجمة في اسفل العمود الايمن في هامش الصفحة ويذكر بعدها محل عمل الباحث وبريده الالكتروني ان وجد واسفل العمود الايسر في هامش الصفحة اذا كان البحث باللغة الانكليزية.
٩ - توضع اسفل الخلاصة باللغة العربية - الكلمات الدالة وكذلك اسفل الخلاصة باللغة الانكليزية Key words.
١٠ - يكتب عنوان البحث على العمود الايمن للبحوث باللغة العربية وعلى العمود الايسر للبحوث باللغة العربية في كل صفحات البحث (ضمن هامش الصفحة) وعلى العمود الايسر لكل صفحات البحوث باللغة الانكليزية. لاتخص الفقرة التالية الباحث وهي يكتب اسم المجلة والمجلد والعدد في الجهة المقابلة التي كتب فبها عنوان البحث.
١١ - المراجع: ترتب حسب الاشارة اليها في المتن (وضع رقم المصدر في قوس مربع). ويوصف كل مرجع كالاتي:
أ - الكتب: يوضع الاسم الثالث في البداية يلية فارزة ثم الاسماء الاخرى او الحروف الاولى منها. توضع نقطة بين مؤلف واخر. ثم اسم الكتاب ويلاحظ ان تكتب كل كلمة من عنوان الكتاب بحرف كبير ثم يليه اسم الناشر والسنة.
ب - البحوث او المقالات: يكتب اسم الباحث كما في الكتب اعلاه . يكتب الحرف الاول من العنوان بحرف كبير. ويوضع عنوان المقالة بين علامتي اقتباس. ثم اسم المجلة والجزء، العدد، الصفحات ثم السنة وتفصل بينهم فوارز.

أقامت

جمعية المهندسين العراقية

بالتعاون مع مجلس محافظة بغداد

مؤتمر الطاقة المستدامة والمتجددة الأول

تحت شعار

(ضمان الطاقات المتجددة لبيئة افضل)

اهداف المؤتمر

١ ـ اطلاع المشاركين على احدث التجارب الوطنية في تكنولوجية الطاقة المستدامة والمتجددة والشركات العاملة في مجال الطاقة الشمسية وطاقة الرياح وطاقة الوقود الحيوي.
٢ ـ تقديم الدراسات والبحوث العلمية التي تهدف لتطوير الطاقات المستدامة والمتجددة.
٣ ـ وسيلة من وسائل التواصل والتعارف بين المختصين والباحثين واساتذة الجامعات في هذا المجال من الاختصاص.
٤ ـ تسليط الضوء على استخدامات الطاقات المستدامة والمتجددة وتوظيف التطبيقات العملية لها.
٥ ـ الاعداد لإقامة معارض في مجال الطاقات المستدامة والمتجددة من قبل مراكز البحوث والشركات المتخصصة.
٦ ـ مراجعة التشريعات القانونية في مجال الطاقة المستدامة والمتجددة في العراق.
٧ ـ ايجاد وسائل اسناد للدراسات ودعم للتجارب العملية بغية استثمارها.

عقدت الجلسات الرئيسية والنقاشية على قاعات فندق فلسطين الدولي.

محاور المؤتمر

١ ـ تطبيقات الطاقة الشمسية (ASE).
٢ ـ تطبيقات طاقة الرياح (AWE).
٣ ـ تطبيقات طاقة الكتلة الحيوية (ABE).
٤ ـ تطبيقات الطاقة المتجددة الاخرى (ORE).
٥ ـ تطبيقات العمارة المستدامة (ASA).
٦ ـ التشريعات للطاقة المستدامة والمتجددة (LSE).

اللجنة المشرفة العليا

د. رياض ناصر العضاض	رئيس مجلس محافظة بغداد	رئيسا
م. الاستشاري فالح كاظم زاير	رئيس جمعية المهندسين العراقية	عضوا
أ.د. امين دواي التميمي	رئيس الجامعة التكنولوجية	عضوا
أ.د. نبيل كاظم عبد الصاحب	رئيس جامعة النهرين	عضوا
أ.م.د. ماجد حميد مجيد	رئيس الجامعة التقنية الوسطى	عضوا
أ.د. محمد علي الانباري	الجامعة المستنصرية/ عميد كلية الهندسة	عضوا
أ.د. جاسم عبود الدباغ	جامعة النهرين/ عميد كلية الهندسة	عضوا
أ.د. محمد زكي الفائز	جامعة النهرين/ عميد كلية هندسة المعلومات	عضوا
أ.د. احمد عبد الصاحب	جامعة بغداد/ عميد كلية الهندسة	عضوا
أ.م.د. محمد عبد عطية السراج	جامعة بغداد/ عميد كلية الهندسة الخوارزمي	عضوا
أ.م.د. قادر حمود الشرع	عميد كلية الفارابي الجامعة	عضوا

اللجنة التحضيرية

م. الاستشاري فالح كاظم زاير	رئيس جمعية المهندسين العراقية	رئيسا
أ.م.د. علاء عبد الحسن عطية	الجامعة التكنولوجية/ المساعد العلمي لرئيس الجامعة	عضوا
أ.م.د. علاء كريم محمد	جامعة بغداد/ كليةالهندسة الخوارزمي	عضوا
أ.م.د. عامر حسن الحداد	جامعة بغداد/ كلية الهندسة	عضوا
أ.م.د. نصير عبود الحبوبي	جامعة النهرين/ كلية الهندسة	عضوا
م.م. احمد صالح مهدي	الجامعة المستنصرية/ كلية الهندسة	عضوا
المعمار ألأكاديمي موفق جواد الطائي	جمعية المهندسين العراقية	عضوا
م. الاستشاري وهاب رزوقي المرعب	جمعية المهندسين العراقية	عضوا
م. الاستشاري منعم صالح السبع	جمعية المهندسين العراقية	عضوا
م. حسنين محمد حسن	جمعية المهندسين العراقية	عضوا

اللجنة العلمية

أ.د. حسين يوسف محمود	جامعة بغداد/ كلية الهندسة	رئيسا
أ.د. مظفر علي الجابري	جمعية المهندسين العراقية	عضوا
أ.د. ندى مهدي فوزي	جامعة بغداد/ كلية الهندسة	عضوا
د. مظهر صادق سبع	وزارة الصناعة والمعادن	عضوا
أ.م.د. عبد الجبار نعمة خليفة	جامعة النهرين/ المساعد العلمي لرئيس الجامعة	عضوا
أ.م.د. ضاري يوسف محمود	الجامعة التكنولوجية/ رئيس قسم الهندسة الكهربائية	عضوا
أ.م.د. علي هادي الحمداني	الجامعة التكنولوجية/ مدير مركز تكنولوجيا الطاقة	عضوا
أ.م.د أحمد قاسم محمد	الجامعة التقنية الوسطى/ الكلية التقنية الهندسية	عضوا
أ.م.د. ناصر احمد العواد	الجامعة المستنصرية/ كلية الهندسة	عضوا
م.د. اميل محمد رحمن	جامعة بغداد/ كلية الهندسة الخوارزمي	عضوا
م.د. وائل رشيد عبد المجيد	جامعة بغداد/ كلية الهندسة الخوارزمي	عضوا
م.د. شذى عباس حسن	جامعة بغداد/ كلية الهندسة	عضوا
أ.م.د. لبنى عبد الجبار الزبيدي	الجامعة المستنصرية/ كلية الهندسة	عضوا

محتويات العدد

بحوث القسم العربي **رقم الصفحة**

تأثير المواد المستدامة على خواص الخرسانة ذاتية القرص **٧**

أ.د.ندى مهدي فوزي الجبلاوي هديل ابراهيم احمد

تحويل الاطارات المستهلكة الى مصدر للطاقة بالطرق الحرارية المختلفة **٢٣**

ميسون جودة زعيتر

أستخراج غاز الميثان كوقود لتوليد الطاقة الكهربائية **٣٣**

م.م.وديان هادي عبد الامير

تأثير المواد المستدامة على خواص الخرسانة ذاتية الرص

أ.د. ندى مهدي فوزي الجيلاوي / استاذ / الهندسة المدنية / جامعة بغداد

هديل ابراهيم احمد / مدرس مساعد / معهد التكنولوجيا / هيئة التعليم التقني

الخلاصة

الخرسانة ذاتية الرص هي صنف جديد من الخرسانة عالية الأداء التي تكون لها القابلية على الانسياب تحت تأثير وزنها وبمستو أفقي، ولها القابلية على ملئ القالب كاملاً حتى في وجود تسليح كثيف وتكون مرصوصة بشكل جيد و بأقل الفجوات من غير الحاجة الى هزاز مع المحافظة على تجانسها بصورة جيدة نتيجة الى مقاومتها العالية للانعزال.

تم في هذا البحث إنتاج خرسانة ذاتية الرص حاوية على الرماد المتطاير وهو نوع من المخلفات الصناعية واستخدم كاستبدال من وزن السمنت . و بينت الدراسة ان للرماد المتطاير تأثير ايجابي على الخواص الطرية والمتصلبة للخرسانة ذاتية الرص.

الكلمات الرئيسية : الخرسانة ذاتية الرص ، الرماد المتطاير ، الخواص الطرية للخرسانة ذاتية الرص، خواص الخرسانة ذاتية الرص المتصلبة

١- المقدمة :-

الخرسانة ذاتية الرص(Self Compacting Concrete) و يرمز لها (SCC) هي واحدة من أحدث الابتكارات في تكنولوجيا الخرسانة، إذ أَخذت بالانتشار في جميع أنحاء العالم لِما لها من خصائص و مميزات في حالتها الطرية و كذلك بعد التصلب،وهي ذات قابلية تشغيل عالية حيث تنساب خلال التسليح الكثيف او العناصر الإنشائية المعقدة هندسياً تحت تأثير وزنها الذاتي فقط على نحو كافي لتملأ الفراغات بدون أي انعزال او نضوح

متجاوز الحد دون الحاجة الى تسليط الاهتزازات عليها (Ravindrarajah,٢٠٠٣)،(Tviksta,٢٠٠٠)، (Vachon,٢٠٠٢). وان للخرسانة ذاتية الرص(SCC) لزوجة تشبه العسل(Honey) وتمتلك هذه الخرسانة سطحاً مستوياً بعد الصب (Placing) ، حيث تأخذ شكل معين وهذا بسبب انسيابها السريع، وهي ذات سطح صقيل بحيث يكون لها شكل نهائي أفضل من الخرسانة التقليدية،وإنها تمتلك صفة عدم الانعزال وعدم ميلها إلى الإعاقة (Blocking tendency)(Ravindrarajah,٢٠٠٣)، (Dehn,٢٠٠٠).

٢- خصائص المواد الأولية و الإعمال المختبرية :-

٢-١ السمنت :-

السمنت المستخدم في هذا البحث هو سمنت بورتلاندي اعتيادي (Type I) المصنع من قبل شركة السمنت المتحدة المعروف تجاريا باسم (طاسلوجة-بازيان) . و خواصه الفيزيائية و الكيميائية مطابقة للمواصفة العراقية (م.ق.ع /٥ / ١٩٨٤) .

٢-٢ الركام الناعم :-

تم استخدام الركام الناعم (الرمل) وهو مطابق للمواصفة العراقية القياسية (م.ق.ع /٤٥ / ١٩٨٤) .

٢-٣ الركام الخشن :-

تم استخدام حصى مكسر مقاسه الاسمي (٥-١٤ ملم) وهو مطابق للمواصفة العراقية القياسية (م.ق.ع /٤٥ / ١٩٨٤) .

٢-٤ الملدن المتفوق :-

استخدم في هذا البحث مضاف مقلل للماء بدرجة متفوقة والمعروف تجاريا (Glenuim ٥١)

٢-٥ الرماد المتطاير (Fly ash) :-

الرماد المتطاير هو مادة بوزولانية صناعية مستوردة مطابقة للمواصفة الأمريكية (ASTM C ٦١٨-٠٣). يعرف الرماد المتطاير صنف (F) على انه ناتج من احتراق انثرسايت او الفحم الحجري ، الذي يلبي الشروط المتطابقة مع ذلك الصنف في هذه المواصفة . هذا الصنف من الرماد المتطاير يمتلك خواص بوزولانية . اجري فحص خواصه الكيمائية و الفيزيائية في الشركة العامة للمسح الجيولوجي و التعدين و نتيجة الفحص تبين ان الرماد المتطاير مطابق للصنف(F) بموجب المواصفة الأمريكية (ASTM C٦١٨-٠٣) كما موضح في الجدول (٢-١) ، (٢-٢) على التوالي

الجدول (٢-١) التحليل الفيزيائي للرماد المتطاير

الخواص الفيزيائية	الرماد المتطاير
المظهر الفيزيائي	مسحوق
اللون	رمادي
الوزن النوعي	٢
المساحة السطحية (طريقة Blaine) سم^2 / غم	٦٢٠٠
دليل فعالية المقاومة (S.A.I)	٨٨

الجدول (٢-٢) التحليل الكيمائي للرماد المتطاير

المركبات	المحتوى %	المواصفة ٠٣/ ٦١٨ .ASTM C صنف F
SiO_2	٦١,٩٥	الحد الأدنى ٧٠%
Fe_2O_3	٢,٦٧	
Al_2O_3	٢٨,٨٢	
CaO	٠,٨٨	
MgO	٠,٣٤	
SO_3	اقل من ٠,٠٧	الحد الأعلى ٥%
Na_2O	٠,٢٦	
L.O.I.	٠,٨٦	الحد الأعلى ٦ %

٣- الخلطات الخرسانية :-

لأجل تحقيق الهدف من الدراسة تم تقسيم التجارب المختبرية الى تسع خلطات ما عدا الخلطات المرجعية فهي عبارة عن ثلاث خلطات فقط و تم استخدام طريقة المنظمة الأوروبية للخرسانة جاهزة الخلط (The EMRCO,٢٠٠٥) في تصميم هذه الخلطات كما في الجدول (٢-٣) .

الجدول(٣-١) : تفاصيل الخلطات المستخدمة .

رمز الخلطة	السمنت كغم/ م^3	الرماد المتطاير كغم/ م^3	الرمل كغم/ م^3	الحصى كغم/ م^3	الماء لتر/ م^3	محتوى الملدن المستخدم لتر لكل ١٠٠ كغم من السمنت	الملدن المتفوق لتر/ م^3	w/Cm
R١	٥٠٠	-	٨٢٥	٨٥٠	١٧٠	٠,٩	٤,٥	٠,٣٤
R٢	٥٠٠	-	٨٢٥	٨٥٠	١٨٠	٠,٩	٤,٥	٠,٣٦
R٣	٥٠٠	-	٨٢٥	٨٥٠	١٩٠	٠,٩	٤,٥	٠,٣٨
FA١	٤٧٥	٢٥	٨٢٥	٨٥٠	١٧٠	٠,٩	٤,٥	٠,٣٤
FA٢	٤٥٠	٥٠	٨٢٥	٨٥٠	١٧٠	٠,٩	٤,٥	٠,٣٤
FA٣	٤٢٥	٧٥	٨٢٥	٨٥٠	١٧٠	٠,٩	٤,٥	٠,٣٤
FA٤	٤٧٥	٢٥	٨٢٥	٨٥٠	١٨٠	٠,٩	٤,٥	٠,٣٦
FA٥	٤٥٠	٥٠	٨٢٥	٨٥٠	١٨٠	٠,٩	٤,٥	٠,٣٦
FA٦	٤٢٥	٧٥	٨٢٥	٨٥٠	١٨٠	٠,٩	٤,٥	٠,٣٦
FA٧	٤٧٥	٢٥	٨٢٥	٨٥٠	١٩٠	٠,٩	٤,٥	٠,٣٨
FA٨	٤٥٠	٥٠	٨٢٥	٨٥٠	١٩٠	٠,٩	٤,٥	٠,٣٨
FA٩	٤٢٥	٧٥	٨٢٥	٨٥٠	١٩٠	٠,٩	٤,٥	٠,٣٨

٤- طرق اختبار الخواص الطرية للخرسانة ذاتية الرص :-

٤-١ اختبار القمع على شكل حرف V :-

ان هذا الفحص يقيم الخواص الطرية للخرسانة ذاتية الرص بأسلوب يختلف عن فحص انسياب الهطول . والشكل (٤-١) يبين الجهاز المستخدم في اختبار القمع على شكل (V) . وتم خلال هذا الفحص قياس الزمن اللازم من لحظة فتح بوابة القمع الى لحظة خروج كل الخرسانة من القمع وهي لحظة رؤية الضوء من

خلال فتحة البوابة ويعبر عنه ب (T_{0min}) . وتعتبر الخرسانة ذات خواص رص ذاتي إذا كان هذا الزمن ضمن حدود ٦-١٢ ثانية .

٤-٢ صندوق الاختبار على شكل حرف U :-

يختص هذا الفحص بالتحقق من قدرة الملئ وإمكانية انسياب الخرسانة ذاتية الرص المحتوية على مختلف أنواع الركام من خلال قضبان حديد التسليح بدون حدوث انفصال حبيبي أو انسداد . يتم حساب قيمة الفرق في ارتفاع سطح الخرسانة بين الحجرتين ($H_1 - H_2$) ويجب إن يكون اقل من أو يساوي ٣٠ ملم ، وكلما كان الفرق اقرب للصفر كلما كانت الخرسانة ذات درجة انسياب عالية ولها مقدرة عالية على الانسياب بين قضبان التسليح .

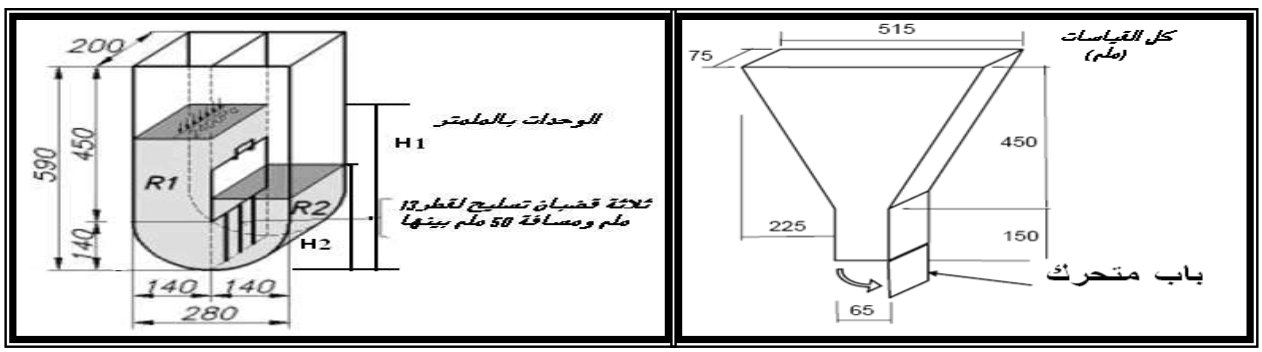

الشكل (٤-١) : اختبار القمع على شكل حرفV على اليمين وصندوق الاختبار على شكل حرف U على اليسار

٥- طرق اختبار خواص الخرسانة المتصلبة :-

٥-١ مقاومة الانضغاط :-

اجري فحص مقاومة الانضغاط بموجب المواصفة البريطانية(BS١٨٨١-part١١٦/١٩٨٣)وتم استخدام نماذج مكعبة الشكل بإبعاد (١٠٠×١٠٠× ١٠٠) ملم للخلطات الخرسانية تم تسليط الحمل على النموذج مع تسجيل الحمل المسبب للفشل ، و تستخرج مقاومة الانضغاط من حاصل قسمة الحمل على مساحة الوجه المعرض للحمل، و تم الفحص بأعمار(٢٨ ، ٦٠ ، ٩٠) يوم واخذ معدل ثلاث مكعبات .

٥-٢ مقاومة الانثناء :-

تم فحص مقاومة الانثناء لاعتاب بأبعاد (٤٠٠×١٠٠× ١٠٠) ملم للخلطات الخرسانية بموجب المواصفة الأميركية(ASTM C ٢٩٣-٠٧) علما بان النموذج وضع داخل الجهاز بحيث تكون السطوح الجانبية و المواجهة لجوانب القالب إثناء الفحص ملامسة للمساند عمودي على اتجاه الصب .يؤخذ معدل مقاومة الانثناء لثلاثة نماذج لكل خلطة و تم الفحص بأعمار(٢٨ ، ٦٠ ، ٩٠) يوم و يعبر عنه بميكا باسكال(نيوتن / ملم^2) و يتم حسابه وفقا للمعادلة الآتية :

$$R = {}^3PL / {}^2 bd^2 \qquad \text{..... (١)}$$

إذ ان

R = مقاومة الانثناء (ميكا باسكال) .

P = أعلى حمل مسبب للفشل (نيوتن) .

L = المسافة بين نقطتي الارتكاز (٣٠٠) ملم .

b = العرض (١٠٠) ملم .

d = الارتفاع (١٠٠) ملم .

٣- النتائج و مناقشة البيانات :-

٦-الاستنتاجات

الخواص الطرية للخرسانة ذاتية الرص :-

تمت دراسة تأثير اضافة نسب مختلفة من الرماد المتطاير (٥ ، ١٠ ، ١٥) % كاستبدال جزئي من وزن السمنت مع ثلاث محتويات مختلفة من الماء و هي (١٧٠ ، ١٨٠، ١٩٠) كغم / م^3 كما موضحة بالجدول (٦-١) و (٦-٢) . فان اضافة الرماد المتطاير أدت الى زيادة في زمن الانسياب (Tv , Tv٥min) و زيادة فرق ارتفاع الملئ بشكل كبير مقارنة بالخلطات المرجعية(R١,R٢,R٣) الحاوية على السمنت بدون اضافة المادة البوزولانية .حيث كلما تزداد نسب الاستبدال للمجموعة الاولى ذات محتوى الماء ١٧٠ كغم / م^3 للخلطات الحاوية على الرماد المتطاير كلما يزداد زمن الانسياب للـ (Tv , Tv٥min) و كما يزداد فرق ارتفاع الملئ يعود السبب الى لزوجة الخلطات الخرسانية التي تزداد في الخلطات الحاوية الرماد المتطاير والسمنت نتيجة لزيادة المواد الناعمة و الى قابلية الانسياب للخرسانة من مقطع الى أخر. و هذا الكلام ينطبق على المجموعة الثانية ذات محتوى الماء ١٨٠ كغم / م^3 والثالثة ذات محتوى الماء ١٩٠ كغم / م^3 . اما زيادة محتوى الماء من (١٧٠-١٩٠) كغم / م^3 للخلطات الحاوية على الرماد المتطاير يقلل من زمن الانسياب لكل من (Tv , Tv٥min) و ذلك يعود الى سرعة الانسياب نتيجة لتقليل لزوجة الخلطة و يؤدي الى زيادة سرعة الانسيابية لهذه الخلطات الذي يؤدي الى تقليل من الاحتكاك الداخلي بين حبيبات الركام او بين الخرسانة و السطح الملامس لها.

اما لزيادة محتوى الماء من (١٧٠-١٩٠) كغم / م^3 للخلطات الحاوية على الرماد المتطاير فيؤدي الى زيادة فرق ارتفاع الملئ وذلك بسبب نقصان قابلية التشغيل للخلطات و نقصان سرعة الانسياب للمقطع الآخر من دون حصول أي انعزال او نضوح للخلطات الخرسانية.

مقاومة الانضغاط و مقاومة الانثناء :-

يلاحظ زيادة مقاومة الانضغاط و مقاومة الانثناء للخلطات الحاوية على الرماد المتطاير مع زيادة نسب الاستبدال الجزئي له و بمقدار (٥ ، ١٠ ، ١٥) % من وزن السمنت للمجموعة الاولى ذات محتوى الماء ١٧٠ كغم/م^3 . ان ما توصل إليه الباحث (Banthia , ٢٠٠١) حول هذا الموضوع حيث بزيادة نسب اضافة المضافات المعدنية تقل نسبة المسامات و هذا ما يميز الفعل الرابط للمضافات المعدنية الطريقة النسبية نفسها لزيادة مقاومة الانضغاط و هذا يعود الى الملئ التدريجي للفجوات الكبيرة بواسطة نواتج الاماهة من المواد السمنتية التكميلية ، وعموما فان ميكانيكية المقاومة للسمنت تزداد مع زيادة هذه المواد و نقصان المسامية و هذا ينطبق على المجموعة الثانية ذات محتوى الماء ١٨٠ كغم/م^3 و الثالثة ذات محتوى الماء ١٩٠ كغم/م^3 . ان زيادة مقاومة الانضغاط للخلطات الحاوية على الرماد المتطاير مع تقدم زمن الإنضاج للمجموعة الاولى ذات محتوى الماء ١٧٠ كغم/م^3 قد يعود ذلك إلى ان المضافات المعدنية ومنها الرماد المتطاير قادرة على زيادة مقاومة الانضغاط في الخرسانة مع تقدم زمن الإنضاج و هذا ناتج من الفعالية البوزولانية لمادة الرماد المتطاير التي تتسبب في إزالة المسام و استبدال المركب الضعيف (هيدروكسيد الكالسيوم) بالمركب الأقوى (سليكات الكالسيوم المميهه) فإذا تم إزالة المسامات الكبيرة و نقصان هيدروكسيد الكالسيوم وهي العناصر الضرورية لإنتاج خرسانة عالية المقاومة فان المضافات المعدنية تلعب دور رئيسي في إنتاج خرسانة عالية المقاومة و هذا ينطبق على المجموعة

الثانية ذات محتوى الماء ١٨٠ كغم/م^3 والثالثة ذات محتوى الماء ١٩٠ كغم/م^3 و هذا يشابه ما توصل إليه الباحث (Mehta , ٢٠٠٦) .

يلاحظ من نتائج مقاومة الانضغاط و مقاومة الانثناء المذكورة في الجدول (٦-٣) و (٦-٤) بان مقاومة الانضغاط و مقاومة الانثناء للخرسانة الحاوية على الرماد المتطاير تتناقص مع زيادة محتوى الماء من (١٧٠-١٩٠) كغم/م^3 و هذا يعود الى ان زيادة كمية ماء الخلطة تعمل على تحسين قابلية التشغيل لكنها تعمل على أضعاف بنية عجينة السمنت و هذا يؤدي الى انخفاض في مقاومة الانضغاط و زيادة نفاذية الخلطة و هذا يشابه ما توصل إليه الباحث (البدري،٢٠٠١).

٧- مناقشة النتائج:-

أ- ان اضافة الرماد المتطاير بنسب استبدال جزئي (٥ ، ١٠ ، ١٥) % من وزن السمنت أدى الى زيادة زمن الانسياب(Tv) و (Tv٥min) زيادة في فرق ارتفاع الملئ مع زيادة نسب الاستبدال الجزئي . و لكن بزيادة محتوى الماء يقل زمن الانسياب (Tv) و(Tv٥min) ويزداد فرق ارتفاع الملئ ، أي له تاثير ايجابي على الخواص الطرية.

ب- زيادة مقاومة الانضغاط مع زيادة نسب الاستبدال الجزئي الرماد المتطاير يتراوح بين (٢٢ ،٣٣، ٥٠) % للنسب (٥ ، ١٠ ، ١٥) % من وزن السمنت و بزمن إنضاج ٩٠ يوم و ذات محتوى الماء ١٧٠ كغم/م^3 و تقل قليلا بزيادة محتوى الماء.

ج- زيادة مقاومة الانثناء مع زيادة نسب الاستبدال الجزئي الرماد المتطاير يتراوح بين (٧ ،١٤، ١٧) % للنسب (٥ ، ١٠ ، ١٥) % من وزن السمنت و بزمن إنضاج ٩٠ يوم و ذات محتوى الماء ١٧٠ كغم/م^3 و تقل قليلا بزيادة محتوى الماء.

الجدول (٦-١) : نتائج اختبار القمع على شكل حرف v

أنواع الخلطات	رمز الخلطة	القمع على شكل حرف V	
		الزمن (ثانية)	الزمن بعد ٥ دقيقة (ثانية)
المجموعة الاولى ذات محتوى الماء ١٧٠ كغم/ م^3	R١	٧,٥	٨,٨
	FA١	٧,٦	٩,٠
	FA٢	٨,٥	١٠,٠
	FA٣	٩,٥	١٢,٠
المجموعة الثانية ذات محتوى الماء ١٨٠ كغم/ م^3	R٢	٧,٢	٨,٥
	FA٤	٧,٣	٨,٧
	FA٥	٧,٥	٩,٥
	FA٦	٩,٥	١١,٥
المجموعة الثالثة ذات محتوى الماء ١٩٠ كغم/ م^3	R٣	٦,٥	٧,٥
	FA٧	٧,٠	٨,٠
	FA٨	٧,٢	١٠,٠
	FA٩	٩,٠	١٢,٠

الجدول (٦-٢) : نتائج فرق ارتفاع الملئ لصندوق الاختبار على شكل حرف U .

أنواع الخلطات	رمز الخلطة	فرق ارتفاع الملئ لصندوق الاختبار على شكل حرف U ΔH (ملم)
المجموعة الاولى ذات محتوى الماء ١٧٠ كغم/ م^3	R١	٨
	FA١	١٠
	FA٢	١٣
	FA٣	١٦
المجموعة الثانية ذات محتوى الماء ١٨٠ كغم/ م^3	R٢	١٠
	FA٤	١٢
	FA٥	١٥
	FA٦	١٩
المجموعة الثالثة ذات محتوى الماء ١٩٠ كغم/ م^3	R٣	١٥
	FA٧	١٨
	FA٨	٢٠
	FA٩	٢٤

الجدول (٦-٣) : نتائج فحص مقاومة الانضغاط للتجارب المختبرية للخرسانة ذاتية الرص .

أنواع الخلطات	رمز الخلطة	مقاومة الانضغاط (ميكا باسكال) بعمر (يوم):		
		٢٨	٦٠	٩٠
المجموعة الاولى ذات محتوى الماء ١٧٠ كغم/ م^3	R١	٤١,٢٧	٤٣,٤٥	٤٧,٧٢
	FA١	٤٢,٠٣	٤٨,١٨	٥٨,٣٦
	FA٢	٤٤,٥٤	٥٤,٧١	٦٣,٤٥
	FA٣	٤٦,٣٦	٥٦,٩١	٧١,٣٦
المجموعة الثانية ذات محتوى الماء ١٨٠ كغم/ م^3	R٢	٣٩,٢٧	٤٣,٢٣	٤٦,٣٦
	FA٤	٤١,٤١	٤٧,٢٧	٥٤,٦٤
	FA٥	٤٢,٨٤	٥٤,٢٣	٥٩,٦٠
	FA٦	٤٤,٣١	٥٥,٩١	٦٩,٩٩
المجموعة الثالثة ذات محتوى الماء ١٩٠ كغم/ م^3	R٣	٣٦,٥٧	٣٨,٩١	٤١,٤٨
	FA٧	٤٠,٢٣	٤٣,٣٦	٥٠,٧٠
	FA٨	٤٠,٤٦	٤٧,٩٥	٥٢,٣٦
	FA٩	٤٤,٢٧	٥٠,٠٠	٥٨,٧٢

الجدول (٦-٤) : نتائج فحص مقاومة الانثناء للتجارب المختبرية للخرسانة ذاتية الرص .

أنواع الخلطات	رمز الخلطة	مقاومة الانثناء (ميكا باسكال) بعمر (يوم):		
		٢٨	٦٠	٩٠
المجموعة الاولى ذات محتوى الماء ١٧٠ كغم/ م^3	R١	٦,٢٤	٦,٤٦	٦,٩٩
	FA١	٦,٥٥	٦,٨٥	٧,٤٥
	FA٢	٦,٩٠	٧,٣٣	٧,٩٥
	FA٣	٧,١٥	٧,٤٦	٨,١٥
المجموعة الثانية ذات محتوى الماء ١٨٠ كغم/ م^3	R٢	٦,١٥	٦,٢٧	٦,٨٠
	FA٤	٦,٤٥	٦,٦١	٧,٢٠
	FA٥	٦,٧٣	٦,٩٧	٧,٦٦
	FA٦	٦,٨٥	٧,٢١	٨,٠٢
المجموعة الثالثة ذات محتوى الماء ١٩٠ كغم/ م^3	R٣	٦,٠٤	٦,١٨	٦,٣٧
	FA٧	٦,٣٠	٦,٤٩	٧,١٥
	FA٨	٦,٦٧	٦,٨٥	٧,٣٦
	FA٩	٧,١٥	٧,٤١	٧,٧٥

٨- المصادر :-

٨-١ المصادر الأجنبية :-

١- ASTM C٢٩٣-٠٧, "Standard Test Method for Flexural Strength of Concrete (Using Simple Beam With Center-Point Loading)" ASTM International .

٢- ASTM C٦١٨-٠٣, "Standard Specification for Coal Fly Ash and Raw or Calcined Natural Pozzolan for Use in Concrete" ASTM International .

٣- BS ١٨٨١, part ١١٦, "Method for determination of compressive strength of concrete cubes" British standards institution, ١٩٨٩.

٤- Banthia, N., and Sakai, K. ," Concrete Under Sever Conditions Environment and Loading", Vancourer BC , ٢nd.ed, Canada, ٢٠٠١, pp.

٥- Dehn, F., K. Holschemacher, and D. Weisse, "Self-Compacting Concrete - Time Development of the Material Properties and the Bond Behavior", LACER No. ٥, (٢٠٠٠), pp.١١٥-١٢٣.

٦- Mehta, P.K., and Monteiro, P.J., "Concrete: Microstructure, Properties and Materials", Department of Civil and Environmental, Engineering University of California at Berkeley, Thrid Edition,٢٠٠٦.

٧- Ravindrarajah, R., Farrokhzadi, and Lahoud, A.," Properties of Flowing Concrete and Self-Compacting Concrete with High Performance Superplasticizer", RILEM Publications, Vol. ١, August ٢٠٠٣, pp.١٠٤٨-١٠٥٨

٨- Ravindrajah R.S., Siladyi D. and Adamopoulos B., " Development of High Strength Self-compacting Concrete With Reduced Segregation Potential ",Proceeding of the ٣rd International RILEM Symbosium, Vol.١, pp.١٠٤٨, Reykjavik, Iceland, (August ٢٠٠٣).

٩- Tviksta L.G., "Guideline for SCC ", Brite EuRam, Task ٩ End Product, (٢٠٠٠) pp.٣-١١.

١٠- "The Europen Guidelines for Self-compacting Concrete", European Ready-Mix Concrete Organisation (ERMCO), May ٢٠٠٥, ٦٨ pp.

١١- Vachon, M., '' ASTM Puts Self-Consolidating Concrete to the Test'' , Ohio, ٢٠٠٢, ١ pp.

٨-٢ المصادر العربية :-

١- البدري ،فراس فاضل "تقييم الخرسانة عالية الأداء بطرق غير إتلافية" اطروحة ماجستير، جامعة بغداد ٢٠٠١.

تحويل الإطارات المستهلكة إلى مصدر للطاقة بالطرق الحرارية

ميسون جودة زعيتر

جهة العمل: وزارة العلوم والتكنولوجيا/ دائرة الطاقات المتجددة

mj_zaiter@yahoo.com

الكلمات الدالة: الإطارات المستهلكة، انحلال حراري، تحويل حراري، زيت بايروليكي.

المستخلص

تصنف الإطارات المستهلكة إلى كونها نفايات خطرة لأنها قابلة للاشتعال وإذا نشب فيها حريق لا يمكن إن ينطفئ بسهولة بالإضافة إلى انبعاث غازات PAH المسرطنة. إن تدوير الإطارات Recycling أصبح ضرورة بسبب الأكوام الضخمة من هذه المخلفات التي تمثل تهديدا للبيئة. من الناحية الإحصائية للبلدان المتقدمة هناك ما يقرب إتلاف إطار بالي واحد للشخص سنوياً. تعتبر الإطارات المستهلكة مصدرا للطاقة والمنتجات الكيماوية وذلك لاحتوائها على قيمة حرارية عالية. بواسطة التحلل الحراري للمطاط تحت ضغط معين، من الممكن الحصول على مصدر طاقة بالإضافة إلى المركبات المفيدة الأخرى.

تم التركيز على تحويل مخلفات الإطارات إلى منتجات مفيدة من خلال عملية كيميائية حرارية، بتسخين حبيبات المطاط في غياب غاز الأوكسجين يؤدي إلى إنتاج منتج يسمى بالزيت البايروليكي الذي من الممكن استخدامه في مكائن الاحتراق الداخلي كمحطات إنتاج الكهرباء ووقود سيارات مشابها بذلك وقود الديزل الناتج عن تكرير الوقود التقليدي(الاحفوري).

أظهرت النتائج إن اعلي إنتاجية للزيت البايروليكي عند درجة حرارة ٤١٥ درجة مئوية وضغط مطلق ٢ كيلو باسكال . كان الوزن النوعي للزيت ٠,٩٥ والمحتوى الحراري بلغ ٤٣ ميغا جول لكل كيلو غرام ومحتوى الكبريت الكلي حوالي ٠,٨% . وكان المنتج النهائي غني بمركبات البنزول.

هنالك طرق بديلة لتدوير الإطارات المستهلكة، وبسبب خاصية المطاط في امتصاص الأصوات والصدمات من الممكن التالي:

- **استخدام الاطار بكامله كحواجز سلامة في منعطفات الطرق السريعة وحدود لمسار مضمار سباق .**
- **تقطيعها وخلطها مع الإسفلت لرص الشوارع .**
- **تقطيعها على شكل حبيبات وخلطها مع مادة لاصقة واستخدامها في تغطية أرضيات الملاعب.**

١ - المقدمة:

يستهلك سنويا حول العالم أكثر من ٣بليون أطار لسيارات صالون وسيارات حمل، وأكثر من ١٠ بليون أطار متراكم في مواقع الطمرالصحي. هذه الاطارات المستهلكة لها القابلية على الاحتراق، وهي تقاوم التحلل البايولوجي وتوفر بيئة ملائمة لنمو القوارض.

متانة الاطارات لتحمل الاحمال العالية تجعلها صعبة التدوير بشكل مربح.

الخيارات الحالية لتدوير الاطارات هي وضعها كحدود امان للطرق السريعة ، تقطيعها الى حبيبات واستخدامها في تغطية ارضية الملاعب، طرق التحلل الحراري والتغويز والتسخين بالبلازما لانتاج الطاقة.

ردم الاطارات المستهلكة هو مشكلة بيئية واقتصادية في تزايد مستمر. تجارياً مسار ردم هذه المخلفات الى مواقع الطمر الصحي تغير الى الردم المفتوح والانحلال الحراري جذب الانظار لكون الزيت المشتق من العملية ممكن استخدامه بشكل مباشر كوقود أو استخدامه كمصدر للمواد الكيمياوية هذا بالاضافة لكون الغازات المشتقة من عملية الانحلال الحراري للاطارات ذات محتوى حراري عالي كافي لتجهيز ما يتطلبه من طاقة لازمة لاتمام الانحلال الحراري. أما الفحم الناتج عن العملية ممكن ان يستفاد منه كوقود صلب أو يعوض عن أسود الكاربون أو الكاربون المنشط كلاً حسب استخدامه.

الانحلال الحراري لمخلفات الاطارات هوتسخين بغياب عنصر الاوكسجين حيث يؤدي الى انتاج زيت حيوي وغازات وفحم كاربوني وشرائط الحديد.

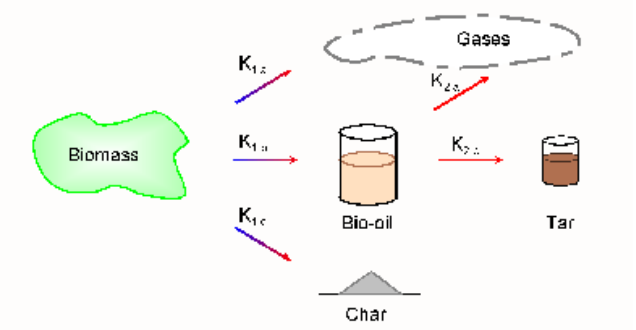

الشكل رقم (١) يوضح رسم تخطيطي لعملية انحلال حراري.

مادة الاطار تحتوي على مركبات كاربونية ثابتة ومتطايرة ذات محتوى حراري أعلى من تلك للفحم **والكتلة** الحيوية. هذه الخواص جعلتها ملائمة كمادة خام للعمليات الحرارية والكيميائية. الانحلال الحراري يعتبر أحد البدائل لأدارة مخلفات الاطارات حيث ينتج عنها ثلاثة اطوار وهي الغازية والسائلة والصلبة ' يتم استخلاص المنتجات السائلة والصلبة وكذلك المتاجرة بها. اما الطور الغازي فيمكن استغلاله مباشرة لتجهيز الطاقة اللازمــة المطلوبة لانجاز العملية [**E. Aylo´n, ٢٠٠٨**].

منظومات تجارب مختبرية مختلفة تم استخدامها لانجاز الانحلال الحراري لمخلفات الاطارات . استخدامت حسابات الموازنة الحرارية (Thermo balance) وتم تثبيتها لأجل توفير المعلومات الديناميكية بأستخدام مفاعلات البرج المتميع (Fluidized bed) من النوع الدفعي. كما استخدام مفاعلات الحشوة الثابتة (Fixed Bed) وتم توثيق النتائج، مع ذلك هنالك اعمال اخرى لعملية معالجة مخلفات الاطارات لمفاعلات مستمرة الانتاجيه (Continuous Reactor). [Dı´ez et al]، ١٩٨٥ مصدر استخدام مفاعل الحشوة المتحركة (Moving Bed) وقارنه بنظام التغذية الدفعي. بالاضافة الى ذلك ان الهدف كان لحرق مخلفات الاطارات في (Supplementary Reactor) حيث يتم حرق الجزء الغازي والصلب معا. الهدف الرئيسي لهذا العمل لاظهار (Viability) الفنية لمحطة ريادية للانحلال الحراري ومقارنتها مع النتائج المتوفرة ذو الحشوة الثابتة من ناحية انتاجية وخصائص الانتاج النهائي.

٢- متطلبات التجربة

٢-١ المواد materials

عينات من حبيبات مخلفات الاطارات الداخلة الى التجربة بعد ازالة شرائط الحديد steel fiber منها وتكون بابعاد قطر لايتجاوز ٥-١٠ ملم ، لذا يتطلب لاجراء التجربة وتهيئة العينات توفر جهاز تقطيع shredder وجهاز فصل شرائط الحديد (Magnetic Separator) فاصل مغناطيسي .

٢-٢ طريقة العمل:

يتم اجراء التجربة باحد الجهازين : الاول مفاعل من الزجاج المقاوم للحرارة (Pyrex Glass Reactor) بنظام دفعي تحت ضغط جوي عادي او اوتوكليف زجاجي كما موضح بالشكل (٢). كمية معينة من مادة مخلفات الاطارات توضح في المفاعل ثابت الحشوة ومن ثم يتم تشغيلها من درجة حرارة الغرفة الى درجة الحرارة النهائية تصل الى ٣٠٠ °م والتجربة الثانية الى ٤٠٠ °م والثالثة الى ٥٠٠ °م ولمدة ساعتين ، يتم التسخين من خلال مسخن كهربائي (Electrical Heater) ويتم قياس درجة الحرارة باستخدام المحرار . كل النواتج الغازية والسائلة والصلبة والمتولدة خلال كل تجربة تجمع ويتم دراسة خواصها .

النواتج الغازية تمر عبر مكثف حيث ينصل الجزء القابل للتكثيف الى سائل ويجمع في وعاء خاص ، اما المتبقي في وعاء التسخين (الجزء الصلب) والذي يكون من اسود الكاربون (Carbon Black)،كل النواتج يتم جمعها ووزنها لمعرفة نسبة الانتاج.

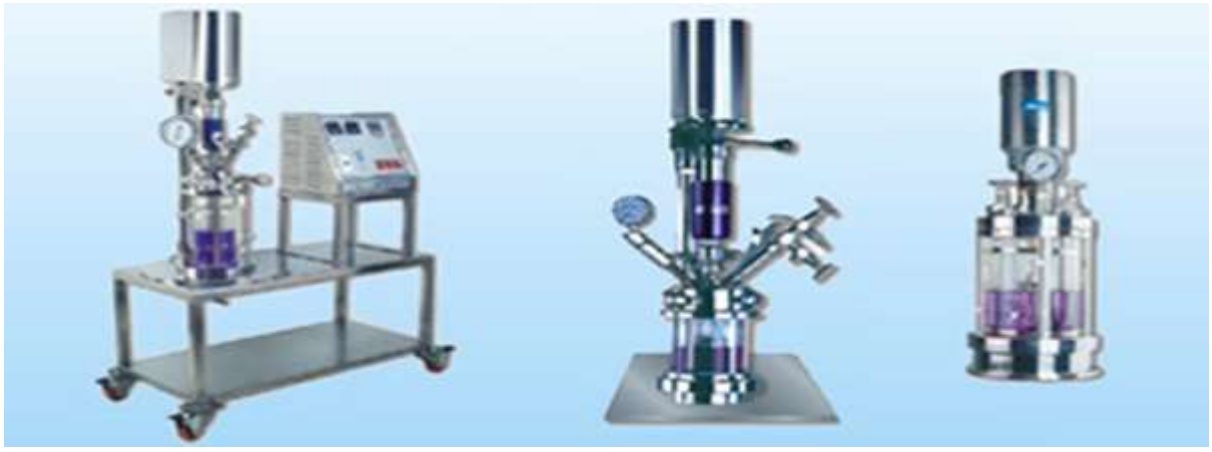

الشكل (٢) اوتوكليف زجاجي

٣- طرق نقل الحرارة :

عملية الانحلال الحراري ماصة للحرارة (Endothermic) [Fang He, ٢٠٠٦] هنالك عدة مرات لنقل الحرارة الى قطع الكتلة الحيوية المتفاعلة

٣-١ الانحلال الحراري بمفاعل ثابت الحشوة Fixed Bed Pyrolysis Reactor

المفاعل مصنوع من الحديد المقاوم للصدأ والتسخين بفرن كهربائي خارجي . يتم حقن غاز النتروجين بشكل مستمر بمعدل ٢لتر بالدقيقة لحمل الغازات الناتجة من منطقة التفاعل .٦٥ غرام من عينة مخلفات الاطارات توضع على مسند داخل المفاعل في مركز المنطقة الساخنة، يتم السيطرة على عملية التسخين بحيث ترتفع درجة حرارة العينة خمس درجات كل دقيقة حتى الوصول الى الدرجة الحرارية النهائية، يتم الابقاء على الدرجة النهائية لمدة عشر دقائق . بعد تبريد الغازات عبر المكثف يتم جمع السائل المتكون في نهاية التجربة ويقياس وزنه المتكون . بعد انتهاء عملية الانحلال الحراري يتم تبريد المفاعل واستخلاص المادة الصلبة المتبقية داخله . ثم يتم قياس وزنها ، اخيرا الغازات الغير قابلة للتكثيف يتم اخذ عينه منها للتحليل بجهاز كروموتوغراف الغاز.وزن الغاز الناتج ونسبة انتاجه يتم حسابها من الفروقات بالاوزان بين المدخلات والمخرجات. خمس تجارب اجريت في هذا المفاعل في ظروف متشابهة ولكن درجة الحرارة النهائية مختلفة لحساب الانتاجية تبين بان الانتاجية هي بعد الوصول الى درجة معينة لن تتأثر برفع المزيد من الحرارة.

٣-٢الانحلال الحراري بمفاعل الحشوة المتحركة :

الرسم التخطيطي في الشكل (٣) يوضح مخطط المفاعل من هذا النوع .يوضح الشكل ان هنالك اربع اجزاء رئيسية :نظام التغذية ،المفاعل ،نظام جمع المادة الصلبة ونظام التكثيف .

نظام التغذية (١)يحوي على جامعين موصلين بصمام نوع (Butterfly) بسعة عشر كيلوغرام من قطع مخلفات الاطارات تقريبا في الساعة. ان هذا النظام يسمح باجراء العملية بشكل مستمر وتحت جو خامل باستخدام غاز النتروجين كغاز حامل .ان حبيبات الاطارات يتم تغذيتها الى المفاعل (٣) بواسطة ناقل حركة لولبي (screw) (٢) الذي يسمح باختياركمية تدفق التغذية من المخلفات الى المفاعل .

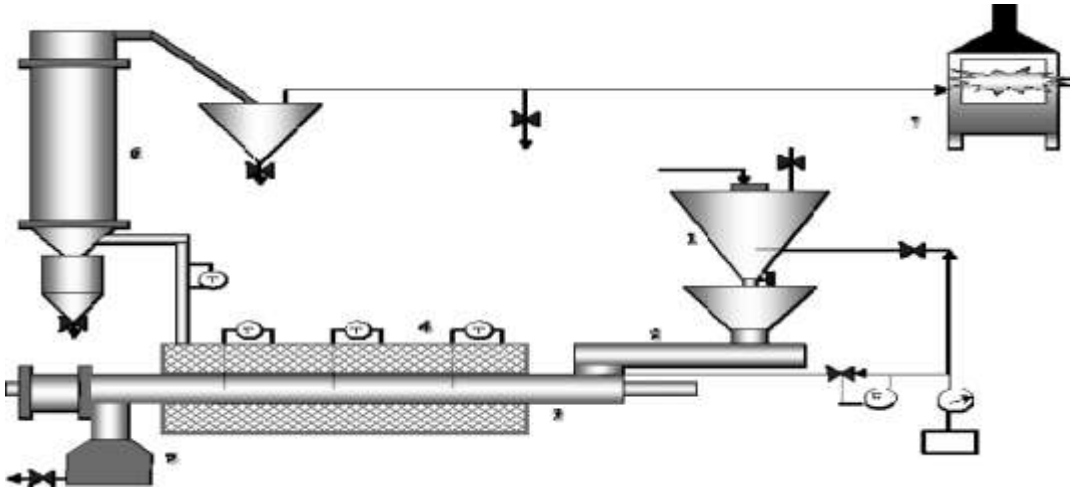

الشكل (٣) منظومة ريادية لمفاعل متحرك الحشوة.

المفاعل عبارة عن ناقل حركة لولبي محاط بسخان كهربائي (٤) وذلك لتجهيز الحرارة اللازمة للتفاعل الماص للحرارة .

ان نظام التسخين مقسم الى ثلاث مناطق ومجهز بمحرار نوع K-type للوصول الى افضل سيطرة على درجة حرارة المفاعل . ان قطع المخلفات تتحرك داخل المفاعل وفي نفس الوقت تتفكك الى غازات مع بقاء جزء من المادة الصلبة .

الجزء الصلب المتبقي يترك المفاعل بواسطة الجاذبية حيث يسقط الى نظام جمع المادة الصلبة واستخلاصها اثناء اجراء التجربة .ان الغاز الناتج من المفاعل يصل الى المكثف بواسطة تيارات الحمل بمساعدة الغاز الحامل (N_2) .ان نظام التكثيف (٦) يتكون من مكثف نوع (Shell and Tube) بعكس التيار Counter Current حيث يحتوي على ماء يتم تدويره في جزء ال(shell) على اعتباره سائل تبريد .

جزء السائل المتكثف ينزل الى داخل الانبوبة بواسطة الجاذبية ويجمع في وعاء خاص تحت المكثف .ان الجزء غير المتكثف من الغاز يتم تغذيته الى مشعل رقم (٧) قبل وصوله الى الجو .

لقد اجريت خمس تجارب في ظروف متشابهة لتحديد انتاجية هذه العملية .تم اختبار تغذية ثابتة حوالي ٦ كغم / ساعة ادخلت الى المفاعل لمدة اربع ساعات . الكمية المناسبة للانحلال الحراري تمت بدرجة ٦٠٠ م^{o} وبمعدل تدفق ١,٢ كغم / ساعة لتر نتروجين /دقيقة .

٤- التركيب الكيمياوي للاطارات

المكونات الاساسية للاطار هي:

- مطاط صناعي
- مطاط طبيعي
- الكبريت والمركبات الكبريتية
- رمل (سليكا)
- راتنج فينولك
- زيت اروماتي نفثاليني، بارافينك
- كتان، بوليستر، نايلون، الخ
- شمع نفط
- اصباغ اوكسيد الزنك ثنائي اوكسيد التيتانيوم ..الخ
- اسود الكاربون
- حوامض شحمية (Fatty acid)
- مواد خاملة
- شرائط حديد

التركيب النوعي الوزني

هذه القوائم لاصناف المواد الداخلة في تصنيع الاطارات وبنسب وزنية الى الوزن الكلي للاطار

٥- تهيئة المواد لعملية الانحلال الحراري

قبل معالجة مخلفات الاطارات في الوحدة الرئيسية ،هنالك خطوة لتهيئة المادة الداخلة وتتضمن تقطيع shredding الاطارات المستهلكة الى قطع صغيرة وازالة شرائط الحديد والنسيج منها

بعد التقطيع وادخال المادة الى وحدة الفاصل المغناطسي اذا كان يتألف من مرحلة واحدة تكون كفاءة ازالة شرائط الحديد تصل الى ٩٥,٦%من وزن الشرائط اما اذا كانت تزال بمرحلتين من الفاصل المغناطيسي فأن كفاءة الازالة تصل الى ٩٩,٨٦% نسبة وزنية للشرائط الاصلية .

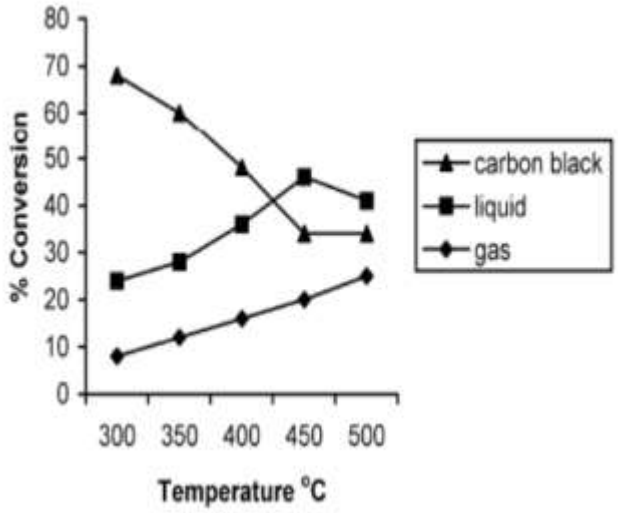

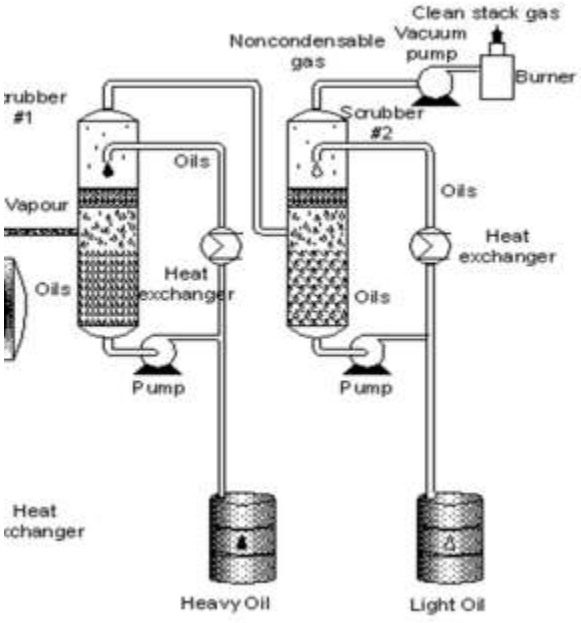

الشكل (٥) يوضح منظومة لانتاج الزيت البايروليكي بنوعيه الخفيف والثقيل

الزيت الثقيل، الزيت الخفيف يتم تكثيفهما خلال وحدتين متعاقبتين (Successive Scrubbers). الانتاج النوعي كالاتي ٥٥% زيت، ٣٥% اسود الكاربون و١٠% غاز.

عند تسخين ١٠ غرام من قطع مخلفات الاطارات في مفاعل دفعي (Batch reactor) من الزجاج المقاوم للحرارة وبعد تسخين من درجة حرارة الغرفة الى الدرجة النهائية ٢٨٠ °م ، ٣٥٠°م و ٥٠٠°م لمدة ساعتين.

في البداية يكون جو المفاعل حاوي على الهواء. بعد التسخين وتفكيك المخلفات الى غازات. هذه الغازات الناتجة تمر عبر مصيدة (Trap) حيث يتم جمع الهيدروكاربونات السائلة. مايتم انتاجه يتم وزنه في كل تجربة وقياس نسبة انتاجه الى المادة الاصل. اما الجزء الغازي يتم حساب وزنه من الفروقات بين مجموع المادة الصلبة والمادة السائلة مطروحة من وزن المادة الاصل. الشكل رقم (٦) يوضح تأثير درجة الحرارة على انتاج كل من الغاز والسائل والمادة الصلبة. الشكل رقم (٦) يوضح تأثير درجة الحرارة

على انتاج كل من الغاز والسائل والمادة الصلبة.

٦- خط انتاج الزيت البايروليكي من الانحلال الحراري لمخلفات الاطارات على مستوى صناعي وتحت الضغط الاعتيادي.

يحتوي خط انتاج الزيت من الانحلال الحراري لمخلفات الاطارات عادة على خمس وحدات ثانوية الزامية وثلاثه وحدات ثانوية اختيارية.

- منظومة تقطيع الاطارات (اختيارية)
- منظومة انحلال حرارية ذات استمرارية
- منظومة انتاج اسود الكاربون (اختياريه)
- منظومة انتزاع الغاز القابل للاحتراق
- منظومة تنقية الغاز
- منظومة سيطرة
- منظومة تنقية الزيت وتحسين نوعيته (اختياري)

الانتاجية للمنتجات المختلفة من خط عملية الانحلال الحراري لمخلفات الاطارات تحت الضغط الطبيعي موضحة بالشكل رقم (٧)

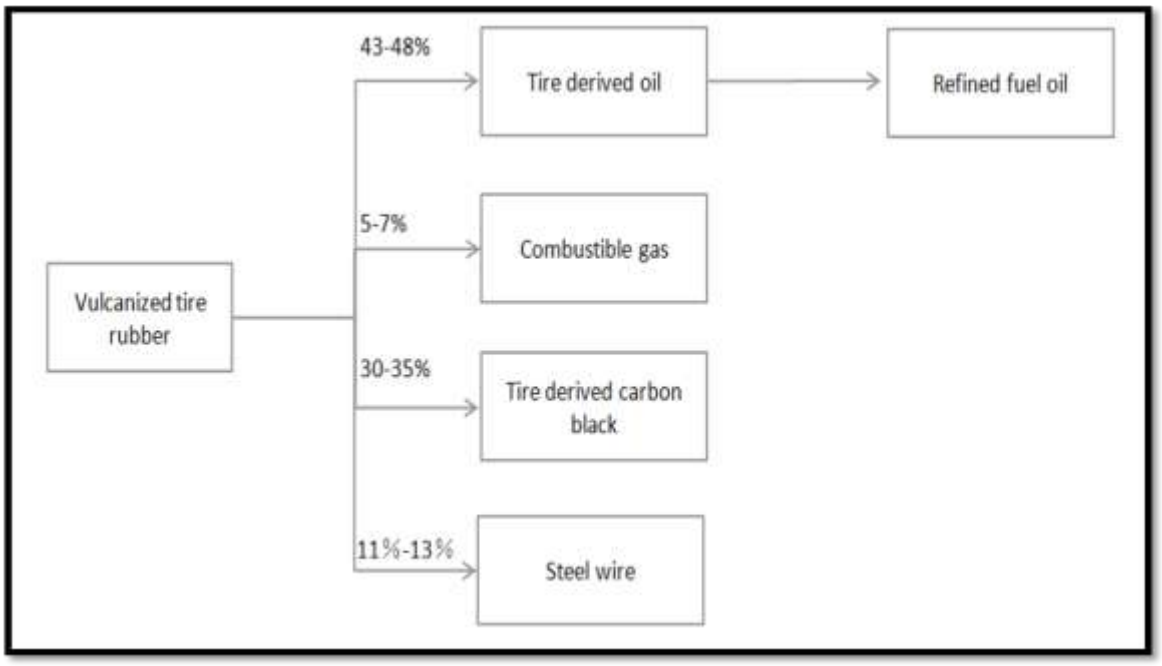

الشكل (٧) انتاجية الخطوط المختلفة

٧- خواص نواتج الانحلال الحراري

تقطير الزيت البايروليكي ينتج تقريبا ٢٠% نفثا خفيفة، ٦،٨% نفثا ثقيلة، ٣٠،٧% ناتج التقطير الوسطي و٤٢،٥% بقايا التقطيرالصلبة من الاسفل. البنزين، التولوين، زايلين ومركبات مشتقة من البانزين تتواجد بنسب متباينة في جزء النفثا. بالاضافة الى مواد كيمياوية مفيدة مثل مادة dl-limoene توجد بنسبة وزنية ١٥%.

الناتج الخفيف من النفثا البايروليكي تحتوي على نسبة عالية من الكبريت والماركبتين (Mercaptans) ومركبات نتروجينية اخرىناتجة عن التفكك للمواد المضافة لمادة الاطار كعامل مساعد للكبريت.

المستوى العالي نسبيا لمركبات الكبريت والنتروجينية والاوليفية وثنائية الاوليفية في الجزء الخفيف من النفثا البايروليكي يجعلها غير ملائمة للخروج مع الكازولين.

عمليات كيمياوية مطلوبة لتحويل مركبات الكازولين ذات القيمة العالية. مقارنه النفثا البايروليكة مع النفثا المشتقة من النفط بالطرق التجارية لتظهر ان الاولى كمركب اكثر تعقيدا من الثانية.

٨- معدات التحليل الكيمياوي:

لتحديد الصفات الفيزياوية والكيمياوية للمنتجات البايروليكية من غاز وسائل ومادة صلبة يستخدم:

جهاز التحليل غاز كروموتوغراف GC ، جهاز تحليل اطياف تحت الحمراء IR.

اجهزة قياس درجة الوميض والكثافة واللزوجة وغيرها من الخصائص الفيزياوية.

٩- تطبيقات حبيبات المطاط

هنالك طرق بديلة لتدوير الإطارات المستهلكة، وبسبب خاصية المطاط في امتصاص الأصوات والصدمات من الممكن التالي:

- استخدام الاطار بكامله كحواجز سلامة في منعطفات الطرق السريعة وحدود لمسار مضمار سباق .
- تقطيعها وخلطها مع الإسفلت لرص الشوارع .
- تقطيعها على شكل حبيبات وخلطها مع مادة لاصقة واستخدامها في تغطية أرضيات الملاعب.

١٠ - الاستنتاجات

الانحلال الحراري يمكن ان يحول الاطارات المستهلكة –التي تعتبر عادة مخلفات- الى تشكيلة من المنتجات المفيدة – الزيت البايروليكي واسود الكاربون وغاز الذي يطلق عليه الغاز الصناعي. الزيت ممكن تقطيره وفصله الى اجزاء مختلفة وهي النفثا والزيت بنوعيه الخفيف والثقيل وبقايا التقطير الثقيلة. كل هذه المنتجات لها قيمة تجارية. من خلال التجارب العديدة التي اجريت وجد انه مهما تغيرت خواص الناتج النهائي للزيت ، الا انه سيكون له نفس التاثير الحراري لما يناظره من مشتقات نفطية. هنالك فقط اختلاف في سلوك المنتج من ناحية التدفق ومرونة الانتقال داخل الانابيب وهذا يعتمد بشكل مباشر على ظروف اجراء عملية الانحلال الحراري. الاختيار الامثل للعملية ومايليها من عمليات تحسين المنتج له اثر كبير في ايصال اداءه الى ذلك من النوع التجاري. بالاضافة الى ذلك ممكن الاستفادة من مادة اسود الكاربون كفلر (مادة مالئة) يخلط مع الاسفلت.القيمة التجارية للمنتوجات تجعل الانحلال الحراري عملية واعدة في معالجة المخلفات الصلبة من الناحيتين كونها اقتصادية وصديقة للبيئة.

References:

Chen, D. T.; Perman, C. A.; Riechert, M. E. & Hoven, J. (١٩٩٥). Depolymerization of tire and natural rubber using supercritical fluids. Journal of Hazardous Materials. No. ٤٤, pp. ٥٣-٦٠, ISSN ٠٣٠٤-٣٨٩٤

E. Aylo´n, A. Ferna´ndez-Colino, M. V. Navarro, R. Murillo,* T. Garcı´a, and A. M. Mastral, "Waste Tire Pyrolysis: Comparison between Fixed Bed Reactor and Moving Bed Reactor" Instituto de Carboquı´mica, CSIC, M Luesma Castan ٤, ٥٠٠١٨-Zaragoza, Spain

Fang He, Weiming Yi and Xueyuan Bai, Investigation on caloric requirement of biomass pyrolysis using TG–DSC analyzer, Energy Conversion and Management, Volume ٤٧, Issues ١٥-١٦, September ٢٠٠٦, Pages ٢٤٦١-٢٤٦٩

Nobeyuki Itoh. Waste Tire Recycling Plant Producing High-Performance Activated Carbon. Available from: http://www.p٢pay s org/ref/١١/١٠٥٠٤/html/biblio/htmls/pyh ١.htm Accessed: ٢٠٠٧-٠٤-١٢

Sangdo, P. & Earnest, F. G. (١٩٩٧). Statistical study of the liquefaction of used rubber tyre in supercritical water. Fuel. Vol.٧٦, No. ١١/١٩٩٧, pp. ٩٩٩-١٠٠٣,ISSN٠٠١٦-٢٣٦١

Tukachinsky, A.; Schworm, D. & Isayev, A. I. (١٩٩٦). Devulcanization of waste tire rubber by powerful ultrasound. Rubber Chem Tech. Vol. ١. No. ٦٩/١٩٩٦ pp. ١٠٤-١١٤, ISSN ٠٠٣٥-٩٤٧٥

of William P.T, "The pyrolysis of automotive tire waste", Journal of the Energy, ١٩٩٥, vol ٦٨]

استخراج غاز الميثان كوقود لتوليد الطاقة الكهربائية من ترسبات المياه الثقيلة بعد المعالجة : لمحيط بغداد

وديان هادي عبد الامير

مدرس مساعد/ قسم الهندسة الكهربائية/كلية الهندسة/الجامعة المستنصرية

الملخص:

في هذا البحث سوفنولي اهتماماعلىمصدر جديدللطاقة المتجددةفي توليد الطاقةالكهربائية، وبالتالي فإن مصادرالطاقةلم تعدمحدودة بعد الآن .غاز الميثان المستخرج منمياه الصرف الصحي CH_4.سيكونالمصدر الرئيسي للطاقةلتوليد الكهرباء .الفكرة الرئيسيةمنالبحث هيبناءمحطة للطاقةتعتمد علىغاز الميثانكوقودطبيعي .و اجراء مقارنة كالتي بين عدد السكان وانبعاث الغازات وانبعاث الغازات مقدرة الطاقة المولدة، فإن زيادة انبعاثات غاز الميثان يزداد بزيادة عدد السكان وقدرة التوليد أيضا سترتفع وسوف تقل التكلفة.

الرموز:

أ. Ch_4غاز الميثان
ب. Kw/hr كيلو واط على ساعة
ت. TS الفضلات الصلبة
ث. ICE مولد الاحتراق الداخلي

١. المقدمة:

كانت الناس تستخدم الغاز الحيوي لأكثر من ٢٠٠ عاما .في الأيام التي سبقت الكهرباء، وكانت تحصل على الغازالحيوي من أنابيب الصرف الصحي تحت الأرض في لندن وأستخدم للانارة مصابيح الشوارع، والتي كانت تعرف باسم "أضواء الغاز." في أجزاء كثيرة من العالم، يتم استخدام الغاز الحيوي للحرارة وإضاءة المنازل، لطهي الطعام، و حتى إلى وقود الحافلات .يتم جمعها من مصادر واسعة النطاق مثل مدافن النفايات وحظائر الخنازير، ومن خلال النظم المحلية أو المجتمع الصغيرة في العديد من القرى .[١] .بالتالي فالطاقة المتجددة في الوقت الحاضر ممكن تصبح مصدر رئيسي لتوليد الطاقة الكهربائية .كما الطاقة المتجددة يمكن أن تاخذ العديد من المجالات، مثل الطاقة الشمسية وطاقة الرياح، وطاقة الوقودالحيويوهذه الطاقةأيضا يمكن تقسيمها إلى أنواع كثيرة، يمكن أن تقسم الى عدة وجوه لتوليد الطاقة من مصادر طبيعية مختلفة، غاز الميثان يمكن أن ينتج من خلال عدة طرق، من قبل تخمير

فضلات الحيوانات أو استخدام المخلفات الزراعية واخيرا المخلفات البشرية[٢].لتوليد غاز الميثان على المراحل الكيميائية المطبقة على النفايات، كالنفايات البلدية، وحمأة مياه الصرف الصحي بعد المعالجة، وهذه العملية استخدمت من قبل العديد من البلدان ونجحت بجمع غاز الميثان واستخدامه كوقود لتوليد الطاقة الكهربائية٣] .، .[٤طبقت الفكرة وأعطى نتائج جيدة خاصة في البلدان المتقدمة أولئك الذين يحتاجون إلى الطاقة في أقل تكلفة وأقل من التلوث .الآن نريد بناء هذا النوع من المحطة في بلدان أخرى لديهم المصدر الرئيسي للطاقة مثل النفط ولكن لديهم مشاكل داخلية كثيرة تتعلق توليد الطاقة مثل العراق ونحن سوف نسلط الضوءعلى غاز الميثان المتولد من حمأة مياه الصرف الصحي التي تم جمعها من محطات معالجة المياه العادمة بعد عملية المعالجة.موقع محطات معالجة مياه الصرف الصحي موزعة على نهر دجلة .وفي الجانب الشرقي من بغداد وخاصة محطتى الرستمية والتوسيع الثالث ممكن ان تكون المكان الامثل للانشاء المحطة الكهربائية .الفكرة تعتمد على بناء محطة توليد للكهرباء تساهم في حل مشاكل التوليد للطاقة الكهربائية في بغداد، والتي تفسر في القسم التالي.

٢. الفكرة الرئيسية:

تعتمد فكرة المشروع على تركيب هاضم اللاهوائي الحيوي مع قدرة استخراج الغاز الحيوي في محطة معالجة مياه الصرف الصحي العضوية الحالية لعلاج الغالبية العظمى من المحتوى العضوي للتحلل في مياه الصرف .بعد هذه المعالجة الأولية الحمأة انتاج وجمع في الهاضم، لتنفيذ التخمير .سيتم استخدام الغاز الحيوي المستخرج لتوليد الكهرباء .وبالتالي فإن نشاط المشروع يقلل من كمية CH_4 المبددة في الغلاف الجوي .من خلال الاستفادة أيضا من الغاز الحيوي لإنتاج الكهرباء للشبكة، بدلا من حرق وCH_4، سيسهم المشروع أيضا إلى تشريد استهلاك الكهرباء، وكذلك الحد من انبعاثات غازات المظرة وبالتالي تقليل التلوث البيئي [٥].شروط التطبيق كالتالي:

- نظام معالجة مياه الصرف الصحي القائمة هو نظام الهاضمات اللاهوائية.
- يستخدم غاز الميثان المستخرج لتوليد الكهرباء. [٦]

في الجزء التالي سوف نناقش بإيجاز المعالم الهامة وحسابات غاز الميثان الناتج عن الجانب الشرقي من مدينة بغداد.

أ. محطة توليد الكهرباء في الموقع المقترح

الفكرة الرئيسية لبدء بناء محطة الغاز الحيوي، تبدأ من اختيار المنطقة مثالية لمحطة توليد الكهرباء والمدينة المختارة لتطبيق هذا المشروع بغداد في العاصمة العراقية، ومحطة معالجة مياه الصرف الصحي ذكر موقعها على الخريطة في الجانب الشرقي

من مدينة. وسيكون المكان المثالي لبدء بناء محطة للطاقة بعد عمليات معالجة مياه الصرف الصحي. سيتم جمع الحمأة في الهاضم، (الهاضم هو استخدام خزان ضخم لهضم الحمأة وتوليد غاز الميثان).

Figure ١. Satellite map for east Baghdad wastewater plant

ب. التصميم الرئيسي لمحطة الكهرباء

وتنقسم محطة توليد الكهرباء إلى ثلاثة أجزاء وهي:

- مدخلات نظام الحمأة للهاضم، وكمية الحمأة تعتمد على عدد الهاضمات للحماة او مخلفات المياة الثقيلة بعد المعالجة(sludge).
- نظام اسطوانات جمع الغاز.
- محطة توليد الطاقة معداتها تكون مشابهة لمحطة الكهرباء الغازية مع استخدام مولد استهلاك الداخلي (ICE). [٧].

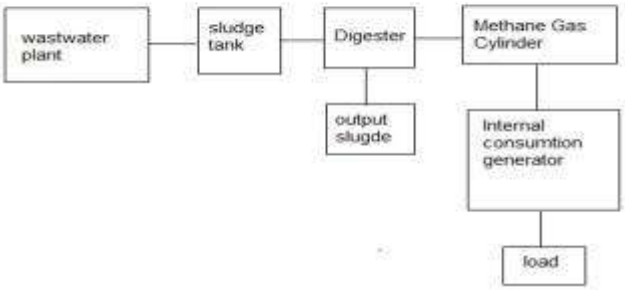

Figure.٢. Power plant design diagram

٣. حسابات انبعاث غاز الميثان من مخلفات المياه الثقيلة بعد المعالجة لمتوسط الفرد لليوم الواحد

انبعاث غاز الميثان الناتج بعد هضم الحمأة مع الزيادة سوف يحسب عدد السكان في هذه المعادلة المذكورة في المعلومات الواردة أدناه:

- ٠,٥ كيلوغرام للنفايات الإنسان في اليوم الواحد. [٧].
- عدد السكان
- درجة الحرارة العادية (C٣٠٠) الغاز الحيوي التي تم الحصول عليها من النفايات البشرية ٠,٣٦٥ M٣ / كغ
- قيمة TS من النفايات البشرية = ٢٠٪

لذلك، بلغ مجموع الغاز الحيوي التي تم الحصول عليها من ن عدد الأشخاص = (٠,٥ × ١٠٥ × ٠,٢ × ٠,٣٦٥) = ٣,٨٣٢٥ m^3 لعدد السكان الأول في الجدول أدناه وسوف حسابات يكون نفسه فقط سيزيد من عدد من الأشخاص.

Table .١.

Methane gas Emission related to Population

No.	Population Number	Gas Emission in (m^3)
١	١٠٥ person	٣,٨
٢	٤٦٨ person	١٧
٣	١٠٠٠ person	٣٦,٥
٤	١٠٠٠٠ person	٣٦٥
٥	٥٠٠٠٠ person	١٨٢٥
٦	١٠٠٠٠٠٠ person	٣٦٥٠٠

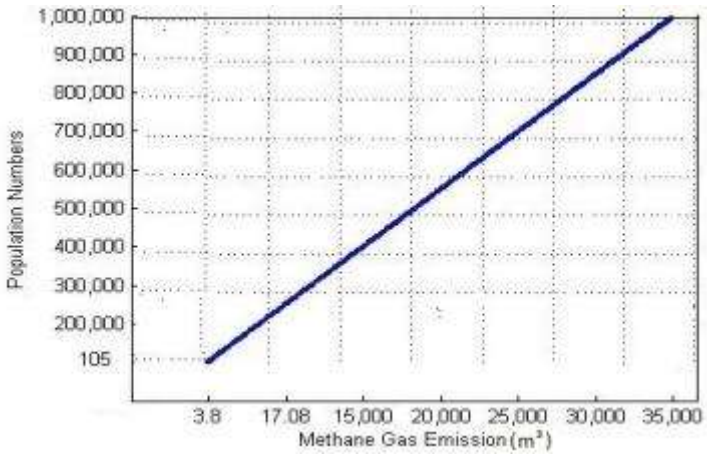

Figure.٣. Methane Gas Emission Per Population

٤. الطاقة الكهربائية المحسوبة بكيلو واط ساعة مقارنة با انبعاث حجم غاز الميثان المستخرج من عملية التخمير

حساباانتاج الطاقةفيساعةواحدة فان انبعاث غاز الميثانفييوم واحدموجود فيالجدول فيالجزء التالي :من كل مترمكعبللغاز الحيوينحصل على١,٤كيلوواط في الساعة.[٨]

Table .٢.

Electric power output related to Methane Emission

No.	Electric Power in kw/hr	Gas Emission in (m^3)
١	٥,٣	٣,٨
٢	٢٣,٨	١٧
٣	٥١	٣٦,٥

٤	٥١١	٣٦٥
٥	٢٥٥٥	١٨٢٥
٦	٥١١٠٠	٣٦٥٠٠

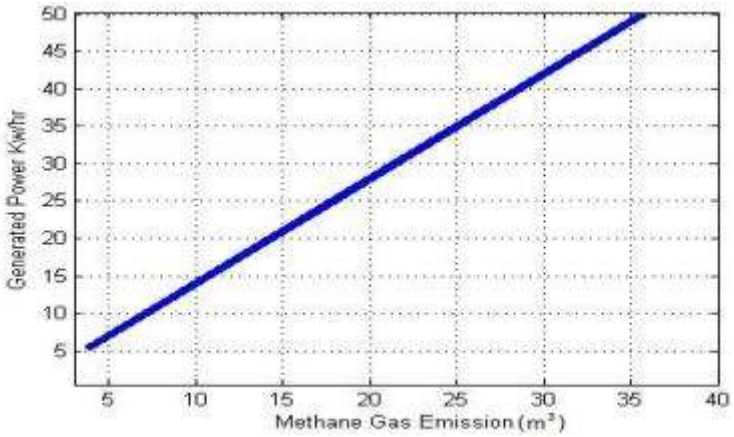

Figure.٤. Electric Power Per Methane Gas Emission

٥. الخاتمة

المشروع يناقش قدرة بناء محطة توليد الطاقة تعتمد على الغاز الطبيعي .(CH_4)انها ولدت من تخمير النفايات البشرية، ثم من الحسابات اكتشفنا أن العلاقة بين عدد السكان مع انبعاث غاز الميثان المتعلقة بالطاقة المتولدة في يوم واحد سوف تكون في حالة تزايد مباشر.

REFERENCES

[١]. Asif Ahsan, Shahriar Ahmed Chowdhury, Feasibility Study of Utilizing Biogas from Urban Waste, United International University, Dhaka, Bangladesh.

[٢]. VLADIMIR LAPCIK, MARTALAPCIKOVA, BIOGAS STATTIONS AND THEIR ENVIRONMENTAL IMPACTS, Technical University of Ostrava, Czech Republic ٢٠١١.

[٣]. Mansour-Al sadi, Design and Building of Biogas Digester for Organic Materials Gained From Solid Waste, ٢٠١٠.

[٤]. Mustafa ErenErsahin, Hale Ozgun, RecepKaanDereli and IzzetOzturk, Istanbul Technical University, Turkey.

[٥]. [Forced Methane extraction from organic wast-water treatment plants for grid-connected electricity supply, AM٠٠١٣/version ٠١, September ٢٠٠٤, htt://cdm.unfccc.int

[٦]. [Forced Methane extraction from organic waste-water treatment plants for grid-connected electricity supply and/or heat Production, May, ٢٠٠٥, http://cdm.unfccc.int/

[٧]. Muhammad BaqerMollah,Design and cost Analysis of Biogas Based Power Plant for Commercial Usage: Bangladesh Perspective, International Islamic University Chittagong, Bangladesh ٢٠١١ IEEE.

[٨]. [Online: October: ٢٠١١] Final Assessment Report: Landfill Biogas Recovery and Utilization;

AL- Muhandis

Scientific Refereed Journal Published by The Iraqi Sosiety of Engineers

Special Issue of The First Scientific Conference on Renewable Energies to Ensure a Better Environment (part 3)

Volume 153,Number 3
ISSN 2413 - 0230

September - 2016
Email: jmise@ise-iq.org

Sixty one year
The Second Issue
September - 2016
All Correspondence Should be on
the e-mail of the Journal
jmise@ise-iq.org
Iraq - Baghdad - Hay Al-Nedhal
103 Dist. - 30 St. - 5 Bldg.

Al-Muhandis Journal

Issued by
Iraqi Society of Engineers
Annual Subscriptions for

Institutions	100.000 ID.
Engineers	60.000 ID.
I.S.E. Members	40.000 ID.
Universities Students	40.000 ID.

Quarterly jour. Deposite No. at the National Library in Baghdad, 510, 1983 Registered by Mail Department No. 56

Forward

There is a direct relationship between population, urbanization and engineering science. During the last 100 years, the world population has grown from 1.5 to 6 billion (may be more) and then enormous needs of human requirements should be satisfied through multidisciplinary engineering topics.

This journal is designed to reflect current developments and advances being made in the general fields of engineering and engineering technology. The word engineering is interpreted in a wide sense, including (not limited) Architectural, Civil, Electrical, Mechanical, Production and manufacturing, Control and Systems, Mechatronics, Chemical, Petroleum and Metallurgy.

The journal has within the above context several specific objectives. It wants to foster a better understanding of engineering issues, provide a forum for unusual and unconventional solutions, the development of low cost energy saving systems and bridge the gap between materials science, engineering performance, environmental effects, field behavior, design, and service life of engineering products.

We know that these topics will continue to develop and we welcome the new and innovative research works and papers that the engineering industry will inevitably evolve.

AL-Muhandis Ed.Board

Iraqi Society of Engineers Founded in1938

Administrative Board 2016

President : Consultant Eng. Falih Kadhim Zayer

Vice President: Consultant Eng . Wahhab Rezooqi Al Murieb

Secretary : Consultant Eng. Sabah Abdul Ridha Al-Jazaieri

Treasurer : Eng. Mohammed Farooq Abdulkhaleq

Members : Professor Dr. Mudhafar Ali Aljabiri
Consultant Eng. Abdullah Dhari Al-Ameri
Consultant Eng. Munim Salih Al-Sab'e
Consultant Eng. Faleh Khedher Aljofy
Consultant Eng. Falah Hasan Almaroof
Consultant Eng. Abdulamir Sabri Kadhum
Consultant Eng. Riadh Ketab Hussain
Eng. Hassanien Mohamed Hassan

Editorial Board

Head : Professor Dr. Mudhafar A. Aljabiri
Editorial Director : Assistant Professor Dr. Maan Salman Hassan
Editorial Secretary: Lecturer Dr. Zainab B. Mohammed
Members : Professor Dr. Najdat Nashat Abdullah
Professor Maher K. Mahmood Al Azawi
Professor Dr. Mohammed Z. Al Faiz
Professor Dr. Rasulcon M. Khalaf
Assistant Professor Dr. Sameera M. Hamdullah
Assistant Professor Dr. Naseer A. Al Habobi
Lecturer Dr. Furat Ebrahim Hassan

Iraqi Society of Engineers:

Administration: 07702526721 – 07901471621

Journal: 07901151092

P.O Box: 18429

Email: Jmise@ise-iq.org
info@ise-iq.org
www.ise-iq.org

instructions for authors

1- **The Kind of Letters should be (Times New Roman) foe English manuscripts, and (Arabic Transparent) for Arabic manuscripts.**
2- **The four margins of the page should be 4cm.**
3- **The header and footer should be 3cm.**
4- **The title font should be bold and in size (14). It should be placed above the abstract in English & Arabic. The subtitles should be without numbering and underlining. For English manuscripts the font should be bold and in size (12).**
5- **Manuscript font in English should be typed bold, and in size (11), and it should be typed bold, and in font (12) for Arabic manuscripts.**
6- **Researcher name should be typed in font (12), with asterisk above the last name. When the authors are more than one, Their names should be typed in one line, with enough space, between each name, and asterisk at the first left name, If they are affiliated the same institution, if they are not the asterisk should be placed above the last name of each author.**
7- **The paper should be typed in two columns each column of 6 cm, with 1cm space between each one. The number of lines should be not less than (42) line, (this not included the abstract, figures, and tables).**
8- **For Arabic manuscripts, an asterisk should be placed at the bottom of the right column margin, refers to the authors work place and his email, if there is. The asterisk should be placed at the bottom of the left column margin, for English margins.**
9- **The Keywords should be placed at the bottom of the abstract, for both English and Arabic manuscripts.**
10- **The title should be write on the right column for Arabic manuscripts, and on the left column for English manuscripts (within the page margin). The following item is not belong to the author, when he/she writes the journal, the volume and the number at the apposite direction, where the title is written.**
11- **References should be arranged as they are mentioned in the manuscripts (its number should be in square brackets). Each reference should be described as following:**
   a. **The books: Authors surname, other names or the first letter, a dot should be placed between the author and the other. It should be in capital letter, followed by the publishers name and the year of publications.**
   b. **The papers and articles: The author name should be written as in (a), the first letter should be in capital letter. The article title should be placed between (" "), then (the journal name, volume, number, pages, and year), they should be separated by commas.**

Iraqi Society of Engineers

Held

The First Conference for

Ensure a Better Environment

with Renewable Energy

In Co operation with

Baghdad Provincial Council

Co sponsored

Iraqi Universities

State, Private Companies and NGOs

December 9 - 10 / 2015

Palestine Int. Hotel

Baghdad

Supreme Supervising Committee

Dr. Riyadh Nasir Al Adhadh	Chairman of Baghdad Governorate Council	President
Consultant Eng. Falih Kadhim Zayer	President of Iraqi Society of Engineers	Member
Prof. Dr. Ameen Daway Thamir	President of University of Technology	Member
Prof. Dr. Nabeel K. Abid Al-Sahib	President of Al-Nahrain University	Member
Assist. Prof. Dr. Majid H. Majeed	President of Middle Technical University	Member
Prof. Dr. Mohammed Ali Al-Anbari	Al-Mustansiriyha University/ Dean of College of Engineering	Member
Prof. Dr. Jassim Al-Dabbagh	Al-Nahrain University/ Dean of College of Engineering	Member
Prof. Dr. Mohammed Z. AL-Faiz	Al-Nahrain University/ Dean of College of Information Engineering	Member
Prof. Dr. Ahmed Abd Alsahib	Baghdad University/ Dean of College of Engineering	Member
Assist. Prof. Dr. Mohammed A. Atiya Al-Sarag	Baghdad University/ Dean of Al-Khwarizmi College of Enginering	Member
Assist. Prof. Dr. Kader Al-Sharaa	Dean of AL-Farabi University College	Member

Preparatory Committee

Consultant Eng. Falih Kadhim Zayer	President of Iraqi Society of Engineers	President
Assist. Prof. Dr. Alaa Abdul Hassan Atiyah	University of Technology/Vice President for Scientific Affairs	Member
Assist. Prof. Dr. Alaa Karim Mohammed	Baghdad University/ Al-Khwarizmi College of Engineering	Member
Assist. Prof. Dr. Amer Hassan Alhadad	Baghdad University/ College of Engineering	Member
Assist. Prof. Dr. Naseer Abood Al-Habobi	AL- Nahrain University/College of Engineering	Member
Assist. Lecturer Ahmed Salih Mahdi	Al-Mustansiriyha University/ College of Engineering	Member
Architect and Academic Mowaffaq Al-Taai	Iraqi Society of Engineers	Member
Consultant Eng. Wahhab Rezooqi AL Murieb	Iraqi Society of Engineers	Member
Consultant Eng. Munim Salih Al-Sab'e	Iraqi Society of Engineers	Member
Eng. Hassanien Mohammed Hassan	Iraqi Society of Engineers	Member

Scientific Committee

Prof. Dr. Hussien yousif Mahmood	Baghdad University/ College of Engineering	President
Prof. Dr. Mudhafar Ali Aljabiri	Iraq Society of Engineers	Member
Prof. Dr. Nada Mahdi Fawzi	Baghdad University/ College of Engineering	Member
Dr. Mudheher Sadeq Sabea AL-Tameemi	Ministry of Industry and Minerals	Member
Assist. Prof. Dr. Abd Al jabar Nema Kalifa	AL-Nahrain University / Vice President for Scientific affairs	Member
Assist. Prof. Dr. Dhary yousif Mahmood	Technology University/ President of Electricity Engineering	Member
Assist. Prof. Dr. Ali H. Al Hamadani	Technology University/ Manger of Energy Technical Center	Member
Assist. Prof. Dr. Ahmed Qasem Mohammed	Middle Technical University/ Engineering Technical College	Member
Assist. Prof. Dr. Nasser Ahmed Al Aoad	AL-Mustansiriyha University/ College of Engineerin	Member
Lecturer. Dr. Ameel Mohammed Rahman	Baghdad University/ AL-Khwarizmi College of Engineerig	Member
Lecturer. Dr. Wael Rashed Abdul Majeed	Baghdad University/ AL-Khwarizmi College of Engineering	Member
Lecturer. Dr. Shatha Abass Hassan	Baghdad University/ College of Engineering	Member
Assist. Prof. Dr. Lubna Abd Aljabar AL-Zubaidi	AL-Mustansiriyah University/ College of Engineering	Member

Contents Issue

English Section Research **Page No.**

Design and Implementation of Smart Traffic light **7**

Mohammed Ehsan Safi **Dr. Eyad I. Abbas**

Increase Efficiency of Photovoltaic Module by Using a Reflectors **20**

Sarmid.Shakir.Abdulsattar **Emad.Jaleel.Mahdi**
Yasir.Shakir.Abdulsattar **Asmaa.Hassan.M**

Prepare a map for the number of hours of electricity **31**

Rawnak A. Abdulwahab **Firas H. Abdulrazaq** **Sura T. Nassir**

Study the Effect of Rotating Disk Base Temperature on Steam **41**

Dr. Ali Al Assadi **Dr. Akram W. Ezzat** **Dr. Ayser Muneer**

Wastewater treatment by UV **54**

Assistant prof Seroor Atallah Khaleefa Ali

Preliminary investigation study of wind energy at Tuz–Khormatu in Iraq **71**

Samah Shyaa Oudah **Mohammed A. Salah**

Design and construction of battery (Deep cycle) specially **81**

Dr. jaafar Ali Al-anbary

Selecting of Renewable Effective Adsorbent for Treating **101**

Ahmed Hassoon Ali

Design and Implementation of Smart Traffic light with Self- Solar Cell Powered Feeding

Mohammed Ehsan Safi
mohammed.ehsan@ymail.com
Mobile: 07700083709

Dr. Eyad I. Abbas
eyad_electdep@yahoo.com
Mobile:07709297560

Department of electrical Engineering- University of Technology

Baghdad- Iraq

Abstract

The increase of population produces an increase of the number of automobiles on the road, which generates heavy traffic in the streets and that causes many problems for the Citizens and traffic policemen an additional two emergency cases therefore it's important with development technology of embedded systems to solve this problem. In this paper new traffic light controller was designed and built to optimization using the Arduino UNO microcontroller board with self-powered solar cell feeding. The system tries to reduce traffic jams, caused by constant timer traffic lights. The system contains ultrasonic sensors on the side of the roads. Also the system contains switches to control the traffic light manually. The ultrasonic sensor system gets activated when vehicles go along the road against it. Microcontroller controls the traffic light by driver circuit using the sensor network to determine the level of jam in the road. Different ranges of traffic light delay time intervals according to jam level are configured by microcontroller and updated regularly. The jam level displayer tool is another feature added to a system controlled by the microcontroller which is a traffic sign informs the drivers about the level of jam before reaching the road.

Keywords: Microcontroller, ultrasonic sensor, and solar cell

تصميم وبناء اشارة المرور الذكية ذات تغذية قدرة ذاتية من الخلايا الشمسية

محمد احسان صافي د. اياد ابراهيم عباس

الخلاصة

ان زيادة السكان نتج عنه زيادة في عدد المركبات والذي يولد حركة المرور الكثيفة في الشوارع والتي تسبب العديد من المشاكل للمواطنين ورجال شرطة المرور إضافة لحالات الطوارئ وبالتالي فإنه من المهم مع تطور التكنولوجيا في الأنظمة المدمجة حل هذه المشكلة .في هذه الورقة تم تصميم وبناء متحكم ذكي لغرض تحسين الاداء للاشارة المرورية باستخدام لوحة المتحكم الدقيق اردوينو انو وبتغذية قدرة ذاتية من الخلايا الشمسية. النظام يحاول التقليل من الزحام المروري الناتج عن الاشارة المرورية ذات التوقيت الثابت. النظام يستند على المتحكم الدقيق، والذي يمثل العقل للنظام.النظام يحتوي على متحسسات فوق الصوتية على جوانب الطريق.ايضا يحتوي النظام مفاتيح كهربائية للتحكم بالاشارة المرورية يدويا.الحساسات فوق الصوتية تتفعل عندما تمر المركبات على الطريق من امامها. المتحكم الدقيق يتحكم بدائرة قيادة اشارة المرور باستخدام شبكة من المتحسسات لحساب مستوى الزحام في الطريق: بالنتيجة المتحكم الدقيق ياخذ القرار بتحديث زمن التاخير للشارة المرورية. المتحكم الدقيق يعرف مستويات مختلفة من التاخير للاشارة المرورية ويقوم بتحديثها وفقا لمستوى الازدحام. اداة عرض مستوى الازدحام هي ميزة اضافية تضاف للنظام يسيطر عليها من قبل المسيطر الدقيق وهي اشارة مرورية تعلم السائقين بمستوى الازدحام قبل الوصول للطريق.

1. Introduction

The increase of jam produces many losses of countries resources because of the looseness of petrol, exhaustion of automobiles', and lateness of employers, in addition to fatigue for both the Citizens and traffic policemen. Many problems with the ordinary traffic light controller, heavy jam is the most important problem because of never configure the level of jam in each way and set the delay time. Another problem represents when there is no jam, but the waiting still continues. The solution

for these problems is to determine the level of jam and set the delay time. In addition to delay time problems there is problem representing of emergency cars, like the ambulance, police, and fire brigade. This problem need of evaluation of the traffic policeman, then there is need for manual control of the traffic light. The traffic jam can reduce if the driver has the information about the level of the crowd in the road before reach it and takes another way.

The aim of this work is to propose system provide solution for all above problems with minimum cost and self-powered feeding.

A large number of approaches are presented to minimize the problems of the traffic light jams, bellow a literature survey for some solution in the last few years:

- Ganiyu R. A., 2014 [1] introduced a traffic light control system; the design consists of the microcontroller, and light emitting diode (LED). The sensing unit is designed utilizing a pressure switch which will sense the weight of any car that steps on it. When the pressure switch is pushed, a logic one is applied on the microcontroller to inform the control unit that there is car at that particular node. The system was designed to sample all the lanes in turn to detect whether there is an automobile on any lane and this action added a period of 15sec to the delay time by the microcontroller which is configuring the traffic light action.
- Sachin Jaiswal, 2013 [2] presented control system consist of microcontroller, IR sensors, in line of sight configuration across the loads to detect the density at the traffic signal, and for VIP automobile RF transmitters are installed on it while the receivers installed on traffic light control circuit to control the state of the traffic light. Three levels of jam and delays are defined high, medium, low density.
- Rashid Hussian, 2013 [3] presents system of Intelligent Traffic Routing using a Wireless Sensor Networks. The Wireless sensor network technology is used to sense presence of Traffic near any node and then able to route the Traffic based on density in the desired road. The system uses microcontroller with the Wireless sensor for Traffic management.

- A. Ms Promila Sinhmar, 2012 [4] propose multiple traffic light control and monitoring system. The system is based on microcontroller. The system contains IR sensors are mounted on the sides of roads respectively. The IR sensors network sense the vehicle passed through it. Microcontroller controls the IR system and counts the number of vehicles passing on the road. The vehicles count are stored in microcontroller memory. Based on a different vehicle count, the microcontroller takes decision and updates the traffic light delays as a result. Administrator sitting on the computer can command system (microcontroller) to down-load recorded data, update light delays, erase memory, etc. Thus administrator of a central station computer can access traffic conditions on any approachable traffic lights and nearby roads to reduce traffic congestions to an extent.

Shilpa S. Chavan, 2009 [5] introduced Intelligent Traffic Light Controller, which consist of infrared sensor mounted on the road to detect the vehicles, this acts as an input to the ITLC unit. This input signal indicates the length of vehicles on each road. The controller generates output signals for Red, Green and Orange Signal and monitors their timings, taking into consideration the length of vehicles on each road. The same information is transmitted to the mobile user which will request for congestion status. If a vehicle driver at junction sends SMS on GSM mobile phone to ITLC unit, the driver will get a message indicting congestion status of the road. The microcontroller that used is AT89c51.

2. Proposed System

The proposed scheme, as depicted in figure (1), consists of processing unit presented by the microcontroller which control all the process in the system, ultrasonic sensors' that determine the level of jam in the road, switch to switch between the manual mode and auto mode, manual control switches to control the traffic light manually by Traffic policeman, the traffic light circuit, and the jams level displayer.

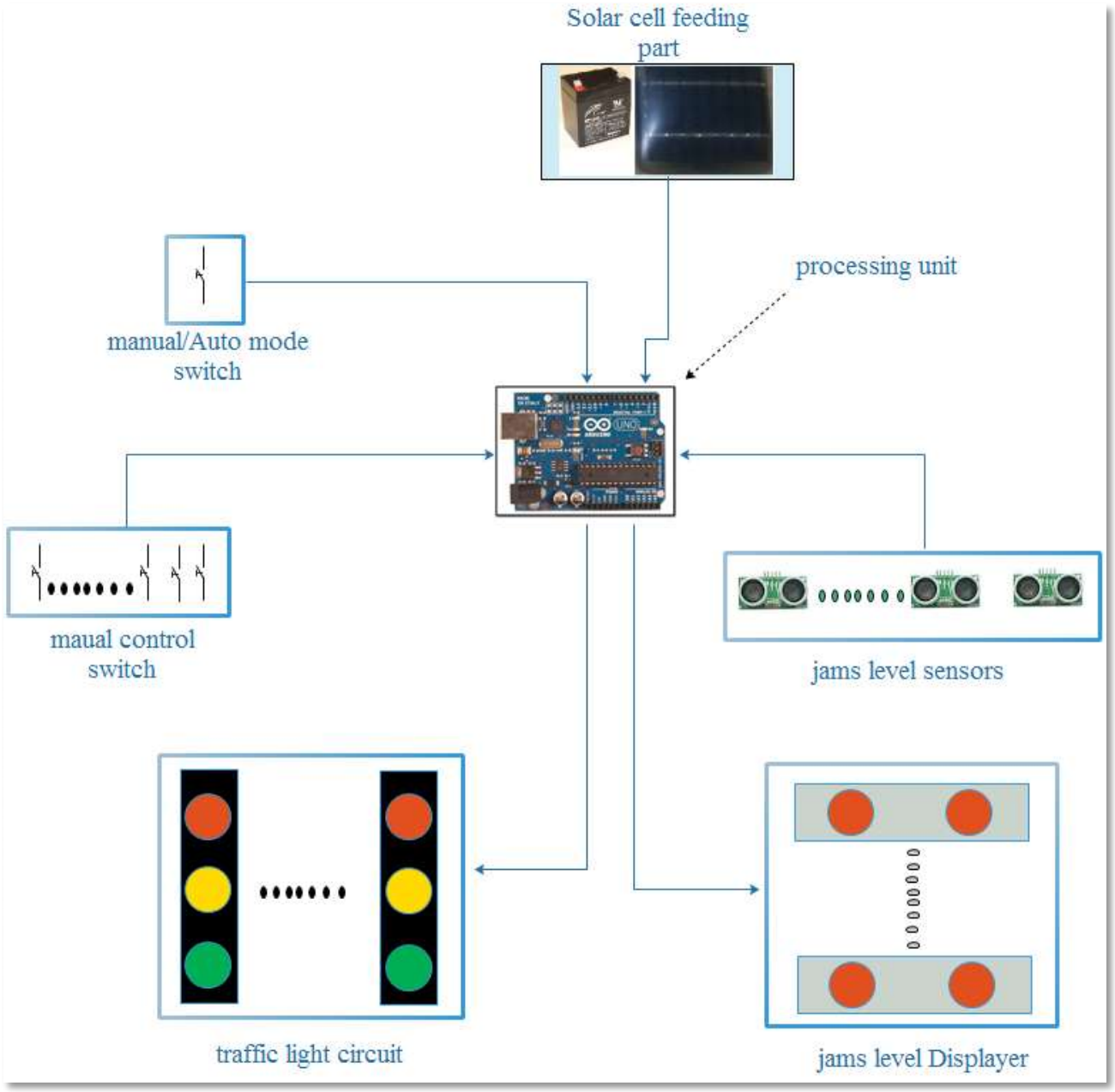

Figure (1): The proposed system organization

2.1 Driver Circuit

Driver circuit was constructed to link up the microcontroller board to drive high power consumption real traffic light and jam level Displayer circuit. The driver circuit as depicted in Figure (2) consists of (ULN2803) chip and relays to supply the force needed to get to the sign on.

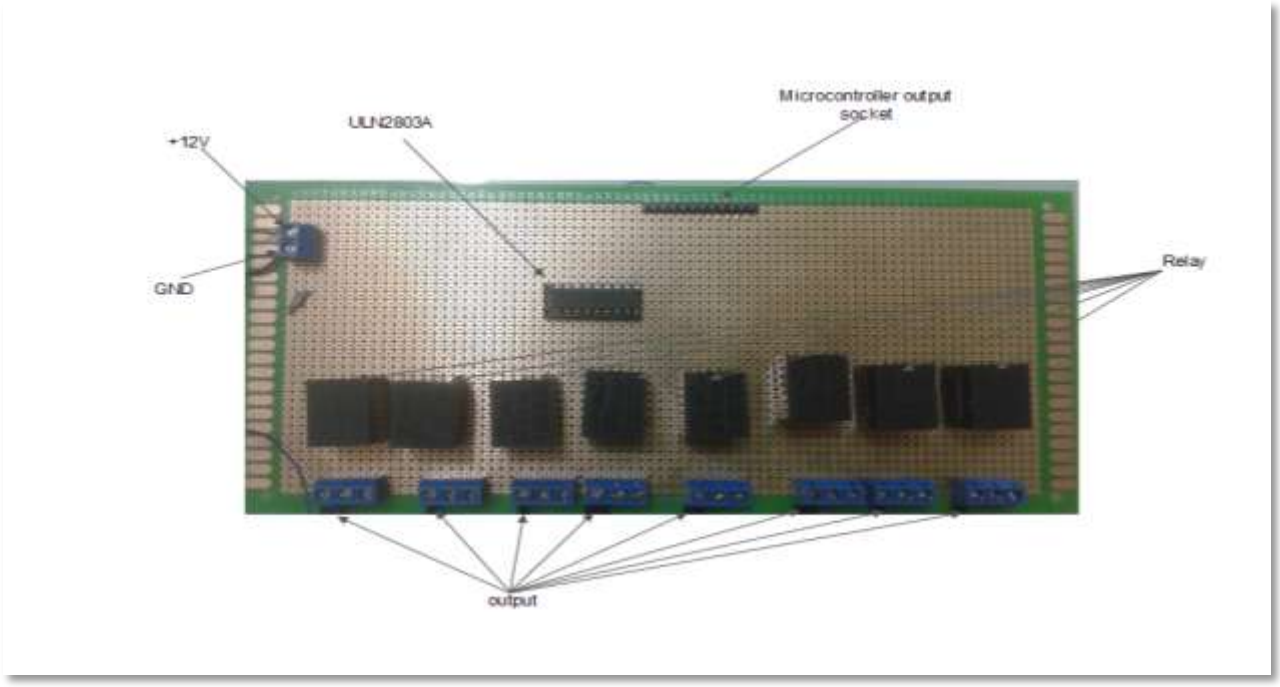

Figure (2): Driver circuit

The ULN2803A is a high-potential, high-current Darlington transistor array. The device consists of eight NPN Darlington pairs that feature high-voltage outputs with common-cathode clamp diodes for switching inductive loads. The collector-current valuation of each Darlington pair is 500mA as seen Figure (3) [6].

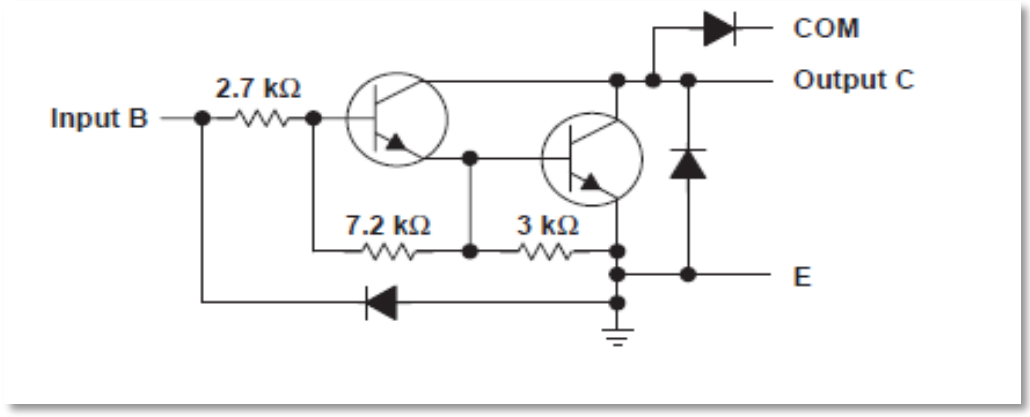

Figure (3): each Darlington pair in ULN2803

The outputs of (ULN2803A) connected to relays which provide the power needed to drive traffic light and jam level Displayer circuit.

3. Procedure of the Proposed System

The proposed system consists of two modes the manual mode and the auto mode adjusted by a manual / auto switch. When the system work in the manual mode the traffic light work according to user (traffic policeman) choices using the manual control switches this mode is important, especially in the emergency that the user evaluate like a police car or ambulance, while the system be in the auto mode is determine the delay time of the traffic light according the sensors in the road by processing unit (microcontroller). The processing unit determines which road has more jam and gives it more delay time for green signal to reduce the crowd, but at the same time isn't determining the level of jam in the other road and give it the delay according to that level.

Jams level displayer is a sign like a traffic light, but it’s located before the road to inform the drivers the level of jam in the road so they decide to take this road or not this tool can reduce the jam too in a simple way. Jams level displayer can made like loading bar or like the street arrows that indicate to the locations its connected to processing unit that evaluate the level of jam in the roads, a flowchart of the proposed system is shown in the Figure (4).

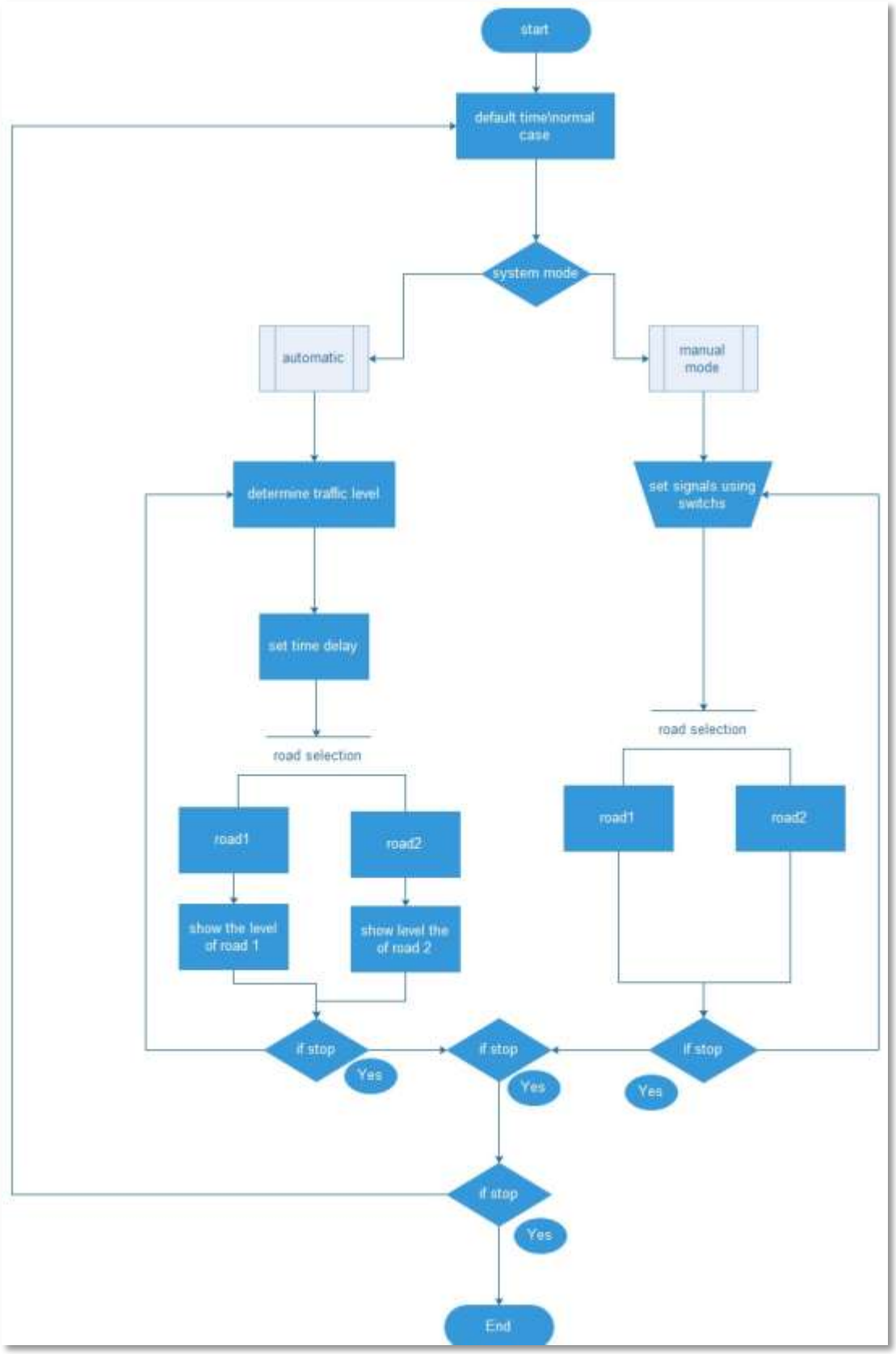

Figure (4): Flow chart of proposed system

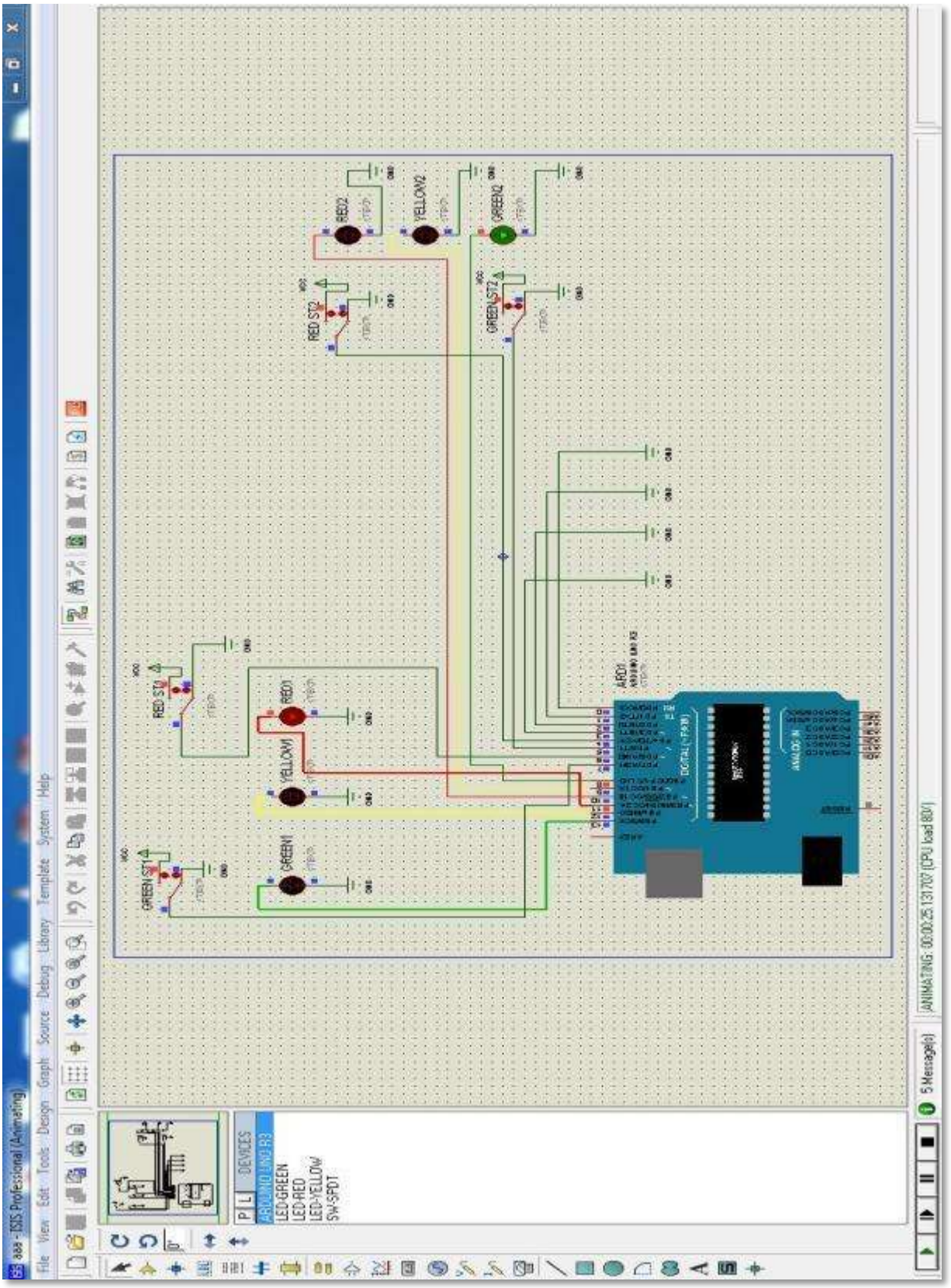

Figure (5): simulation using Proteus program

4. Practical Model and Simulation Results

After design the proposed system its simulated using Proteus program, as show in figure (5).

And so the program loaded to microcontroller through the bootloader of Arduino microcontroller kit and finally the practical control system model was constructed, as shown in figure (6).

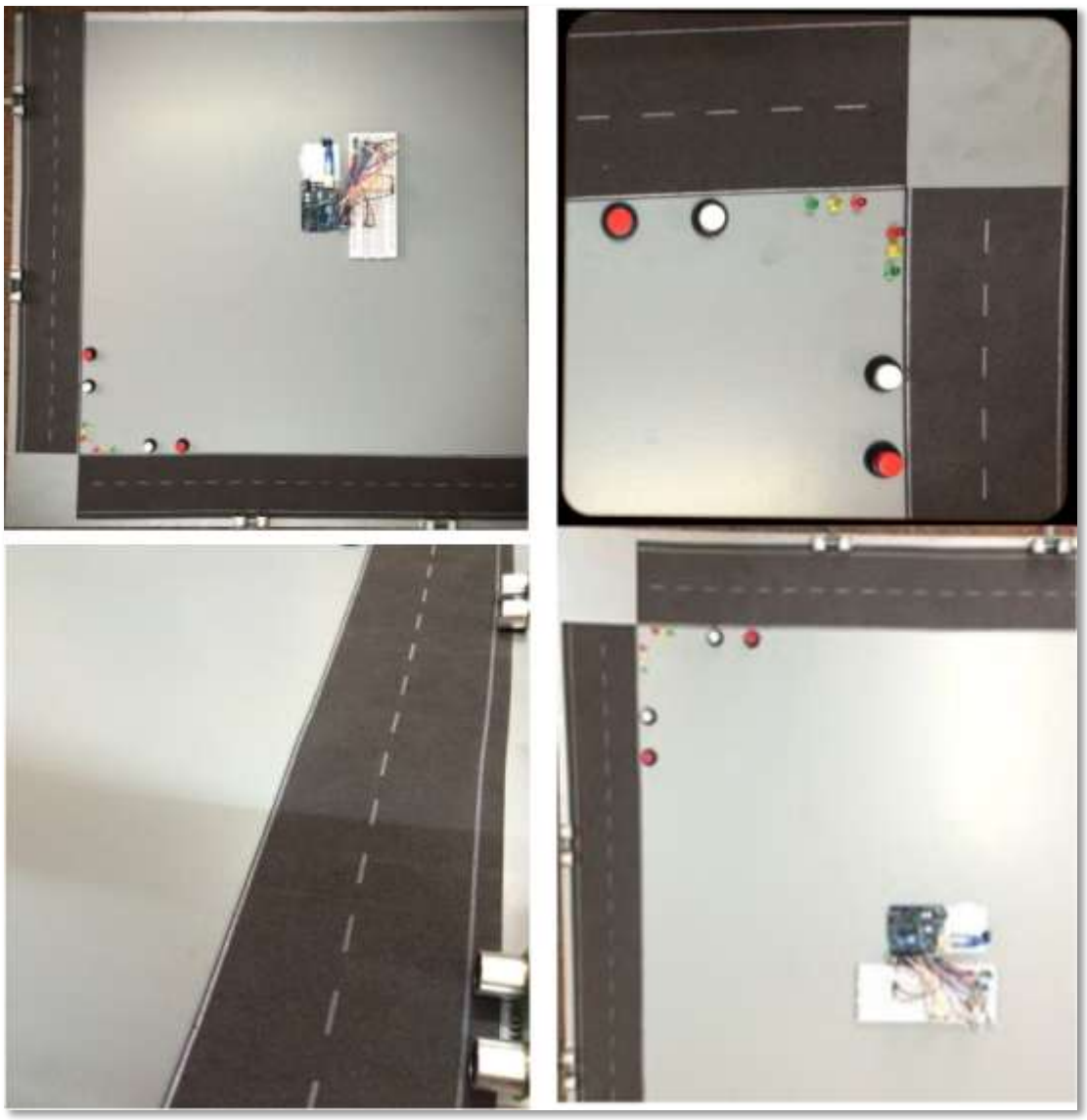

Figure (6): The practical control system model

5. Solar Cell Feeding Part

The power supply of the proposed system mainly depends on the solar power, to make the system more reliable, independent and electricity saving. The solar cell feeding part, as show in figure(7), consists of PV panel provide 7volt and 5w [7], which is the source of power in the system. 7805 IC regulator connects to the panel to convert the voltage from 7 volts to 5 volts [8], and 4.8 battery used to supply the system when the solarcell stop working at the night, while it's charging at the normal mode. Rectifier diode used to protect the panel from reverse current generated by battery when the panel be in the offline mode.

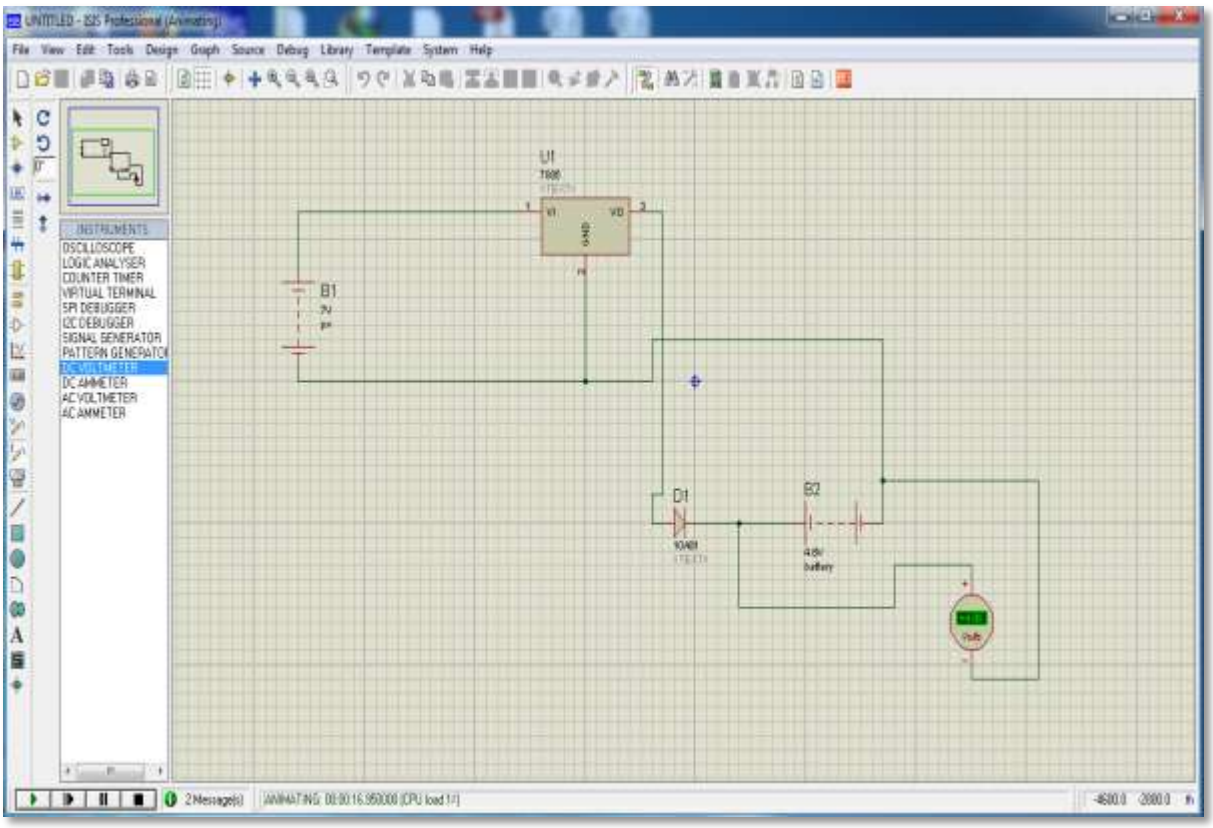

Figure (7): Solar cell feeding circuit

The practical circuit of the Solar cell feeding part show in Figure(8) below :

Figure (8): Practical Solar cell feeding circuit

6. Conclusions

This system solves the problems of crowds on the roads in the present and future using smart traffic light with self-powered feeding from solar cell. The use of The Arduino microcontroller with ArduinoC and solar cell, provide a suitable platform for implementing an embedded control system to meet our future requirements easily and quickly.

7. References

[1] Ganiyu R. A., Arulogun O. T., **"Development Of A Microcontroller-Based Traffic Light System For Road Intersection Control"**, International Journal of Science & Technology Research, Volume 3, ISSUE 5, May 2014.

[2] Sachin Jaiswal,**"Intelligent Traffic Control Unit"**, International Journal of Electrical, Electronics and Computer Engineering, ISSN No. (Online): 2277-2626, 2013.

[3] Rashid Hussian,**" WSN Applications: Automated Intelligent Traffic Control System Using Sensors"**,International Journal of Soft Computing and Engineering, Volume-3, Issue-3, July 2013.

[4] A. Ms Promila Sinhmar, **" INTELLIGENT TRAFFIC LIGHT AND DENSITY CONTROL USING IR SENSORS AND MICROCONTROLLER",** International Journal of Advanced Technology & Engineering Research, VOLUME 2, ISSUE 2, MARCH 2012.

[5] Shilpa S. Chavan, **"Assessment DESIGN OF INTELLIGENT TRAFFIC LIGHT CONTROLLER USING EMBEDDED SYSTEM"**, Second International Conference on Emerging Trends in Engineering and Technology, 2009.

[6] Texas Instruments Incorporated, **"ULN2803A"**, 2006.

[7] http://www.carmanah.com

[8] http://www.alldatasheet.com

Increase Efficiency of Photovoltaic Module by Using a Reflectors

Sarmid.Shakir.Abdulsattar Emad.Jaleel.Mahdi Yasir.Shakir.Abdulsattar Asmaa.Hassan.Moslim

Abstract:-

The known all over the world the efficiency of Photovoltaic module (PV) is too much low compare with other renewable energy devices, for example: concentration solar power (CSP), wind turbine, and biomass efficiencies. The cost per watt for PV module is too much high comparing with cost per watt of the electric power for local diesel generators or private gasoline generator.

In this research use two axis solar tracker system that move into two direction X and Y; this system have two PV modules, the first one has reflectors and the second doesn't has reflectors.

This study focus on the first case that consist of PV module has two reflector mirrors fixed on each sides, and by make a suitable calibration on the angles between reflectors and the module obtain the maximum output power; so that the finding of this research is increase the efficiency for individual PV module by increasing the output power thereby the cost of PV system will reduce.

Introduction:-

PV Cell is an electrical device that convert the sunlight to electricity without moving any part and don't emit harmful pollution [1], many PV cells connected in series and in parallel to obtained the desire power that's called PV module; by connecting the last one in series and parallel to create what's called PV array, also repeat the same connection to obtained what's called PV system.

The tracker system is a mechanic devise using with PV module to increase it's efficiency.

In the other word this system utilize the solar radiation for the whole day, it's able the PV module to be perpendicular on the sunlight during the day, otherwise the steeper motors consume some energy from PV modules in order to move this system.

This study indicate the economic side and the increment in the out power by using two reflectors for each PV modules, each one has the same dimension of the module;

this system able to reduce the number of PV modules per system that has the same output power compare with another PV tracker system without reflectors.

Methodology:-

1- Three PV modules was used, two of them tracker system one with reflectors, and the other without reflectors, also the third one is fixed without reflectors oriented to the south with tilt angle of 33°.

2- These two reflectors on both sides for the individual PV module was connected.

3- Tracker system two axis was used that connected with battery 12V, 7Ah.

4- Fluke multimeter was used to measure the output power for each quarter hour (9:00 am to 1:30 pm) .

5- Solar power meter was used to measure the solar radiation.

6- Several probability was made to obtain the optimum reflector's angle, so that the optimum angle between reflector and PV module was 116º; the site was in Baghdad (latitude = 33.33N and longitude = 44.24E) .

Results and Discussion:-

Figure (1) shows the practical part of the research, each PV module has one solar power meter fix under each one.

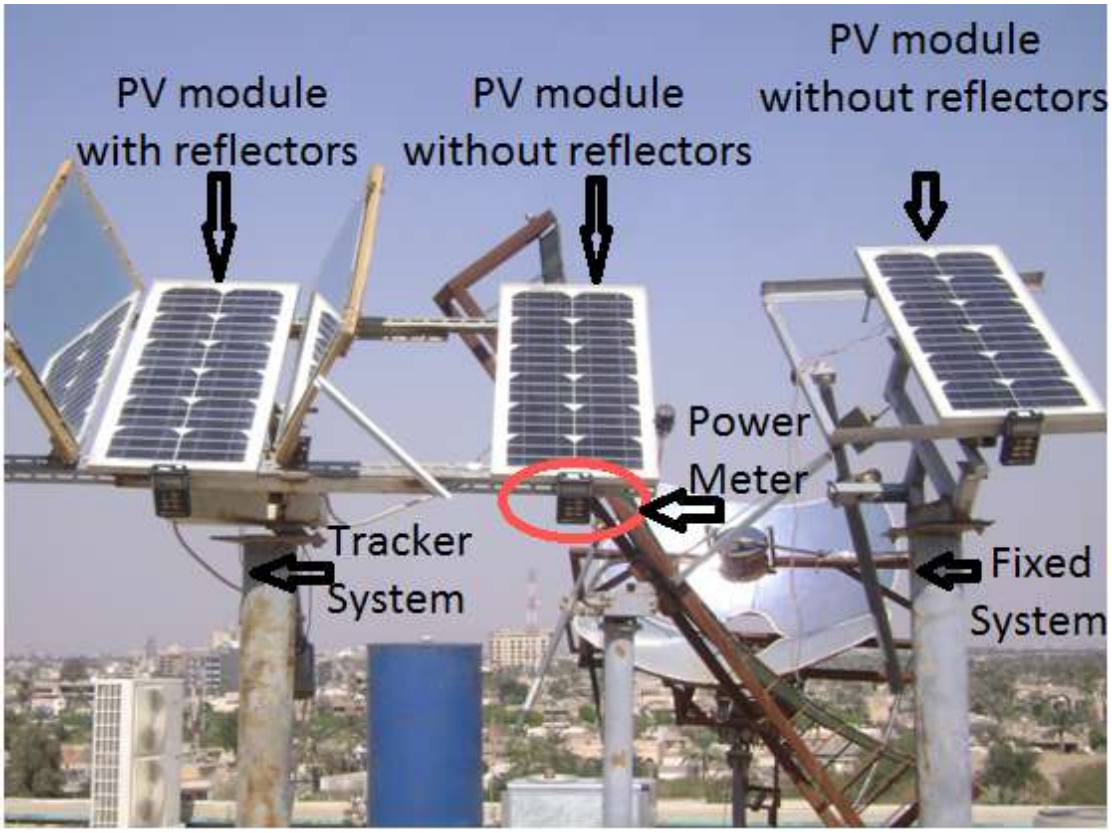

Figure 1: Three PV modules, one of them fixed and the others tracker system.

The comparison will be between two PV modules that have a tracker system one with reflectors, and the other without reflectors; so the finding of output current for the first one indicate in the table A (index A).

These results plot in the diagram (1):

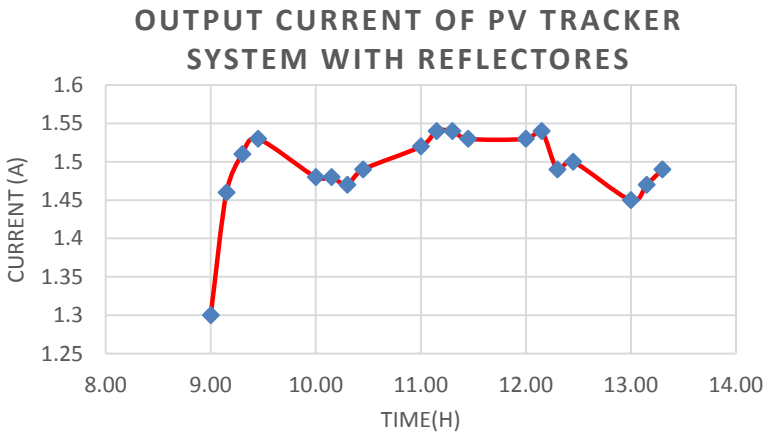

Diagram 1: The output current of PV tracker system with reflectors.

Also the finding of output current for the second one indicate in the table B (Index B).

These results plot in the diagram (2):

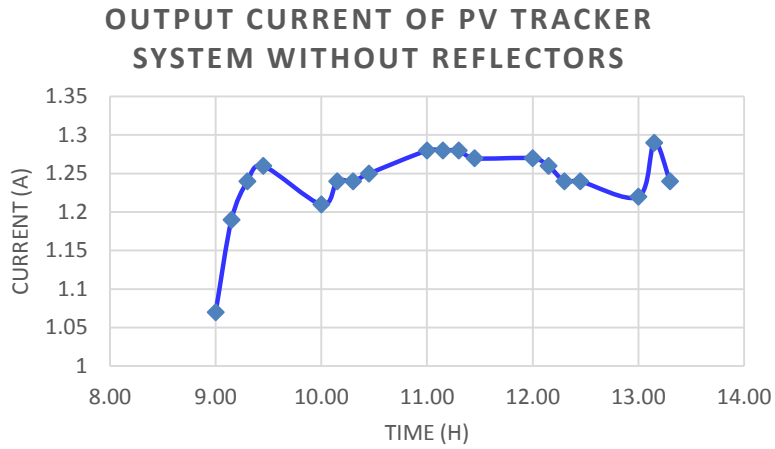

Diagram 2: The output current of PV tracker system without reflectors

Otherwise the output current from the third PV module (fixed without reflectors) indicate in the table C (Index C).

These results plot in the diagram (3):

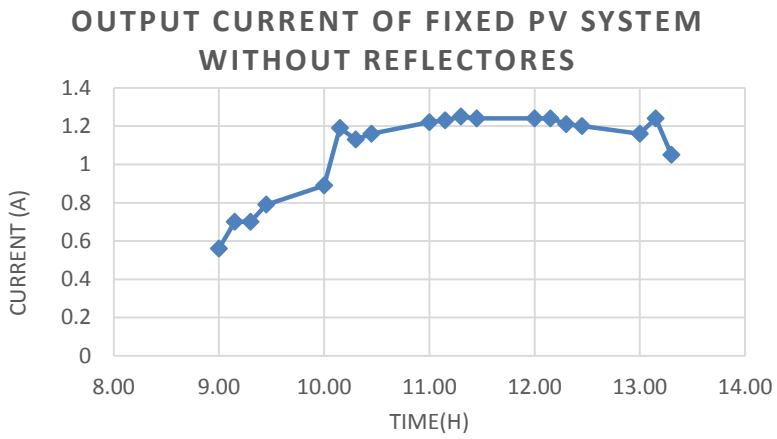

Diagram 3: The output current of fixed PV system without reflectors.

Diagram (4) shows comparison between two tracker system with and without reflectors, the blue curve indicate the output current of PV tracker system without reflectors while the red curve indicate the PV output current with reflectors.

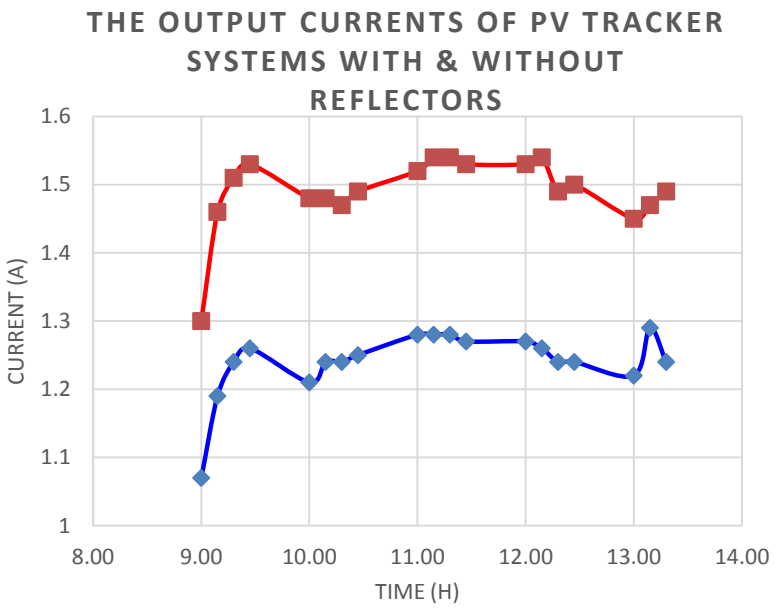

Diagram 4: The output current of PV tracker system with and without reflectors

Also diagram (5) shows the comparison between fixed (green curve) and both PV tracker system with (red curve) and without reflectors (blue curve).

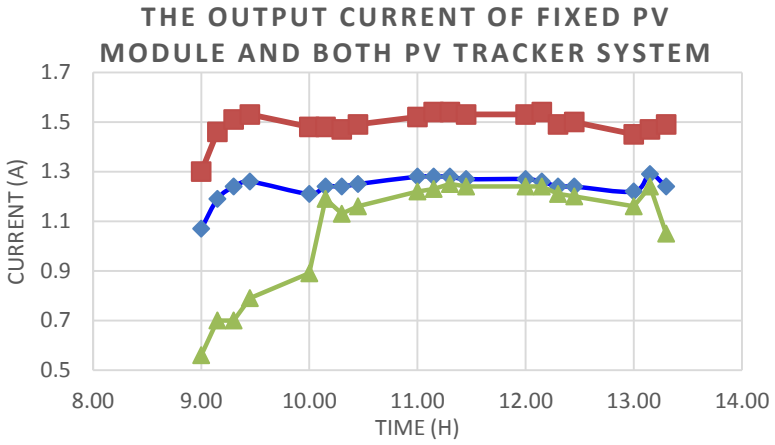

Diagram 5: The output current of fixed PV module and both PV tracker system with and without reflectors

The temperature play an important rule on the photovoltaic modules, that effect on the output voltage. The standard test condition (STC) indicate the typical operation for PV modules, the great voltage at 25 C, that means any increase or decrease in the temperature effect on the output voltage, this effect divided into two cases:

Case 1: when the temperature increase the output voltage decrease.

Case 2: when the temperature decrease the output voltage increase.

Table (4) indicate the difference between two PV tracker systems, one of them has reflectors and the other without reflectors.

Table 4: The voltage at maximum power for two PV modules with and without reflectors.

	without Reflectors	with Reflectors	Difference in Volt between Reflectors and without Reflectors
Time	**V**	**V**	**V**
9.00	**17.01**	**19.26**	2.25
9.15	**19.35**	**19.32**	-0.03
9.30	**19.19**	**19.08**	-0.11
9.45	**19.14**	**18.97**	-0.17
10.00	**19.37**	**19.35**	-0.02
10.15	**19.74**	**19.91**	0.17
10.30	**19.62**	**19.84**	0.22
10.45	**19.51**	**19.71**	0.2
11.00	**19.58**	**19.5**	-0.08
11.15	**19.46**	**19.73**	0.27
11.30	**19.2**	**19.36**	0.16
11.45	**18.97**	**19.06**	0.09
12.00	**18.74**	**18.76**	0.02
12.15	**18.79**	**18.84**	0.05
12.30	**18.98**	**19.02**	0.04
12.45	**19.07**	**19.19**	0.12
13.00	**18.76**	**18.78**	0.02
13.15	**19.04**	**18.91**	-0.13
13.30	**18.9**	**19.05**	0.15

As indicate from table (4), the variation in the output voltage between these two PV modules for the same solar radiation depends on the temperature that has a slightly change related to the wind speed.

At 9:00 o'clock table (4) shows that the high value of the voltage in PV module that has reflectors while the other has low value due to increase in the ratio of wind speed. The next values from 9:15 to 10:00 o'clock, the ratio of wind speed decrease, that cause increase in the voltage value for PV module that doesn't have reflectors.

The temperature of PV module that have reflectors increase due to receive more solar radiation than the other, so that the decreasing in wind speed cause hot region in the surface of PV module thereby cause decrease in the output voltage.

Conclusions:-

The finding of this research indicate the PV tracker system with reflectors increase by 6% compare with PV module without reflectors, and by 11% compare with fixed system as shown in figure 2.

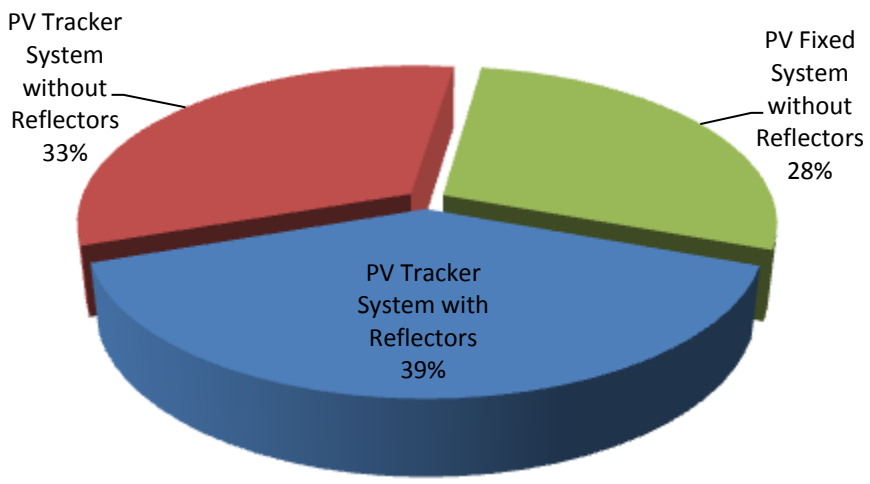

Figure 2: Increment percentage of three PV modules with and without reflectors

Also this result indicate the PV tracker system with reflectors increase the efficiency of PV module by increasing the output power thereby the PV tracker system without reflectors thereby the fixed system that keep the same efficiency (efficiency in the name plate of PV module).

The efficiency of this PV module doesn't written in the nameplate of this module, but in general the efficiency of mono-crystalline PV module ranging from 13.9% to 14.2% at standard test condition (air mass =1.5, solar radiation = 1000 W/m^2, cell temperature =25°) as shown in table 6 (index D), so let us assume the efficiency of this PV module is 14%; and by make some calculation, the efficiencies of these modules are obtain in table 5.

Table 5: New efficiencies of three PV modules with and without reflectors.

	PV Modules Categories	**Efficiencies**
A-	PV module tracker system with reflectors	**20.09%**
B-	PV module tracker system without reflectors	**16.66%**
C-	PV module fixed system without reflectors	**16.54%**

The values of these PV modules consider at noon (12pm) when I calculate the efficiencies, in that time the location of sun will be in the south that means the PV tracker system oriented to the south, and as I mention in the methodology the fixed PV module oriented to the south; that's why the second and third value become very closer in table 5.

Also as you note in the table 5 efficiency is 16.54%, and as I mention before the typical assumption efficiency is 14% (at solar radiation of 1000W/m^2) ; the difference of that back to the amount of solar radiation at noon (1248 W/m^2); see table (3) index C.

References:-

- Photovoltaic application, web: www.ncsun.ncsu.edu

Index A

Table A: Output power of PV tracker system with reflectors.

Time (h)	Power meter	Power = I V	Voltage (V)	Current (I)
9.00	1114	25.04	19.26	1.3
9.15	1220	28.21	19.32	1.46
9.30	1261	28.81	19.08	1.51
9.45	1264	29.02	18.97	1.53
10.00	1270	28.64	19.35	1.48
10.15	1268	29.47	19.91	1.48
10.30	1235	29.16	19.84	1.47
10.45	1258	29.37	19.71	1.49
11.00	1285	29.64	19.5	1.52
11.15	1294	30.38	19.73	1.54

11.30	1297	29.81	19.36	1.54
11.45	1291	29.16	19.06	1.53
12.00	1286	28.70	18.76	1.53
12.15	1283	29.01	18.84	1.54
12.30	1263	28.34	19.02	1.49
12.45	1272	28.79	19.19	1.5
13.00	1225	27.23	18.78	1.45
13.15	1282	27.80	18.91	1.47
13.30	1250	28.38	19.05	1.49

Index B

Table B: Output power of PV tracker system without reflectors.

Time (h)	Power meter	Power = I V	Voltage (V)	Current (I)
9.00	1082	18.20	17.01	1.07
9.15	1193	23.03	19.35	1.19
9.30	1234	23.80	19.19	1.24
9.45	1235	24.12	19.14	1.26
10.00	1240	23.44	19.37	1.21
10.15	1238	24.48	19.74	1.24
10.30	1203	24.33	19.62	1.24
10.45	1229	24.39	19.51	1.25
11.00	1255	25.06	19.58	1.28
11.15	1269	24.91	19.46	1.28

11.30	1271	24.58	19.2	1.28
11.45	1265	24.09	18.97	1.27
12.00	1259	23.80	18.74	1.27
12.15	1259	23.68	18.79	1.26
12.30	1240	23.54	18.98	1.24
12.45	1251	23.65	19.07	1.24
13.00	1260	22.89	18.76	1.22
13.15	1261	24.56	19.04	1.29
13.30	1229	23.44	18.9	1.24

Index C

Table 3: Output power of PV fixed system without reflectors.

Time (h)	Power meter	Power = I V	Voltage (V)	Current (I)
9.00	578.9	11.41	20.38	0.56
9.15	683.5	14.34	20.48	0.7
9.30	772.2	14.25	20.36	0.7
9.45	831.6	16.02	20.28	0.79
10.00	907.7	18.23	20.48	0.89
10.15	984.5	24.44	20.54	1.19
10.30	1110	23.10	20.44	1.13
10.45	1106	23.59	20.34	1.16
11.00	1216	24.92	20.43	1.22
11.15	1237	24.98	20.31	1.23

11.30	1252	25.05	20.04	1.25
11.45	1250	24.24	19.55	1.24
12.00	1248	23.63	19.06	1.24
12.15	1249	24.38	19.66	1.24
12.30	1220	24.02	19.85	1.21
12.45	1216	23.99	19.99	1.2
13.00	1226	22.76	19.62	1.16
13.15	1096	24.74	19.95	1.24
13.30	1095	20.84	19.85	1.05

Index D

Table 6: Electrical characteristic of PV module.

Cell technology	**Mono-crystalline**
Maximum power	**20 Wp**
Open circuit voltage (Voc)	**21.6 V**
Short circuit current (Isc)	**1.25 A**
Voltage at maximum power (Vmpp)	**17.2 V**
Current at maximum power (Impp)	**1.17 A**
Maximum system voltage	**DC 1000 V**
Power tolerance	**$^{+}_{-}$ 5%**

Prepare a map for the number of hours of electricity generation for different wind turbines in the province of Wasit – Iraq

Rawnak A. Abdulwahab, Firas H. Abdulrazaq, Sura T. Nassir

[1]Ministry of Science and Technology, Renewable Energy Directorate, Baghdad , Iraq.

Abstract

The aim of the proposed work is to Prepare a map which represent the number of hours of generate electricity power from wind energy by using different wind turbines at different hight in the province of Wasit, Iraq.

1.Introduction

Wind results from the movement of air due to change in temperature by san radiation which cause a difference in atmospheric pressure. Wind flows from regions of higher to lower pressure in an attempt to equalize imbalance in air pressure. Wind is characterized by its direction, speed, and gustiness.Because air is invisible, we cannot really see it. Rather, we see things being moved by it. Therefore, we can determine wind direction by watching the movement of objects as air passes them [1].

Winds on a surface weather map do not blow exactlyparallel to the isobars; instead, they cross the isobars,moving from higher to lower pressure. The angle atwhich the wind crosses the isobars varies, but averagesabout 30°. The reason for thisbehavior is friction [2].

For many decades thousands of small windmills, their arms spinning in a stiff breeze, have pumped water, sawed wood, and even supplemented the electrical needs of small farms. It was not until the energy crisis of the early 1970s, however, that we seriously considered wind-driven turbines, called wind turbines, to run generators that produce electricity [3].

Wind power seems an attractive way of producing energy, it is nonpolluting and, unlike solar power, is not restricted to daytime use. It does, however, pose some problems, as the cost of a single wind turbine can exceed 1$ million [4].

If the wind turbine is to produce electricity, there must be wind, not just any wind, but a flow of air neither too weak nor too strong. A slight breeze will not turn the blades, and a powerful wind gust could severely damage the machine. Thus, regions with the greatest potential for windgenerated power would have moderate, steady winds [5].

2- Area of study

The feasibility and applicability of wind energy development depends on the physical characteristics of the study area and the wind resource. The region is located in the area between Maysan and Wasit.

It is 112 km from Maysan, 85 km from Wasit, and about 220 km from Baghdad at position 32.77°N 46.70° E; Figure. 1 shows the location of chosen site in eastern region near the border between Iraq and Iran.

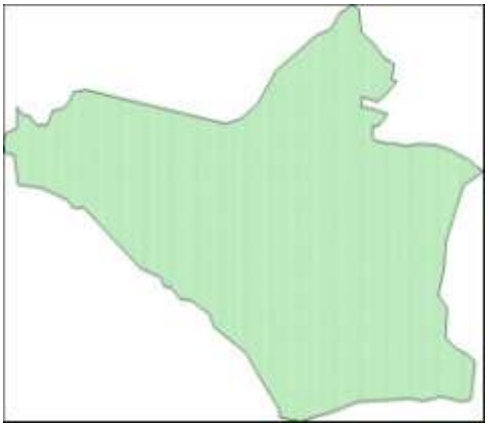

Figure(1). Shows the location of study in iraq

3- Geosun Map

Geosun map is wind resource map or wind energy map of Iraq at 3 heights above ground at high resolution (1 km x 1 km). The wind map is generated with the atmospheric Mesoscale model SKIRON and presented in Geographic Information System (GIS) format.

This map haveWind View allows users to view and query wind data in an interactive environment, as well as modifies, copy, and print maps.With the selected methodology it is possible to obtain virtual hourly datasets at any specified position and any height above ground level.

This study, allowed us to determine the optimum spatial resolution and the best input data to obtain hourly wind forecasts. In the case of wind energy assessment, this methodology allows us to get a wind velocity map, virtual wind series or wind power density map at any height above ground level.

From Geosun Map, it is plotedIraqi Wind map at height 50m in figure (2) and100 m in figure (3), which explained that the wasit site have higher amount of wind speed from (9-10)m/sec at height 100m and from (8-9)m/sec at height 50m.

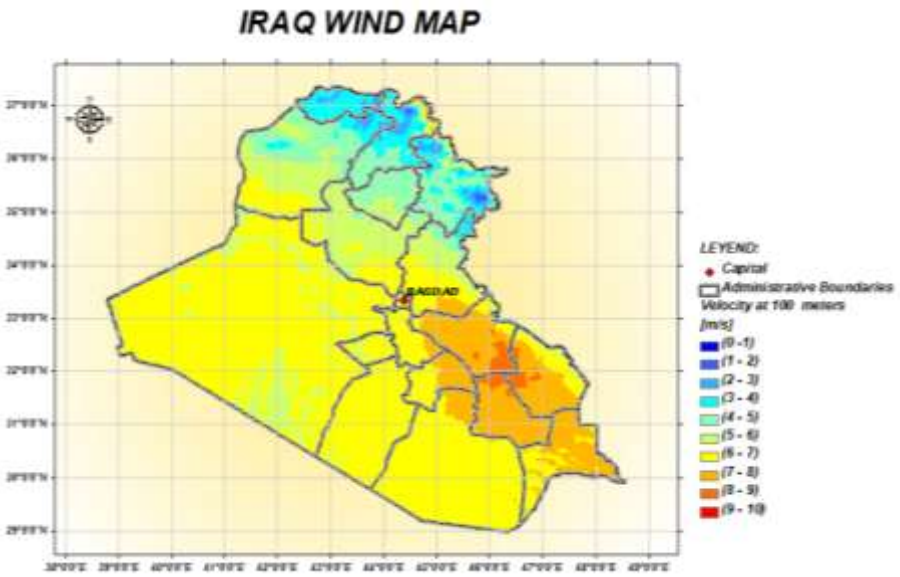

Figure (2). Iraq Wind map at 100 m

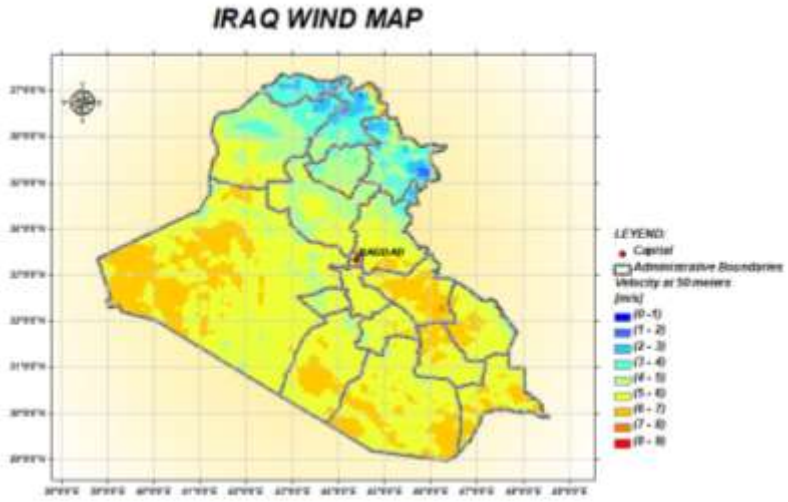

Figure (3).Iraq wind map at 50 m height

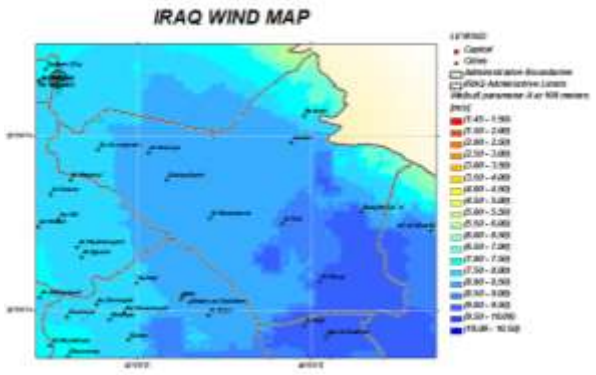

c at 100m

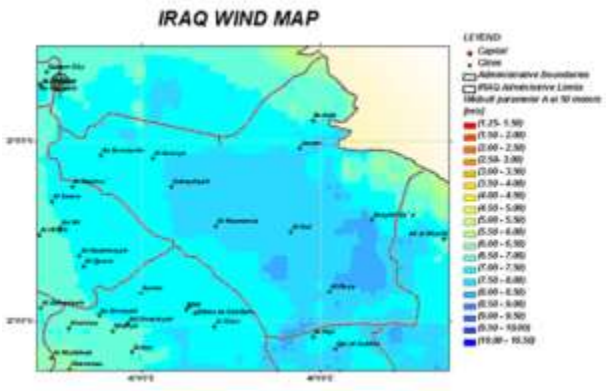

c at 50m

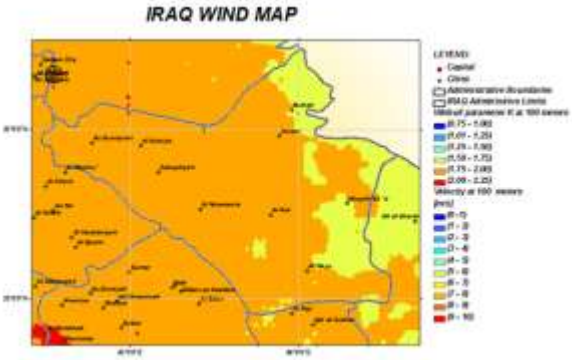

K at 100m

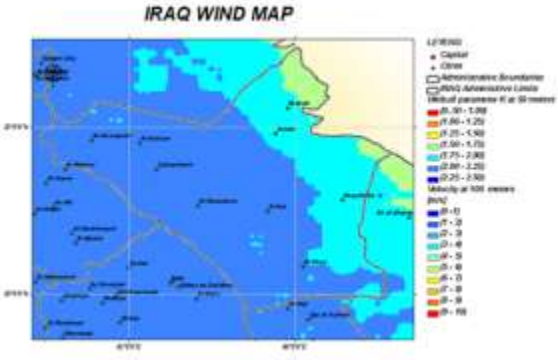

K at 50m

Figure (4). Weibull parameters (C , K) at height 100m and 50m

4. Weibull Distribution

When the percentage frequency distribution is plotted against the wind speed, the frequency distribution emerges as a curve. The top of this curve is the most frequent wind speed. This frequency distribution is used also to identify the most suitable wind turbine for the site [7].

5. Weibull Parameters

The most general expression of the Weibull pdf is given by the threeparameters. An important aspect of the Weibull pdf is how each of

- the shape parameter k,

- the scale parameter c,

- the location parameter g ,

- and the wind speed variable v.

affects the pdf curve. These effects will be shown below.

5-1 Weibull shape parameter, k

Shape factor is a measurement of the width of the distribution. Differentvalues of the shape parameter can have effects on the behavior of the distribution [8].

The Weibull distribution is equivalent to the exponential distribution.	k =1
The Weibull distribution is equivalent to the Rayleigh distribution.	k =2
The Weibull distribution which approximates the normal distribution provides the best estimation.	k = 3- 4
The Weibull distribution approximates the peaked normal distribution.	k =5

5-2 Weibull scale parameter, C

Scale factor is closely related to the mean wind speed. Increasing the value of scale parameter while holding shape parameter constant has the effectScale parameter has the folloeing properties, [9]:

- If c is increased, while k and g are kept the same, the distribution gets stretched out to the right and its height decreases.

- If c is decreased, while k and g are kept the same, the distribution gets pushed in towards the left (i.e. towards its beginning or towards 0), and its height increases.

- c has the same unit as wind speed.

5-3 Weibull locatin parameter, g

The location parameter g , as the name implies, locates the distribution along the wind speed axis. Changing the value of g has the effect of sliding the distribution and its associated function either to the right (if $g > 0$) or to the left (if $g< 0$) [9].

6- Types of used turbines and the power curves

Wind turbine usually has six main components: the rotor, the gearbox, the generator, the control and protection system, the tower and the foundation. These main components of used turbines in this paper is shown below [6]

6.1 Suzlon S64-950kW

- Manufacturer: Suzlon (India)
- Model: S64/950
- Nominal power: 950 kW
- Rotor diameter: 64 m
- No more available
- Offshore model: no
- Swept area: 3,217 m²
- Power density: 3.39 m²/kW
- Number of blades: 3

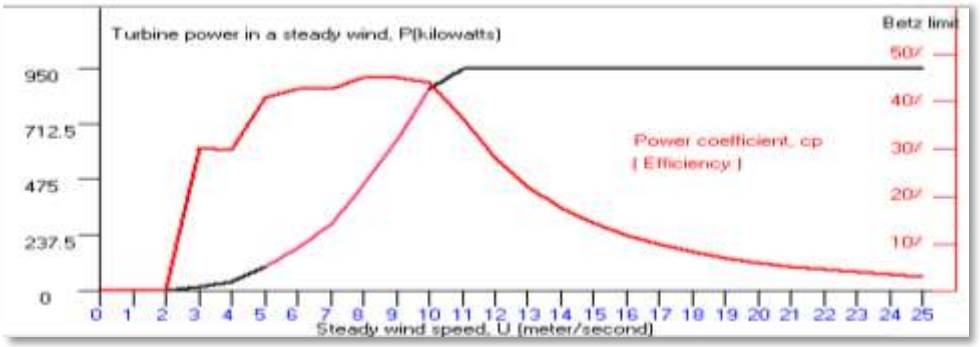

Figure (5). Suzlon S64-950kW power curve and power coefficient

6.2 Gamesa G58-850kW

- Manufacturer: Gamesa (Spain)
- Model: G58/850
- Nominal power: 850 kW
- Rotor diameter: 58 m
- No more available
- Wind class: IEC IIIb/IIa
- Offshore model: no
- Swept area: 2,643 m²
- Power density: 3.11 m²/kW
- Number of blades: 3

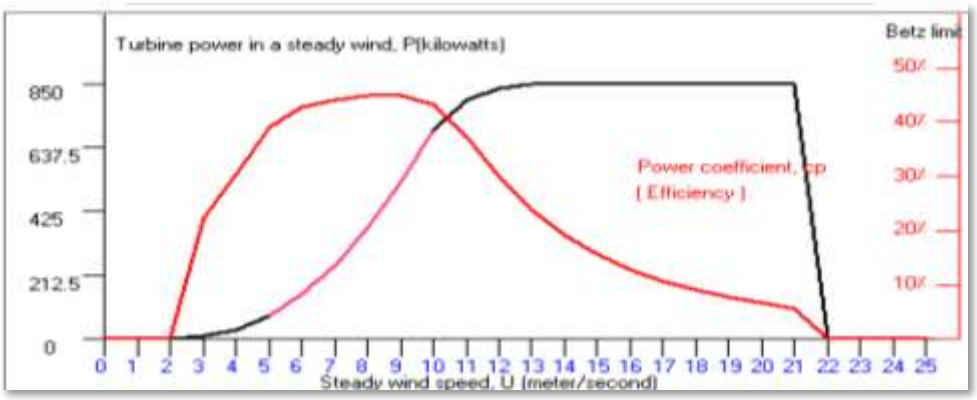

Figure (6). Gamesa G58-850kW power curve and power coefficient

7. The operating hours of the wind turbine

The cumulative distribution can be used for estimating the time for which wind is within a certain velocity interval. The monthly operating hours in a year can be calculated like follow [10]:

$$\boldsymbol{p(v_c < v < v_f) = \left(e^{-\{v_c/c\}^k} - e^{-\{v_f/c\}^k}\right) * tm}$$

Where v_c is the cut-in speed, v_f is the cut-of speed. **tm** is the monthly or yearly hours number (30 day chosen for each month or 365 day for each year), k is the weibull shape factor and c is the weibull scale factor.

8- Results and discussion

The figure (7) shows that the higher hours is about 1050 hour/year at height 50m by using Gamesa turbine which applied in surfer program.

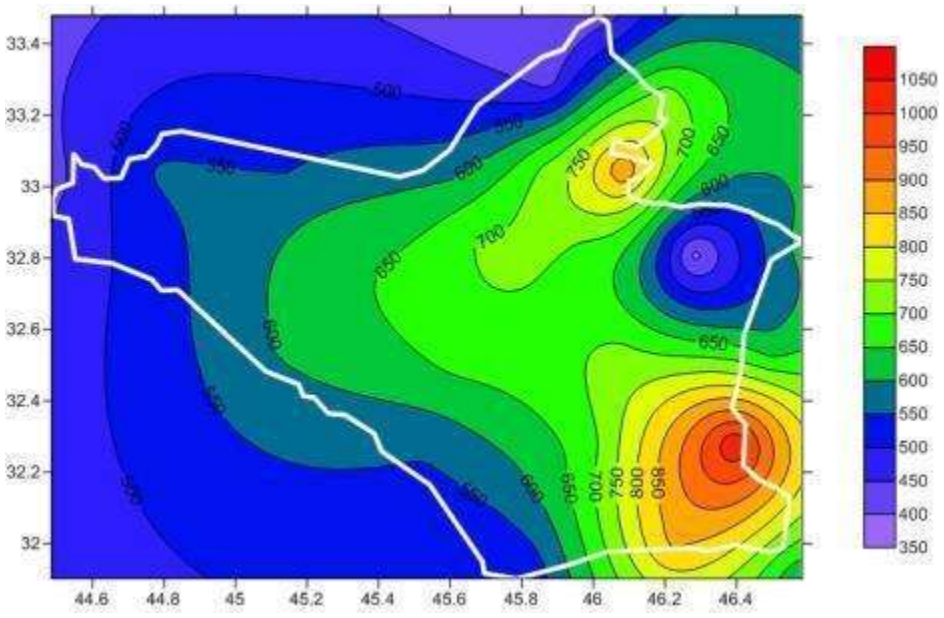

Figure (7). The number of hours of power in Gamesa atheight 50m

The figure (8) shows the higher amount of power is 2000 hour/year at 100m in the south east of wasit by using Gamesa turbine.

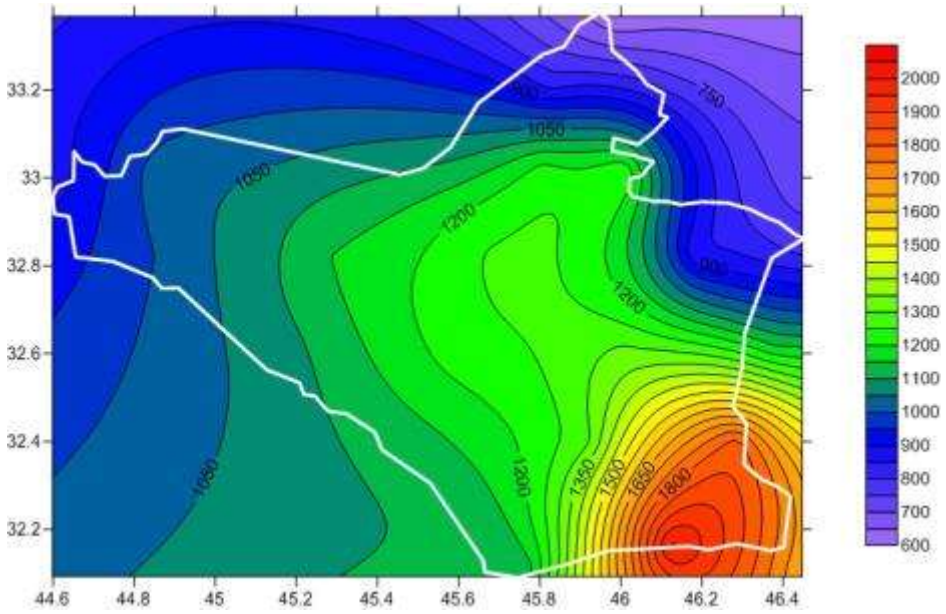

Figure (8). The number of hours of power in Gamesa atheight 100m

The figure (9) and (10) shows the higher amount of power is about 2250 hour/year at 50m and about1450 hour/year at 100m in the south east of wasit by using sezlon turbine.

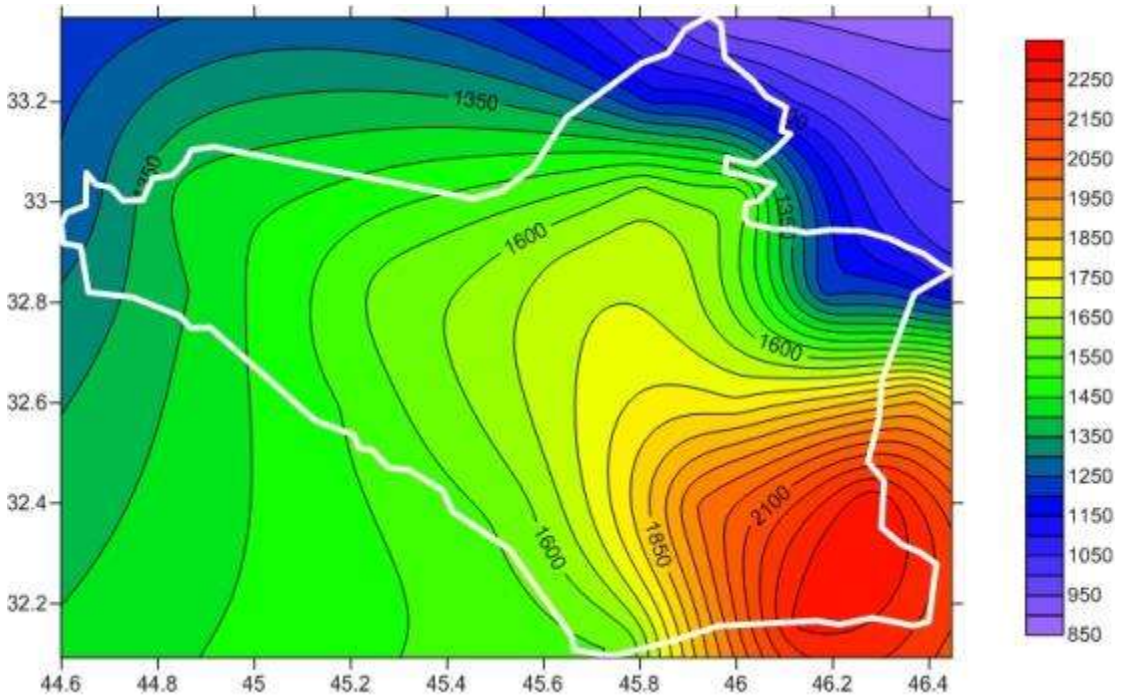

Figure (9).The number of hours of power in Suzlon at height 50m

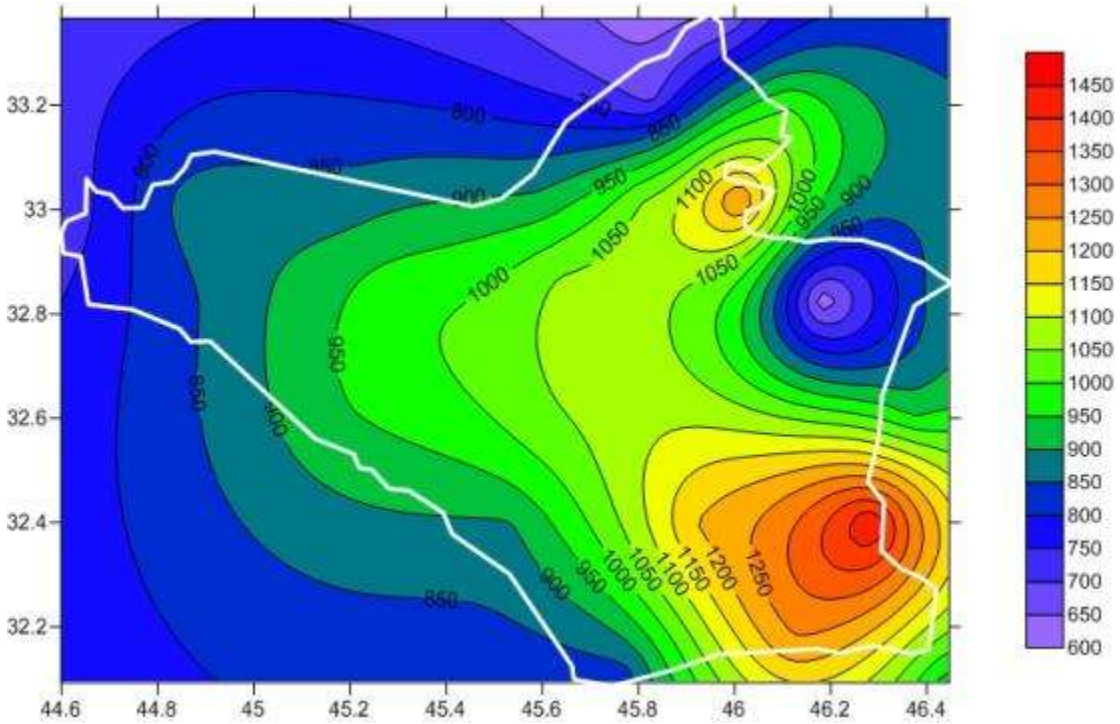

Figure (10).The number of hours of power in Suzlon at height 100m

9- Conclusion

1- The number of hours depend on the range of wind speed which taken in our considration (rated to cutout wind speeds). In Gamesa wind turbine this range located between 12-23m/s, while it is located between 11-25m/s in Suzlon wind turbine type.

2- Gamesa G58-850 KW gives more generated hours per year than Suzlon S64-950KW, such that the 1st one gives about 1050 hour per year at 50 meters height. While the 2nd one gives 2250 hour/year.

References

[1] Botterud, A., Wang, J. , Miranda, V. and Bessa, R.(2010) : Wind power forecasting in U.S. electricity markets. The Electricity Journal .Vol.56, No.7, pp.67-69.

[2] Kusiak, A., Li, W. and Song, Z. (2010) :Dynamic control of wind turbines. Renewable Energy. Vol.25, No.2, pp.56-70.

[3] Chen, S. and Xiao,Y.(2005) :Wind Speed and Generated Power Forecasting in Wind Farm. Proceedings of the CSEE,Vol.234, No.23, PP.1-5 .

[4] Kusiak, A, Zheng, H. and Song, Z. (2009) :Short-term prediction of wind farm power: a data mining approach. IEEE Transactions on Energy Conversion.Vol.34, No.7, pp.75-79.

[5] Dutton, A., Kariniotakis, G., Holliday, J., and Nogaret, E. (1999): Load and Wind Power Forecasting Methods for the Optimal Management of Isolated Power Systems with High Wind Penetration. Wind Engineering,Vol.45, No.3, pp. 69-87.

[6]Ahrens, C.,D., :essential of meteorology; An invitation to the atmosphere, third edition, PP.140-155.

[7] Lysen E. H., "Introduction to Wind Energy (1983):Development corporation information department, 2nd edition.

[8] Ulgen K. and Hepbasli A., (2002) :*Determination of Weibull Parameters for Wind Energy Analysis of Izmir, Turkey*", International Journal of Energy Research.

[9] Salahaddin A. A., (2013): Comparative Study of Four Methods for Estimating Weibull Parameters for Halabja, Iraq", International Journal of Physical Sciences Vol.8, No.5, pp.186-192, February.

[10] Hadi, F., A., (2014) : Construction of Mathematical-Statistical Model of Wind Energy in Iraq Using Different Weibull Distribution Functions. AL-Nahrain University, College of Science, Department of Physics.

Study the Effect of Rotating Disk Base Temperature on Steam Condensation Effectiveness

Dr. Ali Al Assadi
Department of Mechanical Engineering
University of Baghdad

Dr. Akram W. Ezzat
Department of Mechanical Engineering
University of baghdad

Dr. Ayser Muneer
Department of Mechanical Engineering
University of Baghdad

ABSTRACT

Theoretical and experimental study has been conducted to evaluate the effectiveness of rotating disk condenser at different temperature of disk cooling water and power supplied to water evaporation. The experimental investigation involved, special test apparatus designed and fabricated to realize the condensation process of the saturated steam on the upper surface of a disk whose base is kept at low temperature. The designed system consists of three parts; cold water system that designed to ensure low temperature for the base of the disk. Cold water system has the capability to cool the water at different temperatures (5, 11 and 20 ℃). The heater used evaporate the water is regulated to ensure desired water temperature using thermostat. The heating element of the steam production sub-system is capable to work at different power ranging (P_{ev}=385, 270, 168Watt) to ensure water evaporation at different rates. Special slip-ring is fixed on this shaft to transfer the temperature signals from rotating disc to the read out device. The slip ring used in the apparatus is of 6-way mercury type. The ensured experimental results demonstrate that the maximum condensate rate is ensured form high steam power supply (P_{ev}=385watt) and low cooling water temperature (T_{cool}=5℃). It is concluded that local heat transfer is affected by the condensate layer thickness over the upper disc surface.

The disk surface temperature measured values decrease continuously in the radial direction Condensate. Film thickness gradually increases from center to outer portion of the disk based on both condensate rate and centrifugal force that affects this thickness which in turn depend on the speed, cooling water temperature. The agreement between the experimental and theoretical overall heat transfer coefficient appears to be reliable with a deviation of about (1.2-10%).

Keywords: Film condensation, Speed rotating disc, Steam, Different cooling water temperature, Different water Evaporation Rate, Theoretical and experimental study.

دراسة البخار المتكثف على سطح القرص دوار وبسرع مختلفة

د. علي عبد المحسن الأسدي
قسم الهندسة الميكانيكية
كلية الهندسة – جامعة بغداد

د. أكرم وهبي أحمد عزت
قسم الهندسة الميكانيكية
كلية الهندسة – جامعة بغداد

د. أيسر منير
قسم الهندسة الميكانيكية
كلية الهندسة – جامعة بغداد

الخلاصة

يقدم البحث الحالي دراسة عملية ونظرية لانتقال الحرارة على سطح قرص دوار يدور ومدى تأثير الدوران على كمية بخار الماء المتكثف بدرجات حرارة مختلفة لسطح القرص. تم في العمل التجريبي من البحث تصميم وبناء جهاز عملي يقوم بتكثيف بخار الماء المشبع عند درجات حرارة واطئ على سطح القرص العلوي، يتكون الجهاز من ثلاث أجزاء رئيسية، منظومة التبريد وقد تم

أخذ ثلاث درجات حرارة مختلفة لماء البارد (T_{cool}=20, 11, 5C^o) . منظومة توليد البخار التي تستخدم لتوليد بخار الماء ويمكن السيطرة على كمية البخار الداخل الى المنظومة بواسطة المحول ،للتحكم بكمية بخار الماء الداخل الى المنظومة (168,270, P_{ev}=385Watt).ويتصل من أعلى العمود جهاز للقياس درجات الحرارة على سطح القرص الدوار يدعى slip ring يقوم بنقل أشارة درجة الحرارة من سطح القرص الدوار الى Data logger .
لقد اظهرت النتائج العملية أعلى كمية بخار متكثفة على سطح القرص تكون عند أقل درجات حرارة للماء البارد (T_{cool}.=5℃) وأعلى طاقة للبخار المتولد عند (P_{steam}=385Watt). ونستنتج كمية الحرارة المنتقلة من سطح القرص مرتبطة بسمك الطبقة المتكثفة من البخار، وعند زيادة كمية البخار المتدفق أي بزيادة في سمك الطبقة المتكثفة وبتالي أنخفاض بكمية الحراة المنتقلة. درجة حرارة سطح القرص الدوار تكون أعلى قيمة عند المركز وتنخفض تتدريجيا عند المحيط وبالتالي يحصل أعلى تبادل حراري بالقرب من المركز وينخفض تدريجيا عند المحيط.
تزداد درجة حرارة القرص كلما زادت سرعة القرص بسبب أزاحة البخار المتكثف من سطح القرص . سمك الطبقة المتكثفة على سطح القرص تزداد تدريجيا من المركز القرص الى محيط القرص ،ان زيادة سمك الطبقة ونقصانها مرتبط بالمؤثرين هما قوة الطرد المركزي وكمية البخار المتكثف على سطح القرص والذي يعتمدان على سرعة القرص ،درجة حرارة الماء البارد وكمية البخار الماء.أظهرت الحسابات النظرية توافق الى حد معقول ومقبول مع الجزء العملي عند حساب معامل أنتقال الحرارة الكلي وأظهرت النتائج نسبة الخطا تتراوح بين (1.2-10%).

الكلمات الرئيسية:دوران القرص عند سرعة ثابتة، بخار ماءبكميات مختلفة، درجات حرارة الماء البارد مختلفة، دراسة عملية ونظرية مع مناقشة النتائج.

1. INTRODUCTION

Water condensation in desalinations systems using solar energy became one of the important technical aspects that are challenging the engineers worldwide. The enhancement of the evaporated water condensation using rotating disc is governed to this challenge to enhance energy utilization. High energy costs have forced engineers to pay detailed attention to actual energy requirements and their efficient use. Integration of groups of process plant to improve overall energy efficiency has produced great benefits, mainly by removing the more easily identified source of waste and inefficiency. The improvement of operating conditions, better control and maintenance will contribute to this effort. In the future significant improvements in processes are only likely to come with major changes in the actual processes themselves. For example changes in manufacturing method from catalytic to biochemical routes **(Khan 1986)**.

Rotating condensation attractive for space vehicle applications, where the force of gravity is essentially zero. In addition, rotating condensation also seems promising for earthbound applications where higher condensation rates are desired than are obtainable with **gravity (Sparrow and Hartnett 1961).** Since rotating condensation radiators are of great interest in space applications, a condensation experimental has been developed that reduces the effect of gravity. In the ground-based experiments the effect of the gravitational field could be minimized by using a flat plate in which the axis of rotation is parallel to the gravity vector. The flow of a thin liquid film on a horizontally disc is commonly encountered in many engineering application: coating technologies such as the coating of silicon wafers for integrated circuits, for magnetic storage disc and for monitor screens or optical devices **(Ohara et al 1989)**, and heat/mass transfer enhancements such as fast heat/mass exchanges with the surrounding gas phase like water desalination, blood oxygenation and cooling devices **(Leneweit et al 1999)**. Later, **(Hoyle and Matthews 1964)** presented experimentally and theoretically a theory that predicts the transfer of heat from steam to a cooled rotating cylinder. The measured heat transfer coefficients were generally greater than those predicted by this simple theory. The discrepancy due to the instability of the condensate film flow which can cause a wave type of film flow to exit in the laminar flow region. The type of flow controls the heat flux and depends on the properties of the condensate film and the forces that act upon it.

A number of studies related to various aspects of film flow on rotating surface are reported in the literature. These range from the complex flow regimes which were noted above, to the techniques and difficulties associated with the measurement of film parameters such as film thickness and surface velocity. The main area of interest of the present research concerns heat transfer with phase change in thin liquid films. The literature reviewed in this chapter is limited to those papers which make a significant contribution in this area. Subsequently, **(Espig and Hoyle 1968)** studied the heat transfer from steam to cooled rotating cylinder, in which drainage of the film was perpendicular to the surface by the growth and throwing off of protrusions, carried out a series of experiments to study the transfer of heat from steam to a cooled vertical flat rotating disc. The discussion of results showed that heat flux is high near the cooling sprays and lower at greater radii where the temperature drop through the condensate decreases, the local heat transfer coefficients calculated from the heat fluxes rise with increase of radius. Furthermore **(Wilfried and Roetzel 1975)** worked out experimentally and theoretically to investigate the condensate film thickness and consequently, heat transfer dependence on the method of condensate removal. The conventional rotating condensate siphon is replaced by a stationary one with the tip running in a circumferential groove. The high pressure drop in the rotating siphon is avoided while film thickness is reduced somewhat.

The effects of heat transfer on a rotating surface with and without phase change was investigated by **(KHAN 1986)** studied experimentally and theoretically the heat transfer to liquid films flowing across the surface of a rotating disc. Two cases of heat transfer have been considered, the first dealing with sensible heating of the liquid film, the second with heating and evaporation from the surface of the film. In both cases the heating medium was condensing steam. A model for the thermal performance of such devices has been constructed and compared with experimental data for water and methanol.

(Homam et. al 1995) studied experimentally heat transfer parameters of film condensation on a rotating flat plate. A rotating flat-plate condensation experiment has been developed to investigate the heat transfer characteristics of a rotating flat-plate radiator. The condensing surface is cooled to simulate the rejection of heat to a cold surface. The working fluid is superheated steam. The results obtained including relationship between the overall heat transfer coefficient and the temperature difference between the working fluid and a cold environment, both placed in dimensionless groups, and plate angular rotational speeds. This empirical relationship is useful for choosing the optimum rotational speed for a rotating flat-plate radiator given a desired heat rejection load. This study also provides the basis for designing new heat rejection systems using centrifugal forces and condensation phenomena in both space and ground applications. Then, Beside the same authors, **(Usha and Ravindran 2001)** investigated the numerical study of film cooling on a rotating disk. The development of a heat conducting fluid film on a rotating disk has been investigated numerically under the planar interface assumption and the film thickness, the flow characteristic, the temperature distribution and the rate of heat transfer are determined. The range of validity of the time scale and Reynolds number bounds have been presented for the existing asymptotic solution for film cooling on a rotating disk. The effects of the Reynolds number (Re), cooling parameter β and the Prandtl number σ on the variation of film thickness, and temperature distribution have been examined. It is concluded that the film thickness decreases with time for fixed angular velocity of the rotating disk and this was in agreement with the results presented by (Emslie et al. 1958), (Higgins 1986), (Rehg and Higgins 1988) and (Dandapat and Ray 1990). It is also observed that the (Dandapat and Ray 1990) asymptotic solution is in good agreement with the numerical results at short times $\tau \leq 1$ but the agreement was poor at longer times.

(Basu, Cetegen 2006), studied the problem of analysis of hydrodynamics and heat transfer in a

thin liquid film flowing over a rotating disc by the integral method. An integral analysis of hydrodynamics and heat transfer in a thin liquid film flowing over a rotating disk surface is presented for both constant temperature and constant heat flux boundary conditions. The model was found to capture the correct trends of the liquid film thickness variation over the disk surface and compare reasonably well with experimental results over the range of Reynolds and Rossby numbers covering both inertia and rotation dominated regimes. Nusselt number variation over the disk surface shows two types of behavior. At low rotation rates, the Nusselt number exhibits a radial decay and Nusselt number magnitudes increasing with higher inlet Reynolds number for both constant wall temperature and heat flux cases. At high rotation rates, the Nusselt number profiles exhibit a peak whose location advances radially outward with increasing film Reynolds number or inertia. The results also compared favorably with the full numerical simulation results from an earlier study as well as with the reported experimental results. Another related problem is that of **(Sung Kim and Uhn Kim 2009)** studied the flow of a liquid film on a rotating disc in the case where a liquid is supplied at a constant flow rate. The authors proposed thin film equation by the integral method with a simple approach to satisfy the boundary conditions on a disc and a free surface, and the results were compared with those of the Navier-Stokes equations. The radial film velocity was assumed to be a quadratic profile in their analysis. The basic flow and its stability were analyzed using the thin film equation even in the region where the inertia force is not negligible. A local stability analysis of the flow conducted using the linear disturbance equation and correctly predicts Needham' simple instability criterion. The thin film equation gave good approximation of the Navier-Stokes equation.

(Muhammad et. al 2011) presented experimentally and theoretically, the paper describes hydrothermal characteristics of liquid flowing on horizontal rotating disk. The liquid was introduced at the center of the disk in the form of a falling jet. Liquid spread out due to the simultaneous action of surface and body forces and forms a thin film over the disk. The effect of nozzle to plate spacing, fluid flow rate and disk rotational speed on the film thickness, local heat transfer coefficient and local Nusselt number along the radial direction was investigated. It was observed that local heat transfer coefficient and local Nusselt number strongly depends upon flow rate and disk rotational speed and has no influence of nozzle to plate spacing. The study also concludes that the process of heat transfer is intensified manifold by rotating the surface, which will be helpful in the future heat and mass transfer applications.

The main objectives of the present work are:

- Investigate experimentally and theoretically the steam condensation process on rotating disc condenser at certain rotation speed (N =150 rpm) and different cooling water temperature (T_{cool} = 20, 11, 5℃) at different water evaporation power ranging (P_{ev}= 385, 270, 168W)..
- Investigate the relation between the disc base temperature versus its radius at different cooling system temperature and water evaporation power.
- Investigate the relation between condensate film thickness versus disc radius at different cooling system temperature and water evaporation power.

Figure (1) and **Figure (2)** shows the elementary principles of the condensation process on rotating disc and the different parameters effects on this process.

2. EXPERIMENTAL WORK

The test rig consists of rotating disc shown **figure (3)**, which has a diameter of 150 mm and thickness of 2 mm is made from high-strength, high conductivity stainless steel alloy, this assembly rotates about a hollow shaft using proper ball bearing. The rotating shaft is of 450 mm length and is bored out to 18mm, while the outer diameter is machined to suit the ball bearing internal diameter. Two pulleys of 200 mm and 250 mm diameter are made from aluminum and fixed to the rotating shaft by screw. The two pulleys and their accessories that represent disc rotating mechanism are shown in **figure (4)**. The upper driving shaft is clamped on the small shaft,

which has a diameter of 20 mm and 120 mm length. It is made from high-strength stainless steel alloy and screwed to the slip-ring.

The driving pulley is mounted below this housing on the shaft. Both pulleys (driving and driven) are made of Aluminum with different diameters, i.e. 200 mm for the first and 57 mm for the other. A 37 KW D.C. motor (3 Phase, type JL 712-4B3) is provided to the main drive. The variable speed rotation is achieved by a speed controller system (type SV- IC5 Manual). With this arrangement the rotation speeds of 150 rpm are realized, knowing that maximum speed of the motor is 2000 rpm. In view of this problem, the local temperature gradient normal to the disc surface was obtained by smoothing the temperature output from six thermocouples pairs (types K) are placed in (24, 32, 39, 46, 53, and 60 mm) distances from the disc center for the purpose of measuring disc upper surface temperature see **figure (5)**. The ends of thermocouples wires are contacted to slip-ring. The slip- ring is connected to the board of the data logger through the upper end of the shaft. All thermocouples are calibrated in place according to the temperature range that is used during the experiments. The liquid film temperature is measured with a thermistor which had previously been calibrated using a high precision chromium-nickel thermometer ($\pm 10^{-3}$℃). The accuracy of the thermocouples is ±0.5℃. The bolted gasket is fixed by the silicon rubber gasket on the up end cylinder from outer periphery for the purpose of preventing steam leakage to the cooling water vessel. The collector dish is fixed on the cooling vessel surface by 6mm diameter fixtures to ensure uniform water distribution on this surface.

Some auxiliary equipment's in the experimental set-up are used during test rig operation and conducting the related experiments. These are: centrifugal pump to deliver the cold water for rotating disc cooling purpose, stop watch, two thermometers one used to measure temperature of the weather in the laboratory while the other is used to measure the temperature of water in steam condensate collector dish, laboratory flask (laboratory glass blowing).

Saturated water vapor at 45-60℃. The steam is feed continuously towards the rotating disc via 6 nozzle ports which provides the steam on the surface disc, water is fed to the heating tank of 15 liter capacity. The level inside the tank is measured using an L shaped manometer which is attached to the bottom of the tank. An immersed heater of 1.5 kW power rating is used to heat the water inside the tank. The heater power is regulated to ensure desired water temperature using thermostat. Steam is fed to the test rig using 31mm inside diameter and 38mm outside diameter pipe. Stainless steel tubes are used for distributing steam via stationary annular feed channel which delivers the steam to the test section via nozzle, distributor. Another feeding channel made of 15mm inner diameter and 22 mm outside diameter rubber tube. The pressure in the steam chamber is controlled by pressure reducing valve. The condensed steam in liquid droplets moves in the radial direction due to the centrifugal force and collected in circular rubber jacket and drawn through plastic tube to the collection flask.

The cooling liquid is introduced through, cold water system that is designed to ensure low temperature for the base of the disk. Cold water system consists of, condenser (270 mm x 280 mm), evaporated (300 mm x 210mm), expansion valve and compressor (capacity 1/6 hp) to supply the cold water temperature 5℃ from this system by digital thermostat is pumped and distributed from the center of the discs towards its periphery in a thin film under the action of centrifugal force.

3. ANALYSIS OF LIQUID FILM ON ROTATING DISCS

Analytical solution for the condensation mechanism on rotating circular cold surface is modeled using finite difference model. The mathematical model takes under consideration the effect of rotation speed, steam temperature and disk temperature profile on the condensation rate and condensed steam boundary layer growth along its radius.

Following assumptions are taken under consideration during modeling the present case study:

1. Only radial flow of the condensate film is considered indicating that the effect of Coriolis force due to the relative movement of the

condensing film on the disc is negligible under the experimental conditions.

2. The following input parameters are based during conducting theoretical approach:
a) Disc thermal conductivity. **b)** Physical dimension of the disc. **c)** Heat transfer between the steam and the cooled disc which will be calculated based on proper formulas. **d)** Speed of rotation which will be identified based on the characteristics of rotating system. **e)** Physical properties of the condensed steam. **f)**Steam flow rate inside the closed rotation system.

3. The calculations are based on the following assumptions:
a) The fluid properties are constant. **b)** Zero shear stress at the condensate/vapor interface. **c)** The liquid is Newtonian. **d)** Liquid is introduced to the disc surface in an axisymmetric manner. **e)** Incompressible flow. **f)** Steady state condensate film flow. **g)** Film surface is smooth.

Vapor is pure and there is no non-condensable gas. The flow of condensate in the film is laminar within rotation speed range that will be adapted during the experiments.

The hydrodynamics of these flows have been accurately described in terms of a simple balance between centrifugal force and the viscous forces in the film **IZV (1960):**

$$\vartheta \frac{du_r^2}{dy^2} = -r\omega^2 \qquad (1)$$

The radial velocity could be estimated by integrating the equation (1) for the conditions of on slip at the disc surface (y=0) and for stress free ($du_r/dy = 0$) conditions at (y= δ). The redial velocity distribution across the film is found to be parabolic for these conditions:

The average film velocity,

$$\overline{u_r} = \frac{1}{\delta}\int_o^{\delta} u_r dy$$
$$\overline{u_r} = \frac{\omega^2 r\delta^2}{3\nu} \qquad (2)$$

The estimation of the film thickness as a function of radial position, rotational speed, flow rate, and rheological properties of the liquid has been based on the equation (3)

$$u_r = \frac{r\omega^2\delta^2}{\nu}\left[\left(\frac{y}{\delta} - \frac{1}{2}\left(\frac{y}{\delta}\right)^2\right)\right] \qquad (3)$$

The average velocity $\overline{u_r}$ is redefined in terms of flow rate per unit area equating with equation (3), i.e.

$$\overline{u_r} = \frac{Q}{2\pi\delta} = \frac{\omega^2 r\delta^2}{3\nu}$$

$$\text{or} \quad \delta = \left(\frac{3}{2\pi}\frac{Q\nu}{r^2\omega^2}\right)^{0.333} \qquad (4)$$

The Nusselt treatment of condensing heat transfer was based on the assumption that latent heat was conducted from the steam interface at a temperature T_s to the cooled wall at a temperature T_w. this gives rise to a heat transfer coefficient $h = (K/\delta)$. However, in the present case it is assumed that there is no heat flux across the steam interface as the liquid film approaches the wall temperature. The average mixed film temperature which was measured during the experimental is given by

$$T_m = \int_0^{\delta} uTdZ \Big/ \int_0^{\delta} udZ \qquad (5)$$

Noting that the parabolic temperature distribution which satisfies the conditions $T=T_w$ at Z=0, $T=T_s$ at Z=δ, dT/dy=0 at y=δ

$$\left[(T - T_w)/(T_s - T_w)\right] = \left(\frac{3Z}{2\delta} - \frac{1}{2}\frac{Z^3}{\delta^3}\right) \qquad (6)$$

The velocity profile is used from the Nusselt model. It is derived for the similar conditions of flow i.e. laminar

$$\frac{u}{u_\delta} = \frac{2Z}{\delta} - \frac{Z^2}{\delta^2} \tag{7}$$

Substitution of the values of T and u into equation (5) from equation (6) and (7) and then integrating it, leads to

$$\left(\frac{T - T_w}{T_m - T_w}\right) = \frac{40}{61}\left(\frac{3Z}{\delta} - \frac{Z^3}{\delta^3}\right)$$

$$or \tag{8}$$

$$\left(\frac{dT}{dZ}\right)\Big|_{Z=0} = \left(\frac{120}{61\delta}\right)\left(T_m - T_w\right)$$

Rate of heat transfer per unit area can be written as;

$$q' = -K\left(\frac{dT}{dZ}\right)\Big|_{Z=0} = hr\left(T_m - T_w\right) \tag{9}$$

Where (h_r) is the local value of the heat transfer coefficient at the distance 'r' from the origin.
Comparison of equation (8) and (9), led to the following simplified expression, to define local heat transfer coefficient;

$$h_r = \frac{120}{61}\left(\frac{K}{\delta}\right) \tag{10}$$

Where, (δ) is the thickness of the liquid film:

$$\delta = \left(3Q\mu \Big/ 2\pi\omega^2 \rho\ r^2\right)^{0.333} \tag{11}$$

Substituting the value of (δ) into equation (10) and the average value of heat transfer coefficient for the effective heat transfer area is obtained by integrating equation (10)

$$\bar{h}r = \frac{1}{A}\int_{R_I}^{R_o} hrdA \tag{12}$$

$$\bar{h}_r = \frac{90}{61}\left(\frac{r_o^{8/3} - r_i^{8/3}}{r_o^2 - r_i^2}\right)\left[K_L\left(\frac{2\pi\omega 2\rho}{3Q\mu}\right)_L^{0.333}\right]$$

Liquid side film coefficient is estimated using the following correlation, **(Butuzov and Rifert1973)**.

$$h_f = 2.18\left(\frac{K_f^3 \rho_f^2 N^2 r_o^2}{\omega_f \mu_f}\right)^{1/3} \tag{4.12}$$ (13)

Condensate rate

$$Q_c = \left(qA/\rho_c h_{fg}\right) \tag{4.13}$$ (14)

Overall heat transfer coefficient

$$\frac{1}{U} = \frac{1}{h_r} + \frac{1}{h_f} + \frac{x}{K} \tag{15}$$

Experimental overall heat transfer coefficient:

$$U = \frac{q}{(T_s - T_{vessel})} \tag{16}$$

Total effectiveness of system was calculated:

$$\eta_t = \frac{\eta_t}{\eta_{t\,max}} = \left(\frac{q_{cond.}}{q_{rotating}+q_{cooling}+q_{steam}}\right) \Bigg/ \left(\frac{q_{cond.}}{q_{rotating}+q_{cooling}+q_{steam}}\right)_{max} \quad (17)$$

4. RESULTS AND DISCUSSION

The effect of the following parameters ranges on the steam condensation rate is investigated in the experimental and theoretical parts:

1. Cooling water temperatures (20, 11, 5℃) at constant rotating disc 150 rpm.
2. The power supplied to the evaporation tank, P_{ev} Range (385, 270 and 168Watt).

4.1 Steam Condensation Rate

The effect of cooling water temperatures on condensate mass rate is shown clearly on the **figure 4.** The figure shows the effect of cooling water temperatures at different power supplied to evaporate the water in the heating tank and constant rotating disc N= 150 rpm. This figure proves that condensate mass rate increase proportionally versus disc surface temperature and this rate of increase depends on the water evaporation which is function of water evaporation power at constant rotation speed of N=150 rpm. The heat transfer on the disc surface have more effect when vapor condensation rate increase with decreasing cooling water temperature (20, 11 and 5℃), i.e. vapor condensation rate is proportional to heat transfer rate and inversely proportional with condensate film thickness over the rotating disc. For comparison, the condensate rate, Qc of 175 ml per 15 minute is realized when the rotational speed, N=150 rpm and T_{cool}=5°C, while Qc decreases to 140 ml per 15 minute when N kept at 150 rpm and T_{cool} increases to11^{o}C. Further decrease in condensate rate to 80 ml per 15 minute during same rotational speed is realized when T_{cool} increases up to 20°C. It is concluded that condensate rate is inversely proportional to cooling water temperature.

4.2 Disc surface temperature

Disc surface temperature was measured at different radial location using typical thermocouple distributed along the radius of the disc at different angles. Temperature variations at the measured points are mainly affected by varying cooling water temperature (20, 11 and 5°C) respectively which in return affect the condensation rate on disc surface.

Figures 5 to 7 show that temperature measured values decrease continuously in the radial direction at constant water evaporation power ranging (385, 270 and 168W) at different cooling water temperature (20, 11 and 5℃).

It is also clear that disc surface temperature increases by increasing water evaporation power (P_{steam}=385, 270 and 168Watt) due to both condensate film thinning versus velocity and augmentation of condensate rate versus steam production rate which increase its condensation rate. While the temperature profile versus distance is proportional to cooling water temperature as it decreases versus cooling water temperature decrease. Table (5-1) shows the effect of water cooling temperature on the expected heat transfer rate across the disc surface.

Table (5-1) Represent effect of water cooling temperature on the heat transfer rate

r (mm)	T_{cool} (C^o)	T_{sur} (^{o}C)	P_{ev} (W)	N (rpm)	q (watt)
31	20	27	385	150	1.5432e+004
31	11	19	385	150	1.7411e+004
31	5	9.4	385	150	2.0534e+004

4.3 Film Thickness

Figures 8-10 describe the effect of cooling water temperatures (20, 11 and 5°C) respectively on film thickness versus disc radius at constant water evaporation power. It could be seen that film thickness increases versus radial locations, while this thickness is inversely proportional to the

cooling water temperatures. This decrease is justified by increasing the centrifugal force effect. As clarified in theoretical condensate thickness is governed with the mass balance of the condensation rate of the steam on the specified disc sector and the effect of the condensate mass entering and leaving each sector due to the centrifugal force in addition to the proportionality of sector area with radius of each sector.

Theoretical show that at water evaporation power, P=168W the film thickness, δ=0.127μm at radius =31mm, while δ=0.19μm when P=270W and δ=0.2μm when P=385W at a constant cooling temperature (T_{cool}=20℃).

The film thickness peak location shifts to δ=0.45μm when rotational speed N=150 rpm ,T_{cool}=5℃ and water evaporation power 385W.

4.4 Overall Heat Transfer Coefficient

Figures 11-13 illustrate the influence of cooling water temperatures on the overall heat transfer coefficient at constant evaporation power and rotating speed N=150rpm. It is observed that overall heat transfer coefficient increases with decreasing cooling water due to the surface disc temperature decrease. From same figures it is clear that more heat is transferred as the power supplied to the water tank increases

The figures describe the experimental results related to the effect of varying cooling water temperatures on overall heat transfer coefficient at constant evaporation power and rotating disc. Similar behavior to theoretical results is concluded from these figures. However it was noted that experimental overall heat transfer coefficient rate is lower than theoretical values. This difference is estimated to be consistently (1.2-10.4%) below the predictions of the experimental overall heat transfer coefficient rate depending on disc rotation speed, cooling water temperature and water evaporation power.

4.5 Total Effectiveness of Auxiliary Sub-Systems:

Figure 14 show the effect of the whole sub-systems interaction with each other and their effect on the total system effectiveness. Total system effectiveness is plotted versus cooling water temperatures at different evaporation power at constant rotating disc. This figure prove that total efficiency is proportional to cooling water temperatures as it decreases versus this temperatures for the whole range of water evaporation power at constant rotating disc speed N = 150 rpm. It is clear from this figure that maximum effectiveness located at T_{cool}= 5°C and water evaporation power equal 385 watt, while it reaches to its minimum value at T_{cool}= 20°C and water evaporation power equal 168 watt

However the following expression is investigated to show the effect of the cooling and rotating sub-systems on the steam condensation rate at water evaporation power equal 385 Watt, with maximum error of 10%

6. CONCLUSIONS

The research concludes that water condensation rate is proportional to the rotating disc speed, rotating disc cooling system temperature and the water evaporation power. Each mentioned parameter has an effect on the condensation rate and the interaction with other parameters is based to estimate the final effect. The effectiveness of the system based on the consumed power of the related systems and the condensation rate could be used to evaluate the optimum value of the mentioned parameters used to enhance of the condensation process.

7. NOMENCALTURE

D, d	Diameter	
h	Heat transfer Coefficient	W/ m^{2}k
K	Thermal Conductivity	W/m. k
N	Rotational speed	rpm.
p_{ev}	Water Evaporation Power	Watt
Q	Volumetric Flow Rate	m^2/sec
q	Heat Flux	W/m^2
R, r	Radius	m
T	Temperature	℃, k
U	Overall heat transfer coefficient	W/ m^{2}k

Greek Letters

δ Film thickness μm

λ Latent heat J/kg

μ Viscosity of liquid Ns/m^2

ν Kinematics viscosity of the liquid m^2/s

ρ Density kg/m^2

τ Shear stress N/m^2

ω Angular velocity rad/s

8. REFERENCES

Basu S. and Cetegen B. M. (2006),"Analysis of Hydrodynamics and Heat Transfer in a Thin Liquid Film Flowing Over a Rotating Disc by the Integral Method", Int. Heat Transfer, Vol.128, pp. 217-225.

Butuzov, A.I., and Rifert, V.G. (1973), "Heat Transfer in Evaporation of Liquid from a Film on a Rotating Disc" Heat Transfer –Soviet Research, 50(1) pp 88-94.

Dandapat B. S. and Ray P. C.(1990),"Film Cooling on a Rotating Disc", Int. J. Non-Liner Mechanics, Vol. 25, No. 5, pp.569-582.

Emslie A. G., Bonner F. J. and Peck L. G. (1958),"Flow of a Viscous Liquid on a Rotating Disc", J. Appl. Phys., Vol. 29, pp. 858.

Espig H. and Hoyle R. (1986), "The Transfer of Heat from Condensing Steam to a Cooled Rotating disc", Proc. Instn.Mech. Engrs. , Vol.182 Pt 3H.

Higgins B. G. (1986),"Film Flow in Rotating Disc",Phys. Fluids, Vol. 29, pp. 3522.

Homam M. Al-Baroudi and Andrew C. Klein (1995), "Experimental Simulations and Heat Transfer Parameter Measurements of Film Condensation on a Rotating Flat Plate", Experimental Thermal and Fluid Science, pp. 124-135.

Hoyle, R. and Matthews, D. (1965), "The Effect of Speed on the Condensate Layer on a Cold Cylinder Rotating in a Steam atmosphere", Int. J. Heat Mass Transfer, Vol. 22,105.

Khan J. R. (1986), "Heat Transfer on a Rotating Surface with and without phase Chang", Ph.D. Thesis, University of Newcastle upon Tyne.

Leneweit G., Roesner K. G. and Kaoehler R. (1999),"Surface Liquid Film Flow on a Rotating Disc", Exp. Fluids, Vol 26, pp. 75-85.

Muhammad S., Khan J. R., Suleman H., Naveed S. (2011), "Hydrothermal Characteristics of Thin Liquid Film Flow on Horizontal Rotating Disc", J. Quality and Technology Management, Vol. Vll, pp. 131-147.

Ohara T. Matsumoto Y. and Ohashi H. (1989),"The Film Formation Dynamics in Spin Coating ", Phys. Fluids A 1, pp. 1949-59.

Sparrow, F, M, and Hartnett, J. P. (1961), " Condensation on a rotating Con",Int. J. Heat Transfer , vol. 83, pp. 101-107.

Tae-Sung Kim and Moon-UhnKim(2009),"The flow and Hydrodynamic Stability of a Liquid Film on a Rotating Disc", IOP Publishing, Fluid Dynamics Research, Vol.41, pp.1-28.

Usha R. and Ravindran R.(2001),"Numerical Study of Film Cooling on a Rotating Disc", Int. J. Non-Liner Mechanics, Vol.36, pp. 147-154.

WilfriedRoetzel (1975),"Improving Heat Transfer in Steam Heated Fast Rotating Paper Drying Drums", Int. J. Heat Mass Transfer, Vol.18, pp. 79-86.

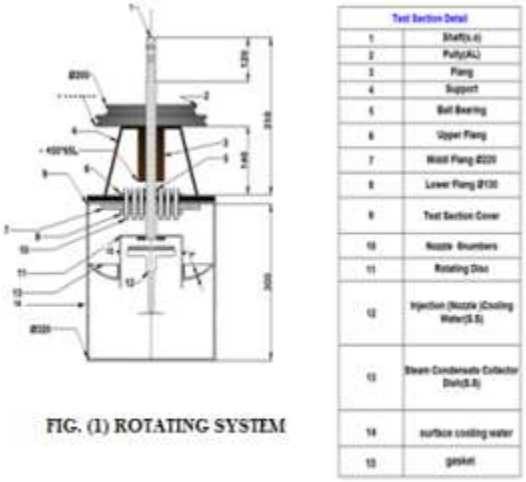

FIG. (1) ROTATING SYSTEM

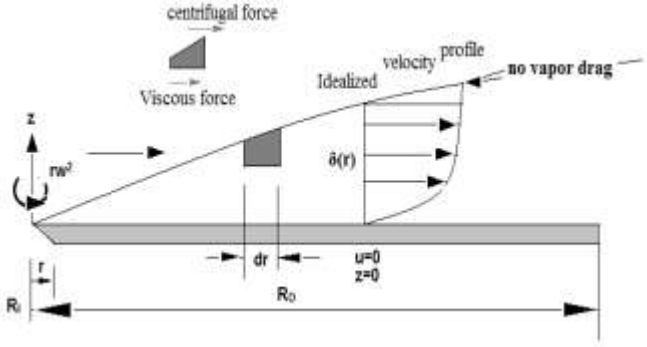

FIG. (3): THE VOLUME ELEMENT OF CONDENSATE ON A ROTATING DISC

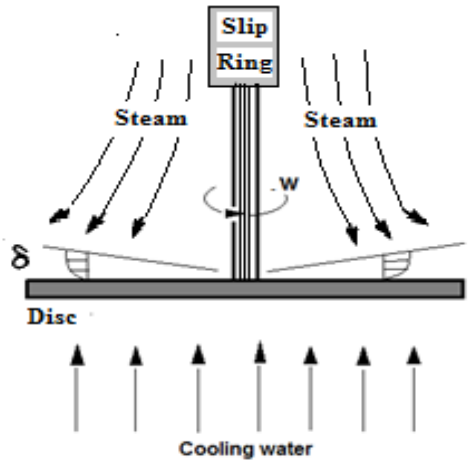

FIG. (2) THE ROTATING DISC SYSTEM

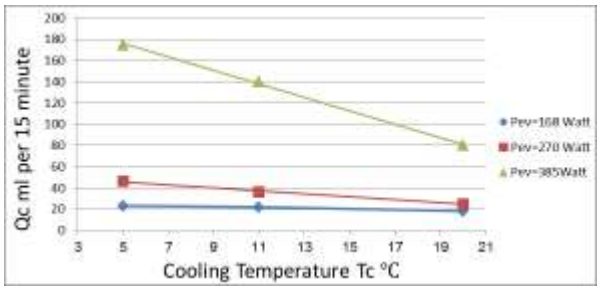

Figure (4) Effect Cooling Water Temperatures on the Steam Condensate Volumetric Rate at Different Evaporation Power (385 Watt)

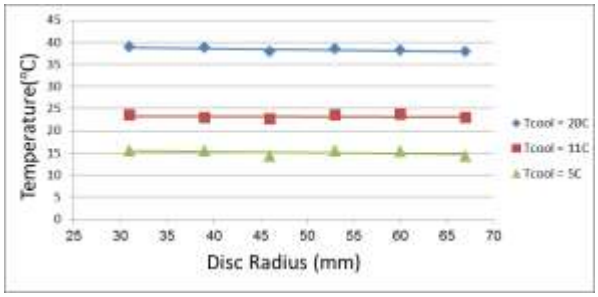

Figure (5) Disc Surface Temperature Variation Versus Disc Radius at Different Cooling Water Temperature and Evaporation Power =385 Watt

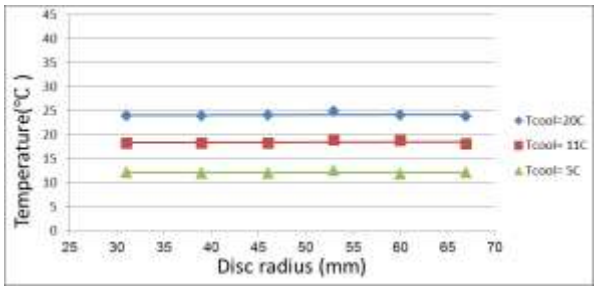

Figure (6) Disc Surface Temperature Variation Versus Disc Radius at Different Cooling Water Temperature and Evaporation Power =270Watt

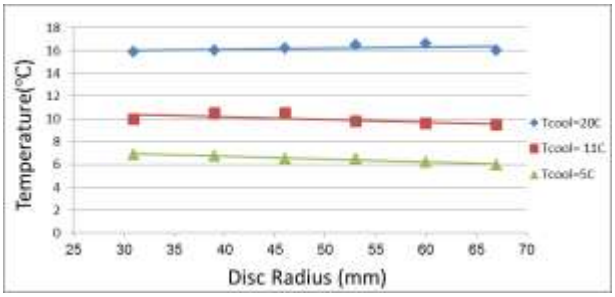

Figure (7) Disc Surface Temperature Variation Versus Disc Radius at Different Cooling Water Temperature and Evaporation Power =168 Watt

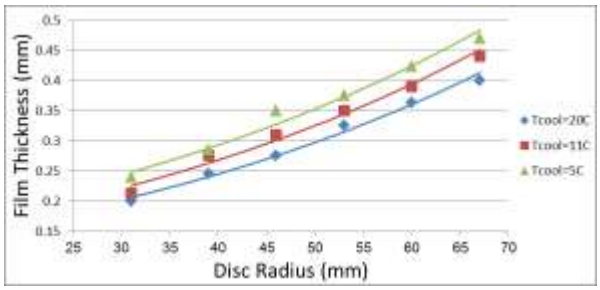

Figure (8) Film Thickness Distribution along The Radius of Different Cooling Water Temperature and Evaporation Power = 385 Watt

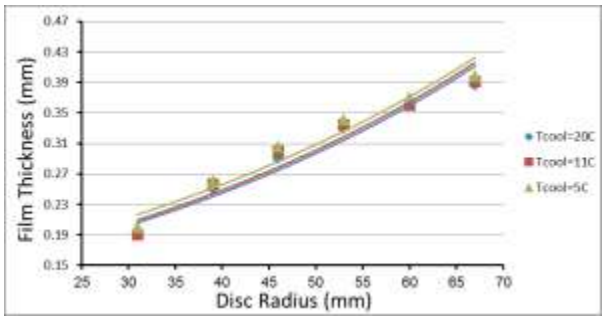

Figure (9) Film Thickness Distribution along The Radius of Different Cooling Water Temperature and Evaporation Power = 270 Watt

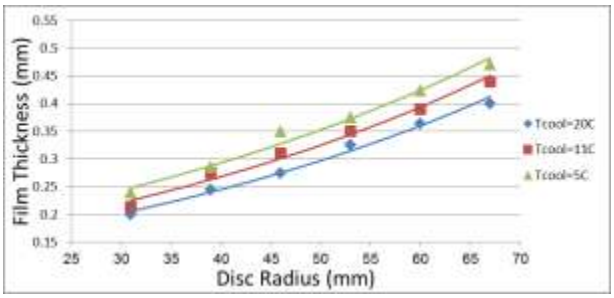

Figure (10) Film Thickness Distribution along The Radius of Different Cooling Water Temperature and Evaporation Power = 385 Watt

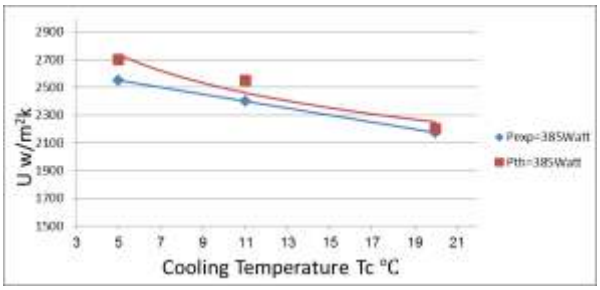

Figure (11): Comparison among Experimental and Theoretical of Overall Heat Transfer Coefficient Versus of Cooling Water Temperature at evaporation Power = 385 Watt.

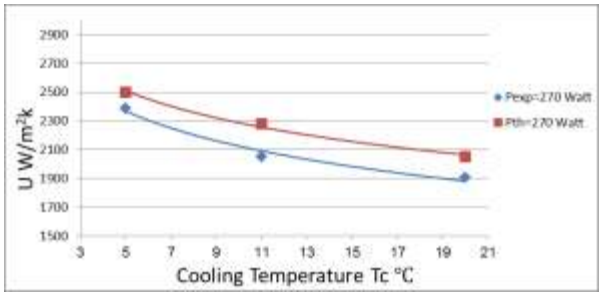

Figure (12): Comparison among Experimental and Theoretical of Overall Heat Transfer Coefficient Versus of Cooling Water Temperature atevaporation Power = 270 Watt.

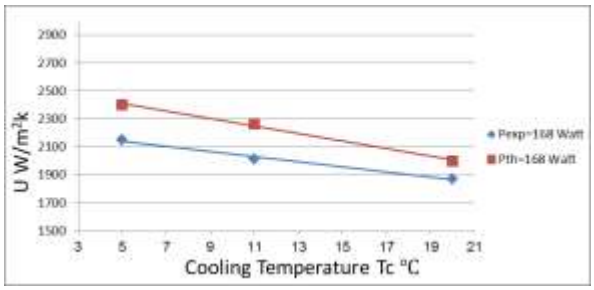

Figure (13) Comparison among Experimental and Theoretical of Overall Heat Transfer Coefficient Versus of Cooling Water Temperature atevaporation Power = 385 Watt.

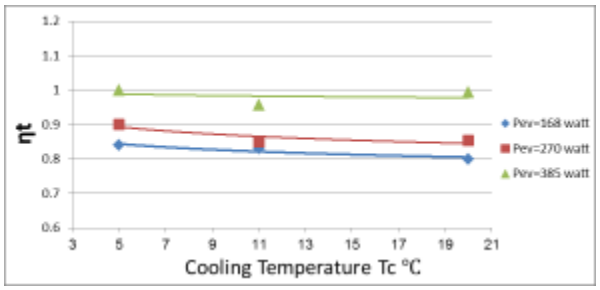

Figure (14): Normalized Total Effectiveness versus Disc Base Temperature at Different Cooling Water Temperature

Wastewater treatment by UV

Assistant prof Seroor Atallah Khaleefa Ali

University of Al Mustansireya / College of Engineering

Abstract

UV wastewater systems are a well established method of wastewater treatment and reuse water treatment safeguarding public health and protecting wildlife. There are different types of wastewater, such as municipal sewage or industrial effluent, and these different wastewaters all have their own types of microbiological environment, microbiological counts, levels of suspended solids, UV transmission rates and temperatures. Depending on whether the effluent is to be discharged into rivers, lakes and seas or re-used for applications such as irrigation, the required microbiological counts are usually specified by local regulations.

Key words: **Ozone, Hydrogen Peroxide, Ultraviolet Radiation Water Treatment Processes**

Introduction

Water disinfection means the removal, deactivation or killing of pathogenic microorganisms. Microorganisms are destroyed or deactivated, resulting in termination of growth and reproduction. When microorganisms are not removed from drinking water , greywater and wastewater, drinking water usage will cause people to fall ill. Sterilization is a process related to disinfection. However, during the sterilization process all present microorganisms are killed, both harmful and harmless microorganisms.
chemical disinfection of water the using disinfectants like Hydrogen peroxide, Hypo chlorite (OCl^-), Detol, Kwartair ammonium salts, soap & detergents.

Ultraviolet or “UV” is a type of energy found in the electromagnetic spectrum, lying between x-rays and visible light. Although we cannot see UV light or rays, we are exposed to them every time we step out into the sun. In fact, UV light is responsible for causing sunburns. Ultraviolet systems use special lamps or bulbs that emit UV light of a particular wavelength. The Ultraviolet energy attacks the genetic core of the

microorganism and rearranges the DNA /RNA eliminating the microorganism's ability to function and reproduce. If the microorganism can no longer reproduce, it cannot replicate, therefore it cannot infect other organisms with which has contact. The process is simple but effective, destroying 99.99 percent of harmful microorganisms without adding chemicals to the water.

UV disinfection is popular around the globe for wastewater treatment and water reuse treatment largely due to the fact that, unlike chlorine, it doesn't increase effluent toxicity.

Using UV have advantages and disadvantages. There are some very important reasons why both homeowners and municipalities are choosing UV technology to treat their water.

For over 25 years, UV technology has been trusted as a safe, cost-effective way to purify water and eliminate harmful microorganisms. It is a proven EPA endorsed technology that is currently being used by thousands of cities, bottled water manufacturers and homeowners around the world.

Chemical free: UV provides water purification without the addition of harmful chemicals such as chlorine. It also avoids the potential of generating harmful chemical disinfection by products. Recent EPA guidelines are forcing cities across the United States to reduce or eliminate the use of chlorine for exactly this reason.

Taste & odor free: UV does not change the taste, odor or color of the water.

More effective than chlorine: Unlike chlorine, UV systems are effective against both Cryptosporidium and Giardia.

Compact and easy to maintain: UV systems are capable of treating a single faucet or an entire home in a minimal amount of space with the only maintenance being an annual lamp and filter replacements.

The adoption of ultraviolet light for wastewater disinfection has grown significantly over the past few decades. Today, over 20% of wastewater treatment plants in North America employ this environmentally-friendly technology. Thousands of municipalities have converted from chemical-

based disinfection, such as chlorine gas, to UV due to the significant safety advantages for their communities, plant employees and local water bodies. As new wastewater treatment plants are constructed around the world, UV is most often selected for disinfection because of the cost savings in both initial construction and long term operation.

Advantages

- No hazardous chemicals involved
- No disinfection by products
- Effective against ALL microbes, including Cryptosporidium and Giardia
- Flexible disinfection performance at lowest cost
-
- Table 1: Infectious Agents Potentially Present in Untreated
- Domestic Wastewater
-
- Organism Disease Caused
-
- Bacteria
- Escherichia coli (enterotoxigenic) Gastroenteritis
  Leptospira (spp.) Leptospirosis
  Salmonella typhi Typhoid fever
  Salmonella (2,100 serotypes) Salmonellosis
- Shigella (4 spp.) Shigellosis (bacillary dysentery)
- Vibrio cholerae Cholera
- Protozoa
- Balantidium coli Balantidiasis
- Cryptosporidium parvum Cryptosporidiosis
- Entamoeba histolytica Amebiasis (amoebic dysentery)
- Giardia lamblia Giardiasis
- Helminths
- Ascaris lumbricoides Ascariasis T. solium
  Taeniasis Trichuris
  trichiura Trichuriasis
- Viruses
- Enteroviruses (72 types, e.g., Gastroenteritis, heart anomalies, polio, echo, and coxsackie viruses) meningitis
- Hepatitis A virus Infectious hepatitis
  Norwalk agent Gastroenteritis Rotavirus
  Gastroenteritis
-
- *Adapted from: Crites and Tchobanoglous (1998) with permission from*
- *The McGraw-Hill Companies*

Number of Bathrooms in Your Home	1 Bathroom	2 Bathrooms	3 Bathrooms	4 Bathrooms	5 Bathrooms	6 Bathrooms
Flow Rates (in gpm)	5	8.5	12	15.5	19	22.5

Limitations in UV Water Systems

Ultraviolet purification itself is not enough to purify water down to drinking water purposes. This is because the UV radiation is only effective for treating bacteria and viruses. UV light does not work to eliminate contaminants such as chlorine, heavy metals and VOC's (Volatile Organic Compounds). UV systems are often paired with Reverse Osmosis Systems to provide a complete purification process for the safest drinking water.

Choosing the Right UV Unit Size

If you draw water from a private water supply it is recommended to treat your entire home. To assure the highest satisfaction, choose the right size (gpm) of UV system that matches your household peak demand flow rate. This is simply a measure of how much water can flow through your main water line if all the water outlets were opened at once.

UV light is a natural process and does not produce harmful chemicals in water. It's a safe, effective and environmentally friendly disinfection method that is widely used for residential and industrial applications around the world.

Sterilization is a process related to disinfection. However, during the sterilization process all present microorganisms are killed, both harmful and harmless microorganisms.

Media

Disinfection can be attained by means of physical or chemical

disinfectants. The agents also remove organic contaminants from water, which serve as nutrients or shelters for microorganisms. Disinfectants should not only kill microorganisms. Disinfectants must also have a residual effect, which means that they remain active in the water after disinfection. A disinfectant should prevent pathogenic microorganisms from growing in the plumbing after disinfection, causing the water te be recontaminated.

For chemical disinfection of water the following disinfectants can be used:

- Chlorine (Cl_2)
- Chlorine dioxide (ClO_2)
- Hypo chlorite (OCl^-)
- Ozone (O_3)
- Halogens: bromine (Br_2), iodene (I)
- Bromine chloride (BrCl)
- Metals: copper (Cu^{2+}), silver (Ag^+)
- Kaliumpermanganate ($KMnO_4$)
- Fenols
- Alcohols
- Soaps and detergents
- Kwartair ammonium salts
- Hydrogen peroxide
- Several acids and bases

For physical disinfection of water the following disinfectants can be used:

- Ultraviolet light (UV)
- Electronic radiation
- Gamma rays
- Sounds
- Heat

Chemical inactivation of microbiological contamination in natural or untreated water is usually one of the final steps to reduce pathogenic microorganisms in drinking water. Combinations of water purification steps (oxidation, coagulation, settling, disinfection, filtration) cause (drinking) water to be safe after production. As an extra measure many countries apply a second disinfection step at the end of the water

purification process, in order to protect the water from microbiological contamination in the water distribution system. Usually one uses a different kind of disinfectant from the one earlier in the process, during this disinfection process. The secundairy disinfection makes sure that bacteria will not multiply in the water during distribution. Bacteria can remain in the water after the first disinfection step or can end up in the water during backflushing of contaminated water (which can contain

Disinfection mechanism

Disinfection commonly takes place because of cell wall corrosion in the cells of microorganisms, or changes in cell permeability, protoplasm or enzyme activity (because of a structural change in enzymes). These disturbances in cell activity cause microorganisms to no longer be able to multiply. This will cause the microorganisms to die out. Oxidizing disinfectants also demolish organic matter in the water, causing a lack of nutrients.

Drinking water is one of the most prominent human needs during exercise daily work, and highlights the citizen's interest in how to maintain the purity of this water and health, and can be fully operational and financial capabilities in access to clean and healthy water covered seeks, and this is probably the direct cause of the spread of the stations, shops and factories that deal with water treatment and sterilized and reach out to a high degree of purity and sterilization and a commitment to the health conditions for Neil buyer satisfaction.

The most important characteristic of bottled drinking water for drinking water, which is pumped in public networks is bottled water quality especially in terms of taste, quality and regularity of water with time. The networks waters some characteristics may change as a result of materials that are exposed or transferred to it from the surrounding environment of the tanks and pipes which travels long distances before it reaches the consumer faucet, while the probability of bottled water pollution are slim because they are placed in airtight containers.

Average annual per capita bottled water consumption of about 24 liters has increased in 1988 to more than 50 liters in 1998. In Saudi Arabia, bottled drinking water industry has grown over the past decade dramatically as the number of packing plants has increased from 15 factories in 1994 to 41 factories in 1999 with a production capacity of about 3478 million liters per year. It is noted that some of these factories produce other products Kalasarat in addition to water. Bottled water is available in different sizes plastic containers used mostly) one-time (small containers such as bottles 0.25 liter, 0.5 liter, 1.5 liter and 3.85 liter) and re-mobilize some of them (as casings 19 Tr.kma available in the market are imported from different countries of the varieties .

Experimental work

Three samples of Contaminated water were taken with three different medias H_2O_2, Chlorine and Dettol with different concentrations. Tests were taken for one week then one month and recorded the change in water specifications. A manufactured unit was used as shown if figs 2&3 .

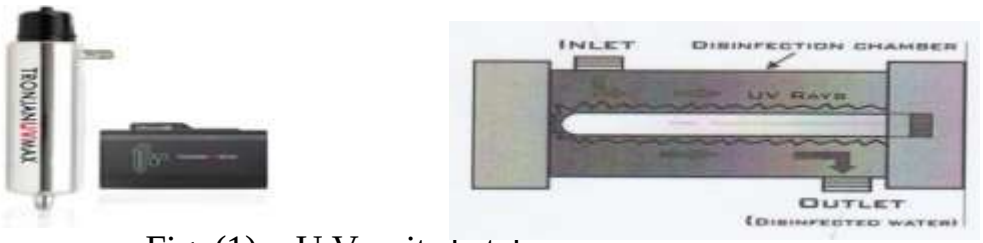

Fig. (1): U V unit sketch

Fig. (2): UV disinfection Unit

Tests were taken for each sample every 15 minutes at the first hour, then daily over a month. Final chemical treated water was disinfected using UV , as shown in the figures below. Results were recorded at final stage.

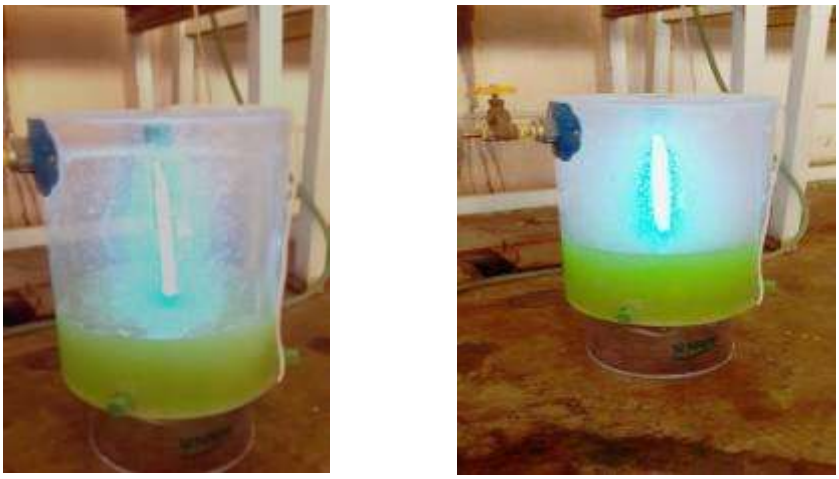

Fig. (3) : UV Unit filled with chemical treated water

Tests of contaminated water were done before and after chemical treatment then by UV treatment

TSS, TDS, PH, Temperature and Electrical Conductivity EC for each sample.

Results

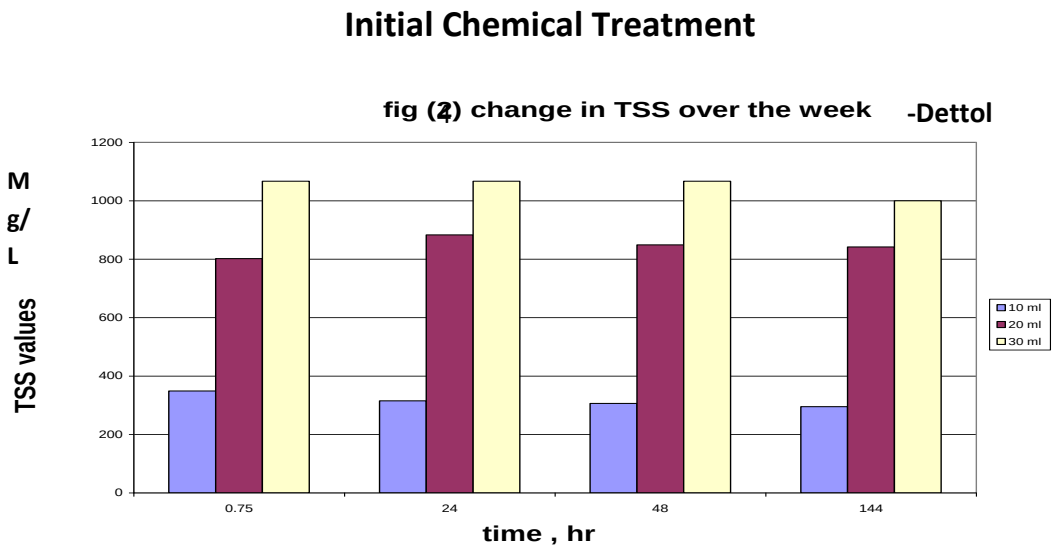

Fig. 5 Change in TSS over the week -chlorine

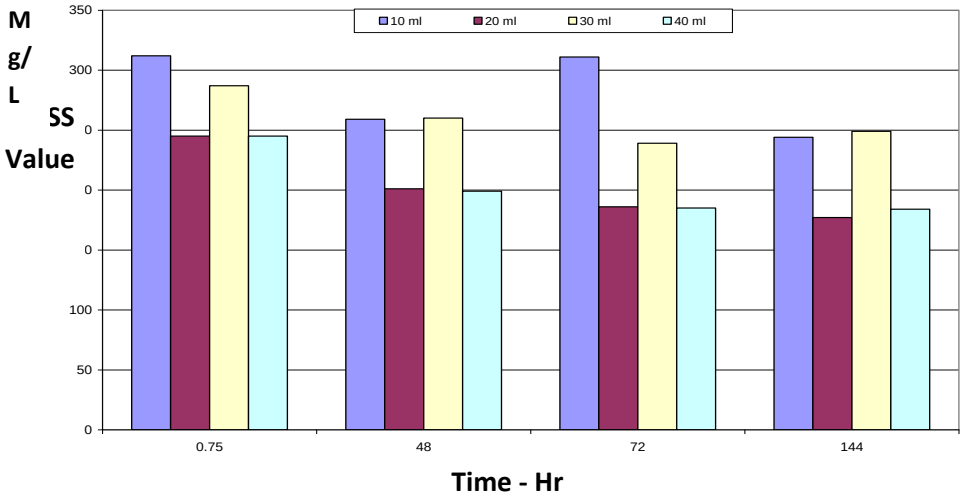

Fig. 6 Change in TSS over a week – C2H2

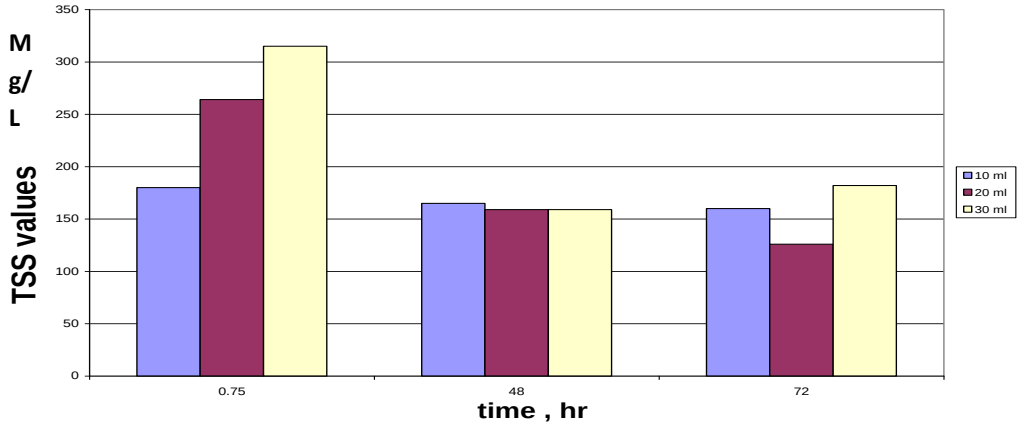

Fig. 7 Change in TDS over a week – Dettol

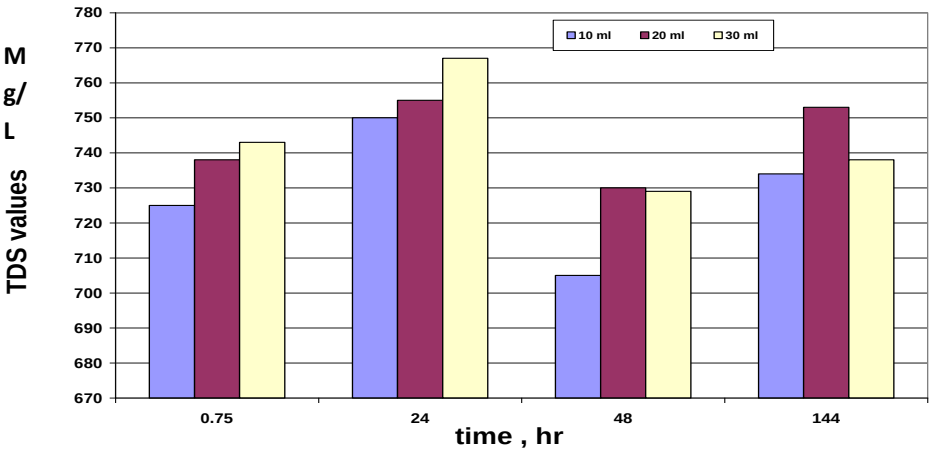

Fig. 8 Change in TDS over a week – Chlorine

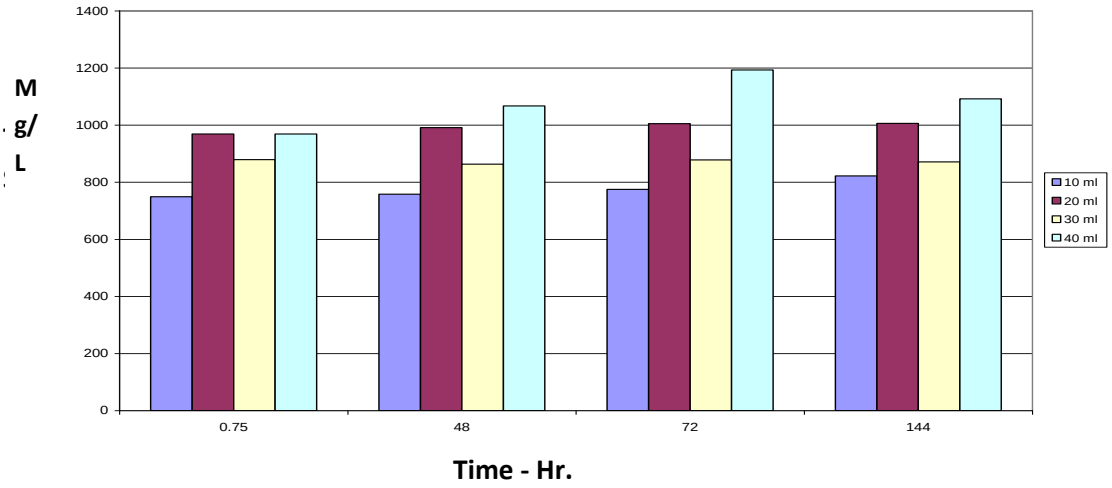

Fig. 9 Change in TDS over a week – C2H2

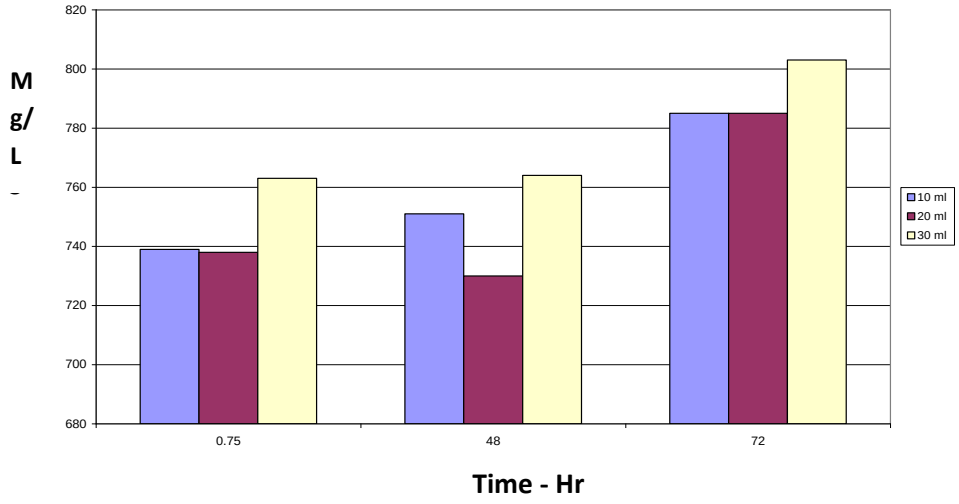

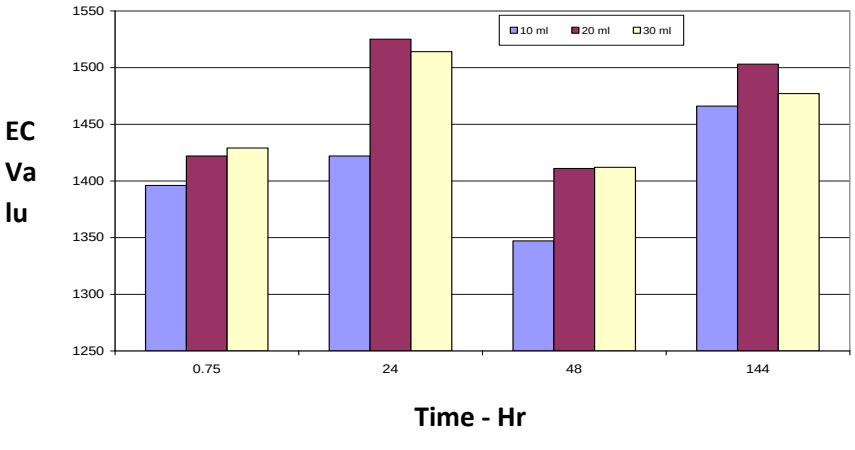

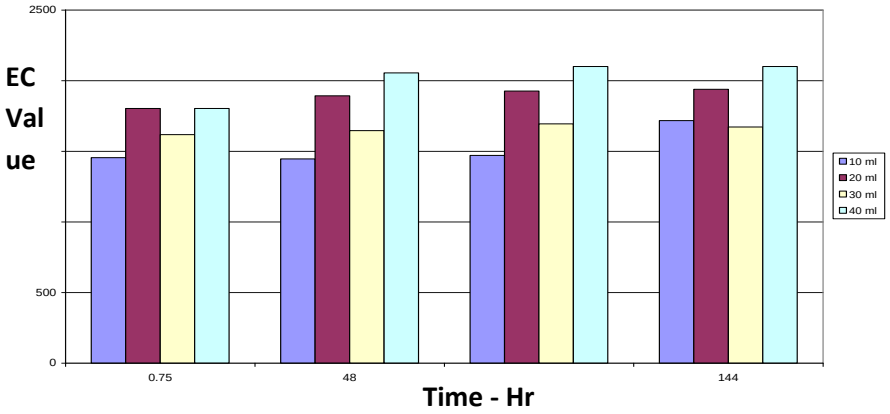
2500
EC
Val
ue
500
0
0.75
48
144
Time - Hr
10 ml
20 ml
30 ml
40 ml

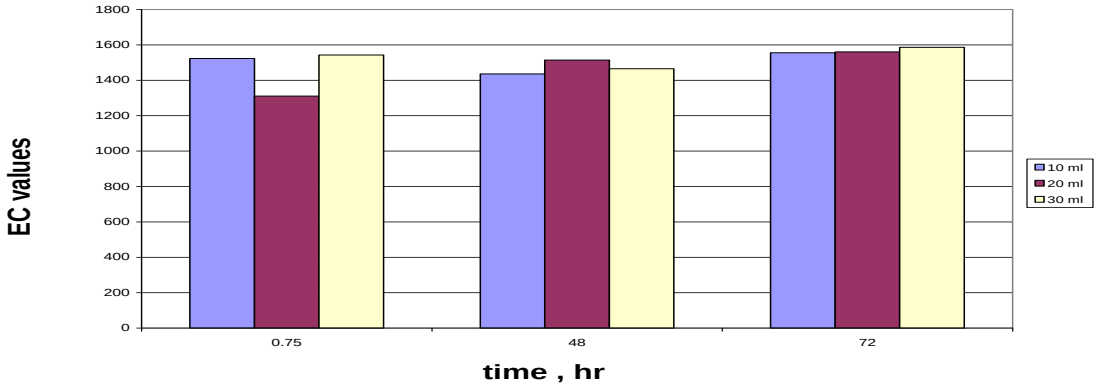
1800
1600
1400
1200
1000
800
600
400
200
0
EC values
0.75
48
72
time , hr
10 ml
20 ml
30 ml

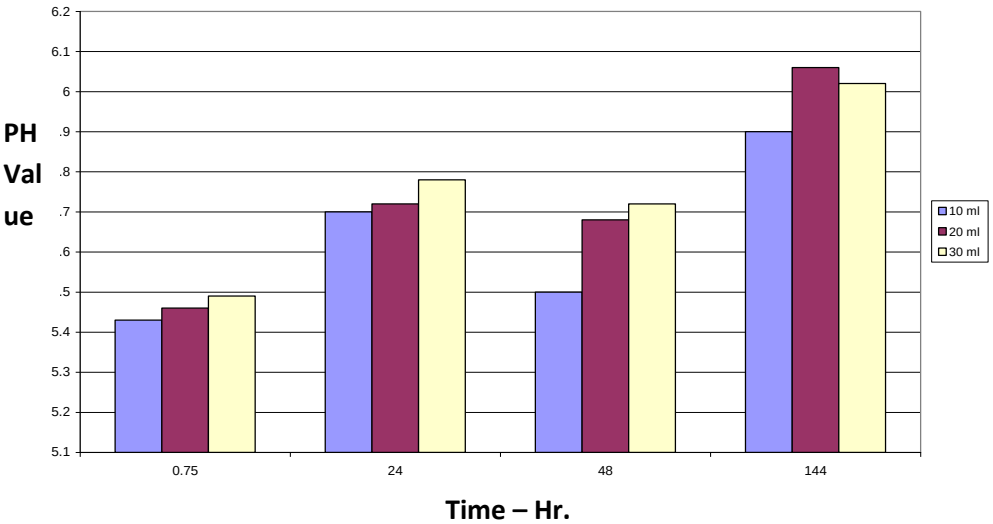
6.2
6.1
6
.9
.8
.7
.6
.5
5.4
5.3
5.2
5.1
PH
Val
ue
0.75
24
48
144
Time – Hr.
10 ml
20 ml
30 ml

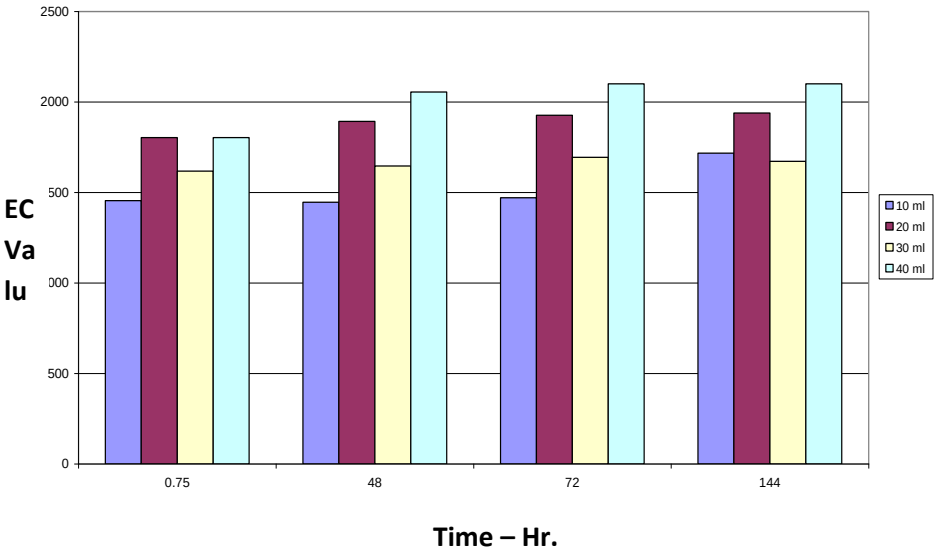
2500
2000
500
000
500
0
EC
Va
lu
10 ml
20 ml
30 ml
40 ml
0.75
48
72
144
Time – Hr.

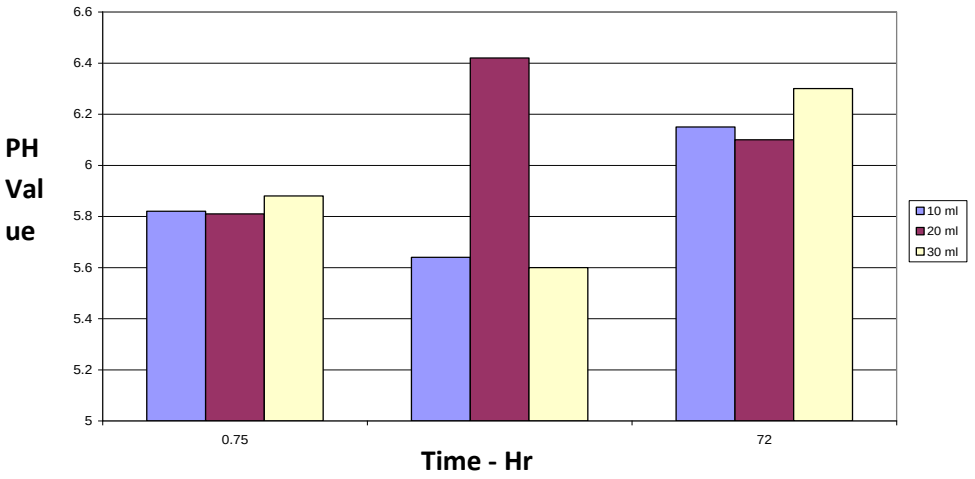
6.6
6.4
6.2
6
5.8
5.6
5.4
5.2
5
PH
Val
ue
10 ml
20 ml
30 ml
0.75
72
Time - Hr

After UV Treatment

Fig. 16: TSS treated after treating with H2S2

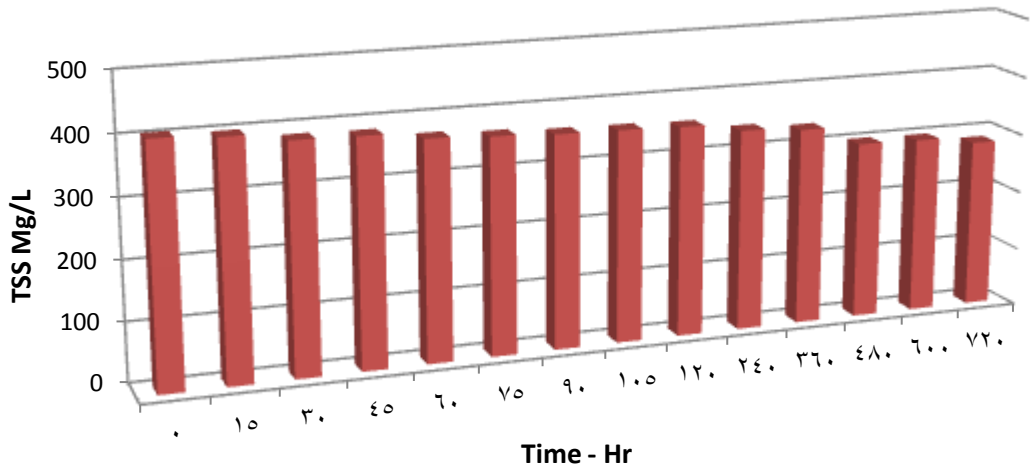

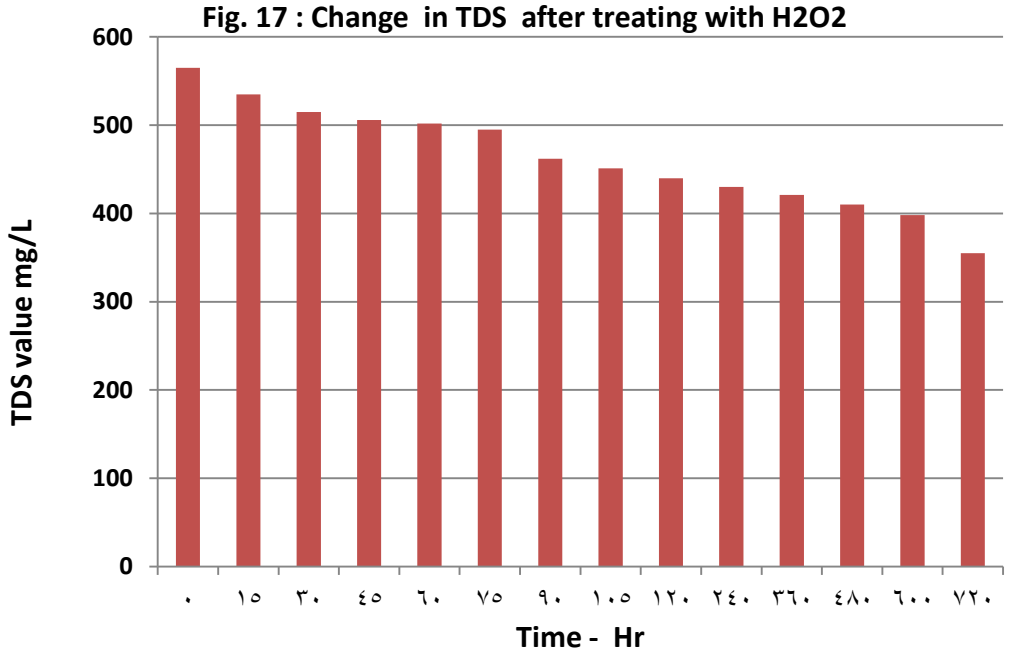

Fig. 18 : Change in EC after treating with H2O2

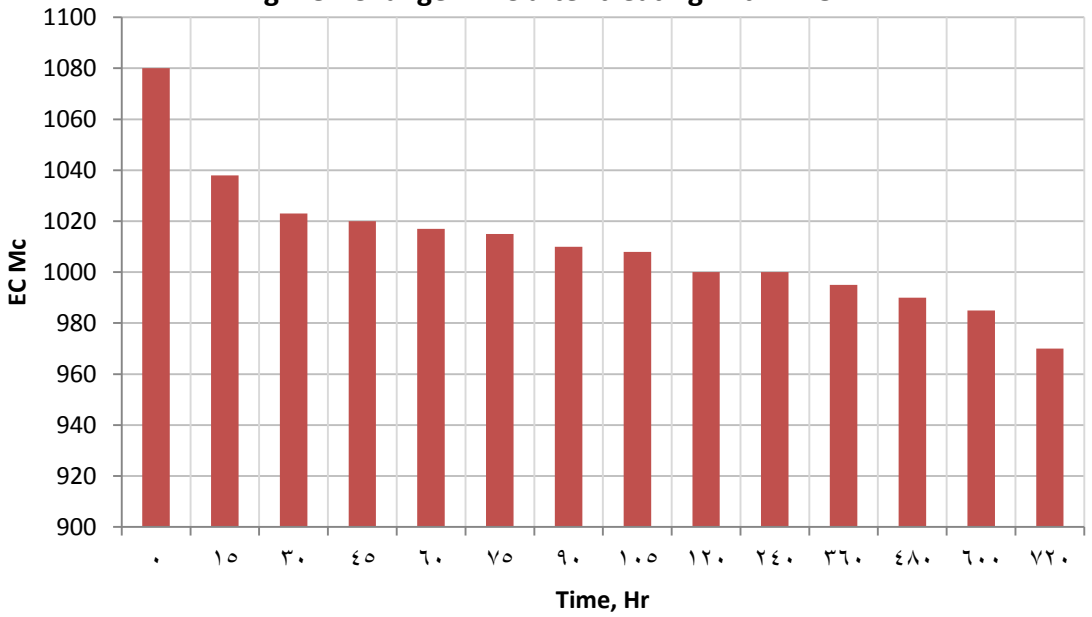

Fig. 20 : Change in PH after treatment H2O2

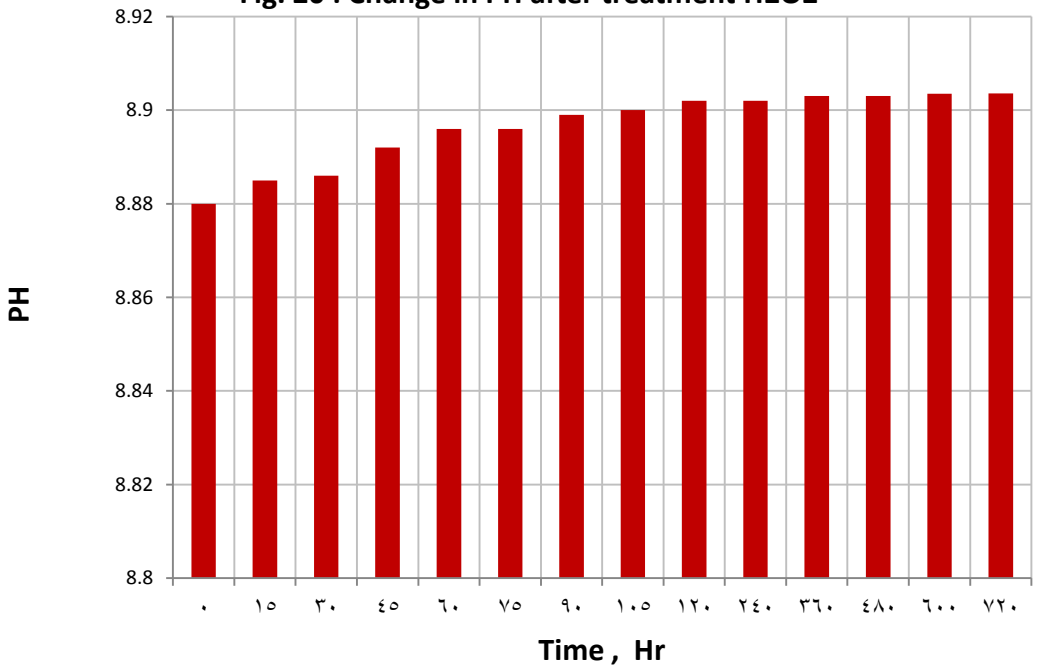

Discussion

Results showed relation between Tss, Tds, Ph, & EC tests to the contaminated water before and after chemical pretreatment by using different medias (H2O2, Chlorine and Detol) in different concentrations where used to treat this water before using final stage ultra violet

treatment. We found that the water at final stage was better after using H2O2 gave best results then it concluded that this media was better in dealing with infected water

Before starting treatment by using UV, preliminary treated the waste water by chemical additives (Dettol, Chlorine and H2O2), we noticed that:

1- Figures 4,5,6 show the change in TSS values over one week , the results showed that H2O2 gave best results were the values ranked between 310-125 mg/L, while the other additives where between 1020-310 mg/L.
2- Figures 7,8,9 , the increase in TDS was in H2O2 Media, where the suspended solids were decreased using H2O2.
3- Figures 10,11,12 the electrical conductivity increased using three additives, the minimum increase in EC was in Dettol additive
4- Figures 13,14,15 showed that the PH is increasing from acidity to nutral value 7 using chlorine but in using H2O2 was more than 8
5- the best chemical treatment was H2O2 , so we used it in UV treatment as it was discussed .

   After one hour UV treatment showed that :
6- Figure 16 for TSS using UV treatment comparing between initial treatment with time was 600 is decreased to 280 mg/L.
7- Figure 17 for TDS using UV treatment comparing between initial treatment with time was 565 is decreased to 375 mg/L.
8- Figure 18 for EC using UV treatment comparing between initial treatment with time was 1080Mc is decreased to 970 Mc.
9- Figure 20 for PH using UV treatment comparing between initial treatment with time was 6.5 is increased to 8.9.

Conclusions

1- Advanced oxidation processes are defined as those which involve the generation of hydroxyl radicals in sufficient quantity to affect water purification. UV light is a natural process and does not produce harmful chemicals in water. It’s a safe, effective and environmentally friendly disinfection method that is widely used for residential and industrial applications around the world.

2- UV does not add any chemical taste or odor to the water
3- One of the most effective ways to kill disease-causing microbes by destroying 99.99%.
4- UV treatment is not enough to purify water down to drinking water purposes. This is because the UV radiation is only effective for treating bacteria and viruses.
5- For future studies must use other chemical s and other techniques.

References

1- Crites, R. and G. Tchobanoglous. 1998. *Small and Decentralized Wastewater Management Systems.* The McGraw-Hill Companies. New York, New York.

2- Darby, J.; M. Heath; J. Jacangelo; F. Loge; P. Swaim; and G. Tchobanoglous. 1995. *Comparison of UV Irradiation to Chlorination: Guidance for Achieving Optimal UV Performance.*

3- Water Environment Research Foundation. Alexandria, Virginia Fahey, R. J. Dec. 1990. "The UV Effect on Wastewater." *WaterEngineering & Management.* vol. 137. no. 12. pp. 15–18.

4- Kwan, A.; J. Archer; F. Soroushian; A. Mohammed; and G. Tchobanoglous. March 17–20, 1996. "Factors for Selection of a High-Intensity UV Disinfection System for a Large-Scale Application." Proceedings from the Wate Environment Federation (WEF) Speciality Conference: *Disinfecting Wastewater for Discharge and Reuse.* WEF. Portla

5- Ozone: science & engineering: the journal of the international ozone association, volume 9, issue 4, 1987

6-Glossary of commonly used terms in wastewater treatment and sewage pollution control

7-http://www.freedrinkingwater.com/whole-house/water-filter-knowledge-base/how-does-ultraviolet-water-purification-work.ht

8- Advanced oxidation of raw and biotreated textile industry wastewater with O_3, H_2O_2 /UV-C and their sequential application/ Idil Arslan and Isil

Akmehmet Balcioglu* , Journal of Chemical Technology and Biotechnology Volume 76, Issue 1, pages 53–60, January 2001.

9- Process Optimization of Chemical Phosphorus, Removal in Wastewater Treatment Facilities/ Jega Jeganathan, Ph.D., P.Eng., R.V. Anderson Associates Limited

Preliminary investigation study of wind energy at Tuz-Khormatu in Iraq.

*Samah Shyaa Oudah, **Mohammed A. Salah.

*Private researcher in wind energy projects.

**Ministry of Electricity/Iraq.

Corresponding Author; Samah Shyaa Oudah, jnbjnb29@yahoo.com

Abstract

The aim of the present work is an investigation of wind energy potential for construction a wind farm in (Tuz-Khormatu) in Iraq using the world wind map of RETScreen software. The wind data were obtained from RETScreen and Windographer programs for 15 years and eight months. Three wind turbines were selected from the library of the RETScreen and matched with wind data to assess the potential of the proposed wind farm at the selected site (Tuz-Khormatu).The wind turbine model (Enercon-33-50m,330KW) has the highest capacity factor 31.5% and the maximum wind energy from the wind farm 6874 MWh/year .

Keywords: RETScreen, Wind Turbine, shape factor, scale factor, wind energy, capacity factor.

1. Introduction

The potential of wind energy in Iraq has not been yet fully explored due to the lack of an accurate reliable and historical wind data at most of the regions in Iraq, so the data is insufficient to evaluate and select the suitable sites for the wind power project development. At present, a few numbers of sampling small scale wind turbines were erected by the ministry of science and technology in Iraq.

To developed more wind energy application; this work will assist in defining the promising site for wind projects for rural electrification in Iraq. The RETScreen software can be used to evaluate the energy production and savings, costs, and other aspects for various types of Renewable-energy and Energy Efficient Technologies (RETs)[1].

H. R. Hermannsson [2] made an examination of two computer programs for estimating wind energy, RETScreen and System Advisor Model (SAM), and compared to measured data from a wind farm. He found that the Wind speed and electrical production estimated by RETScreen underestimates the electrical production by 35% and SAM overestimates it by 26%.

S. Rehman [3] has studied wind farms of 30MW installed capacity at five coastal locations in Saudi Arabia by using RETScreen software. Among the five proposed areas, he found that the only two sites at Yanbo and Dhahran would be an economically feasible for the wind park development considering with 1500, 1000, and 600 kW machine.

In the present work, 6MW proposed wind energy project is supposed for rural electrification at (Tuz-Khormatu). RETScreen software 4 was used to demonstrate the energy modeling of proposed wind farm construction at that site.

2. Wind data source

The assessment of wind resource is the major process to evaluate the potentiality of wind energy of the candidate site. It is recommended to use direct measurements wind data to accurate assessment by tower masts to get long term data acquisition. However, in Iraq the available data is still not covering all the regions. Figure 1 shows the map of Tuz-Khormatu (35.31 latitude, 44.33 longitude).

An hourly wind data were downloaded for this site by using RETScreen at10 m above ground level (a.g.l) and the daily wind data were downloaded from Windographer at 50 m from January of 2000 to August of 2015 (15 years And eight months).

Fig.(1): Tuz-Khormatu map.

3. Wind power density

The wind power density at a site shows expected electrical energy produced by the wind turbine by using wind speed data for selected site. RETScreen calculate wind power using the input wind speed data and air density with a value of 1.225 kg/m³ with standard sea level pressure and a temperature of 15°C. The energy calculations were performed using RETScreen Software, more details can be found in many references [4, 5].

To obtain the Weibull parameters K_h and C_h at different hub heights of wind turbines by using the following equations [6, 7]:-

$$K_h = K_o * \left[1 - 0.0881 * \ln\left(\frac{h_o}{10}\right)\right] / \left[1 - 0.0881 * \ln\left(\frac{h}{10}\right)\right] \quad \text{.....(1)}$$

$$C_h = C_o * \left(\frac{h}{h_o}\right)^{\alpha} \quad \text{.....(2)}$$

Where C_o and K_o are the scale and shape factors, respectively, at the measurement height h_o, and h is the hub height.

The losses of the wind turbines are expressed as coefficient (CL) in the following Eq. (3), specify array loss, airfoil loss and miscellaneous loss are specified in RETScreen models [4,5].

$$CL=(1-\lambda a)\times(1-\lambda s\&i)\times(1-\lambda d)\times(1-\lambda m) \quad \text{.....(3)}$$

Where,

, λa = Array loss, λs&i= Airfoil soiling and icing loss, λd = Downtime loss, λm = Miscellaneous loss.

Table 1 shows the typical and the used values of losses parameters and the rate of electricity absorption which were used in as an input data in RETScreen [7].

Table 1: typical and the used values of losses parameters [7].

Type of losses	Typical value	Used value
Array loss	1-8%	2%
Airfoil soiling and icing loss	1 to 10%	1%
Downtime loss	2 to 7%	3%
Miscellaneous loss	2 to 6%	2.2%
Availability (absorption rate)	98-100%	98

The wind shear coefficient (n) was calculated for each month and the average yearly values were computed using the following equation (4)[8]:-

$$n = [0.37 - 0.088 \ln(c_o)] / \left[1 - 0.088 \ln\left(\frac{h}{10}\right)\right] \quad \text{.....(4)}$$

4. Wind turbine selection

Three wind turbines were selected from the library of RETScreen 4 program to study the proposed site which considers as poor site (class1) according to the classification classes of wind power densities of International Electro technical Commission (IEC61400-1) [9]. The power curve of these turbines is shown in Figure (2). these types of wind turbine can operate at 3m/s.

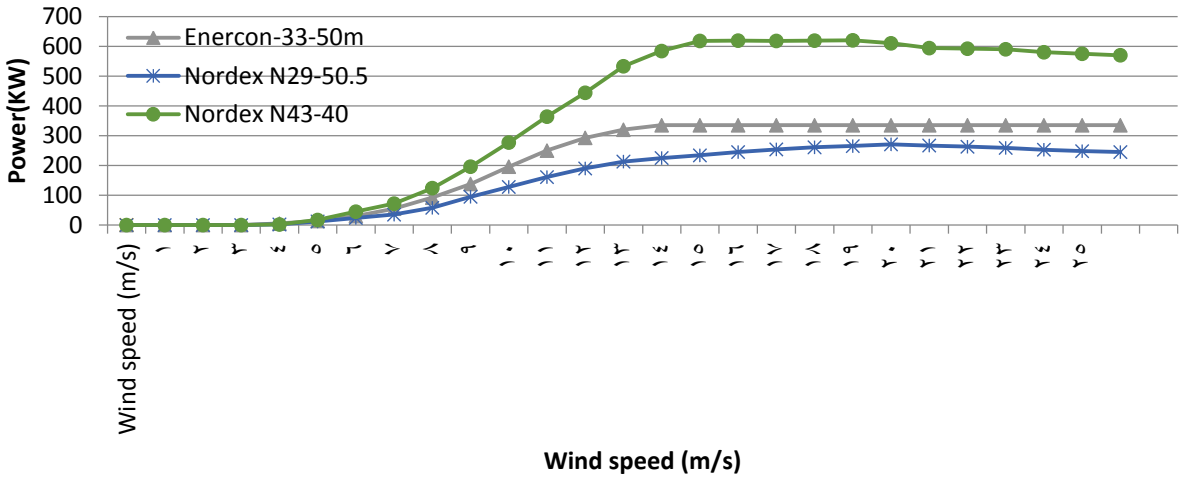

Fig. (2): Power curve of the selected wind turbines at Tuz-Khormatu site[8].

The gross energy production can be computed by the following Eq. [4,5,10].

EG=EU CH CT ... .(5)

Where, EU is the unadjusted energy production, and CH= P/P0 (P is the annual atmospheric pressure at the site and P is the standard atmospheric pressure of 101.3 kPa).

And CT = T0/T (T is the annual average absolute temperature at the site and T0 is the standard absolute atmospheric temperature of 288.1K).

The RETScreen computes the pressure adjustment coefficient and temperature adjustment coefficient automatically from online weather database. The capacity factor can be calculated as the ratio of the energy produced by wind turbine to the energy produced by the operating wind turbine at the rated power throughout the time period expressed in Eq.(6)[5,8].

CF=(EA/(Pr×T))×100 .....

(6)

In which, CF is the capacity factor, EA is the actual energy produced by the wind turbines, Pr is the rated power capacity of the wind turbines, T is the duration of operation in hours. In the models, the gross annual energy production (MWh) and the capacity factor were calculated for the selected wind turbines.

5. Results and Discussions

5.1. Wind data results

The monthly and annual average wind speeds were calculated from the original hourly and daily data from RETScreen and Windographer respectively. The monthly and annual average wind speeds at 10m and 50m are shown in Figure (3).

The average annual wind speed was found to be 3.145 m/s and 3.268 from RETScreen and Windographer at 10m respectively. At 50m, the average annual wind speed was found to be 5.0 m/s and 4.86 from RETScreen and Windographer respectively.

The largest values of wind speeds occur during the summer season, exceeding 6m/s at June month at RETScreen wind data. This is important to generate largest wind energy when maximum demand of electricity is needed while the lowest values were obtained during the winter months.

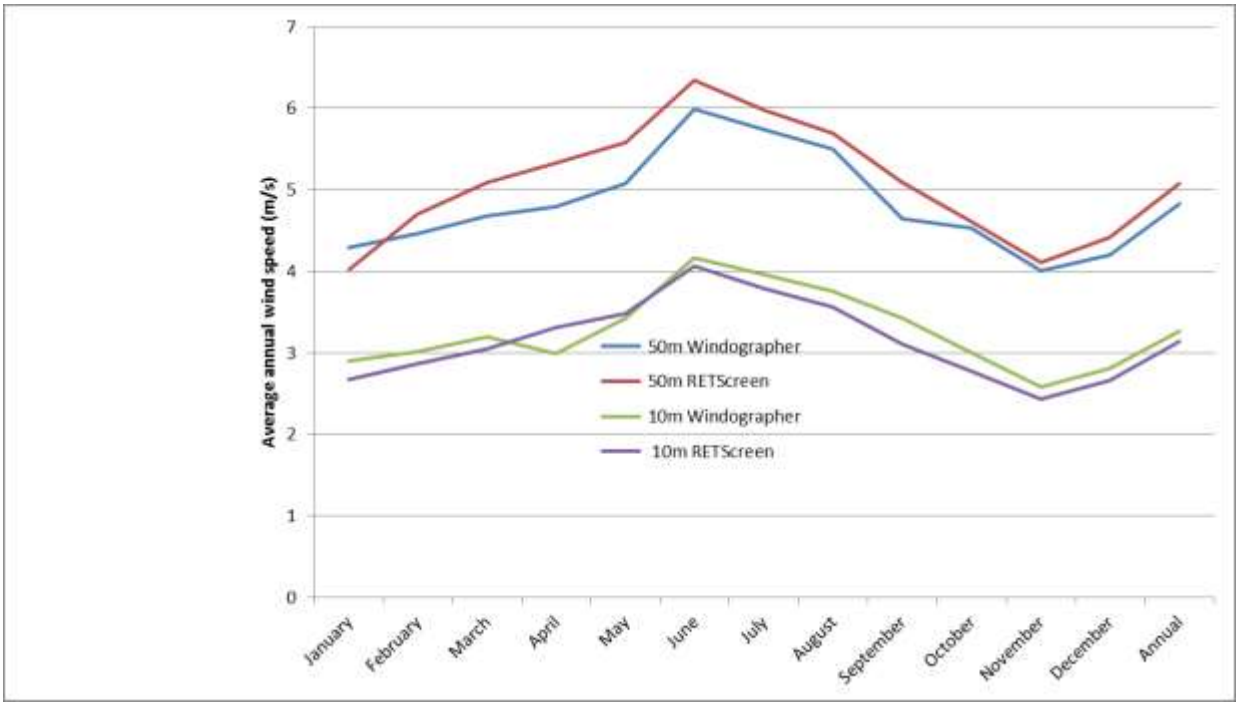

Fig. (3): Monthly and annual average wind speed graphs.

At 10m as shown in Table 2, the average monthly and annually values of the shape factor (k), yielded from RETScreen wind data reflect that the selected site changeable wind regime when k

values less than 2.0 and stable when k values more than 2.0 with an average annual value of 2.26.The stable wind regime site will be more suitable for wind turbines erecting. It was found also that the k values from Windographer wind data were more than 2.0 at all months with an annual value of 3.108, which means more stability wind regime site. The values of scale parameter c is a function of wind speed and represents the breadth of wind distributions along with x axes, The higher scale parameter value, the windier the place is. The maximum values of scale parameter exceeding 4.0 m/s during the summer months when maximum wind speeds were obtained and the average annual values were3.66 m/s and 3.269 m/s from RETScreen and Windographer respectively.

Table 2: Weibull parameters values at 10m.

Month		Jan.	Feb.	March	April	May	Jun.	July	Aug.	Sep.	Oct.	Nov.	Dec.	Ann.
RETS.	K_{10}	1.70	1.82	1.791	1.59	2.60	2.95	2.82	2.95	2.91	2.39	1.86	1.70	2.26
	C_{10}	3.24	3.38	3.591	3.34	3.86	4.66	4.44	4.20	3.84	3.38	2.91	3.14	3.66
Windog.	K_{10}	2.30	2.84	2.395	3.2	3.81	3.85	3.41	3.71	3.18	3.40	2.66	2.46	3.10
	C_{10}	3.26	3.38	3.60	3.34	3.79	4.59	4.40	4.15	3.82	3.34	2.90	3.16	3.26

The wind shear values were computed by using Eq.(4) at both 10m and hub height. The annual average values of wind shear were 0.32 and 0.33 at 10m from RETScreen and Windographer respectively as shown Figure (4), while this value decrease to 0.29 at 50m hub height. It is obvious as the wind speed increase with the altitude, the wind shear decreases and causing more wind energy harvesting at hub height level.

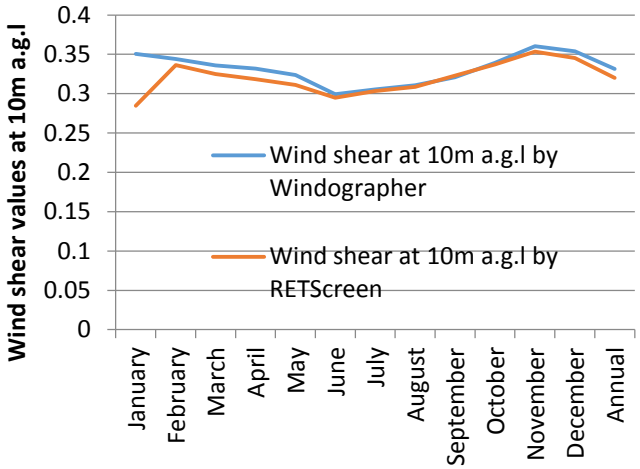

Fig. (4): Wind shear values at 10m.

5.2. Results related to selected wind turbines.

Three wind turbine models were selected and the wind speed characteristics at hub height of selected wind turbines shown in Table 3 and Figure (5). The average wind speed 5.07m/s at the height 50 m for both (Enercon-33, Nordex N29) and 4.7m/s for (Nordex N43) models, These wind speeds are not so high. Both shape and scale parameters were computed at hub height of the wind turbines using Eqs.(1 and 2) and these values are shown in the Figure (5).

Table 3: Wind speed characteristics at hub height of selected wind turbines.

Wind turbine model	Hub height (m)	Average annual Wind shear n_h	Average annual wind speed V_h	Average annual shape factor K_h	Average annual scale factor C_h
Enercon-33	50	0.297	5.077	2.633	5.923
Nordex N29	50.5	0.297	5.077	2.633	5.923
Nordex N43	40	0.291	4.707	2.574	5.492

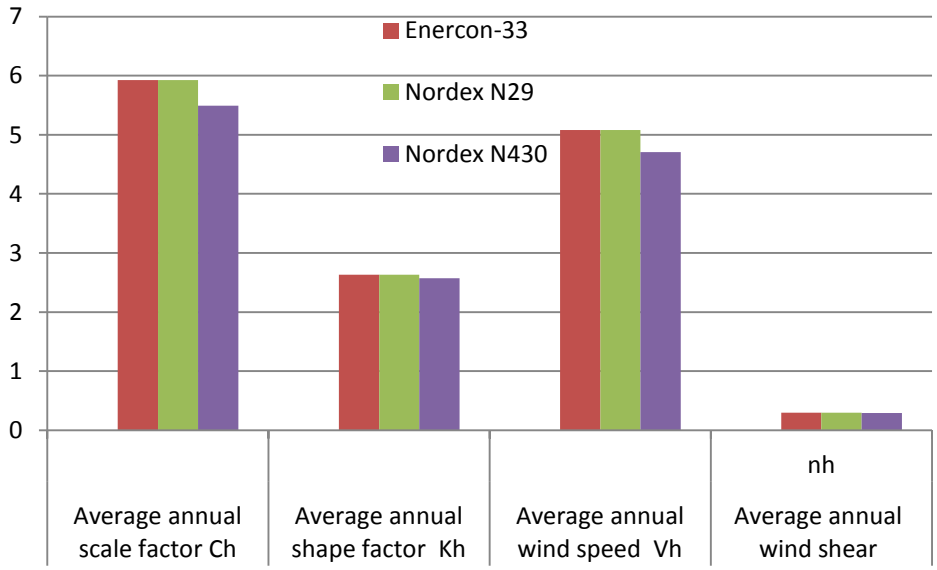

Fig. (5): Wind speed characteristics at hub height of selected wind turbines.

It was found that the results from RETScreen and Windographer software's were closely in their values, so the author neglects the results from Windographer and adopted only the results of RETScreen at all the next calculations.

To construct proposed wind farm at Tuz-Khormatu with a capacity of 6000KW,it was found needing for 19, 24 and 10 wind turbines from the selected models (Enercon-33, Nordex N29, Nordex N43) respectively.

The capacity factor (CF) of each wind turbine was recalculated with respect to RETScreen wind speeds frequencies.

As shown in Table 4,shows that the maximum CF is 31.5% for Enercon-33 wind turbine, hence, the highest capacity factor represents one of the indicators for assessing the performance of wind turbine, while the other two turbines (Nordex N29, NordexN43) have lower a capacity factor of 25.8%.

The calculated delivered energy from RETScreen using the Eqs.(3 and 5) is (6874MWh) from Enercon-33 wind turbines as shown in Table 4 and Figure. (6).

The yearly energy obtained from the wind turbine models (Nordex N29 and Nordex N43) were found with values of 5923MWh and 4138MWh respectively.

Table 4: Results of capacity factor and accumulated energy output for selected wind turbines.

Wind turbine model	No. of wind turbines	Rated Power Pr(KW)	Capacity factor CF	Total wind Energy of the wind farm/year (MWh)
Enercon-33	19	330	0.3151	6874
Nordex N29	24	250	0.2583	5923
Nordex N43	10	600	0.2583	4138

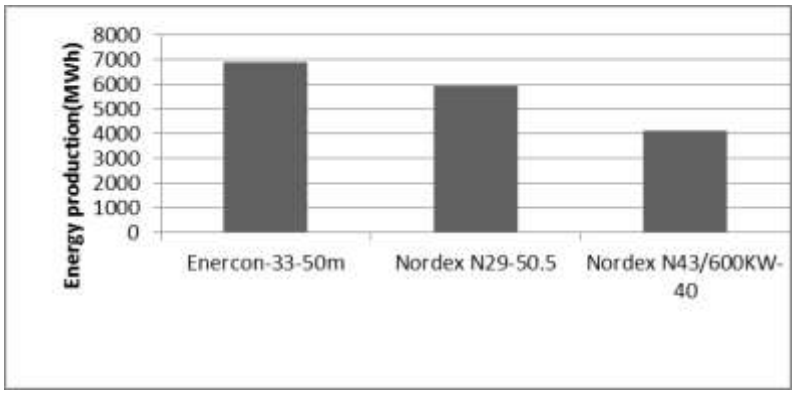

Fig. (6): Annual energy yielding from the wind farm.

6. Conclusion

In this proposed wind farm of 6MW capacity at Tuz-Khormatu site, it can be concluded that the wind turbine model (Enercon-33) with 19 units can produce electricity of 6874MWh/year that is because the highest capacity factor which was found as 31.5%, and represents one of the indicators for assessing the performance of the wind turbine.

From productivity point of view the wind turbine model (Enercon-33) represent the highest choice for constructing the proposed wind farm than the other two models Nordex N29 and Nordex N43, which their capacity factors were found as 25.83%.

The primary founding of wind speeds from RETScreen program shows that the case study site at Tuz-Khormato represent a low wind speed site and suitable for low wind speed wind turbine models.

7. Recommendation

For a reliable and accurate future work, the results from RETScreen will be required to check in comparison with on-site measuring data and observing the error percentage by setting up tower masts and measuring instruments of wind data in the proposed site and comparing the two results.

8. References

[1]. Leng, G. J., Monarque, A., Graham, S., Higgins, S., and Cleghorn, H., "RETScreen International, Results and Impacts: 1996-2012," Minister of National Resources, Canada, 2004.

[2]. Hermann Reynir Hermannsson, "Assessment of Wind Energy Production Software", University of Washington, 2013.

[3]. Shafiqur Rehman, "Prospects of wind farm development in Saudi Arabia", Renewable Energy, vol.30, pp. 447-463, April 2005.

[4]. RETScreen International Clean Energy Decision Support Centre: RET Screen Software Online User Manual; Wind Energy Project Model, Canada

[5]. RETScreen International, Software manual, Chapter 2, Wind energy project analysis. Available from: www.retscreen.net.

[6]. Jaramillo OA, Salaña R, Miranda U. Wind power potential of Baja California Sur, México. Renewable Energy; 29:2087-2100, 2004.

[7] Product data, www.retscreen.net, March 2004.

[8]. RETScreen International, www.retscreen.net.

[9]. "International Electro technical Commission" (IEC), Website www.iec.ch/Design And Application, 2nd edn. Wiley, Chichester (2009).

[10]. Ohunakin, O.S., Adaramola, M.S., Oyewola, O.M., 2011b. Wind energy evaluation for electricity generation using WECS in seven selected locations in Nigeria.Applied Energy http://dx.doi.org/10.1016/j.apenergy.2011.03.022.

Design and construction of battery (Deep cycle) specially for electrical power storage with specifications of 12V/60Ah

Dr. jaafar Ali Al-anbary

Energy and renewable energies technology centre
University of Technology Baghdad

Abstract:

The automotive Lead-acid starting batteries are designed to have high current at short time, low energy storage and relatively low life-cycle, but the batteries specializes for the renewable energies systems must have high storage energy and high life cycle.

The plate design of deep cycle batteries are different than that of automotive starting batteries. Where the grid metal used in the deep cycle battery plate is specifically formulated to increase the adhesion of high-density active paste material and thick lead cell grid to withstand the acid corrosion, this provides high life cycle.

This research clarify the most important properties and the components of the lead-acid battery, for both types automotive starting and renewable energies systems, then defend briefly the effective parameter in its performance, the weight of the effective material, the cell grid thickness, time of charging and discharging cycle, acid density and operating temperature.

After definition of the most factors that prolong battery life and improve its capacity, all this are taken into account in the design and construction of many cells with energy storage capacity about (60A 2V),the grid thickness is increased from 1,5 to 2,5mm, and the acid density is reduced from 1,25 to 1,1 to reduce the grid corrosion. Finally three batteries can be assembled ,the batteries then submit to actual testing process f purpose of the performance evaluation, followed check the percentage of plate corrosion in positive plate along three years, and finally construct three batteries capacity of (60A 12V), it work for long period about three year with acceptable performance.

تحسين أداء بطاريات خزن الطاقة .

الخلاصة:

بطاريات الرصاص الحامضية الخاصة بتشغيل السيارات لها القابلية على إعطاء تيار كهربائي كبير ولفترة تشغيل قليلة وقصر عمرها التشغيلي. ولكن البطاريات الخاصة بخزن الطاقات المتجددة تمتاز بالسعة العالية للطاقة المخزونة وعمرها الطويل.

إن تصميم الشبكة والتركيب الكيميائي لخلايا بطارية خزن الطاقة تختلف عن مثيلاتها المستخدمة لتشغيل السيارات، حيث أن شبكات خلايا خزن الطاقة لها خاصية التصاق كبير بالمادة الفعالة ذات السعة الكبيرة لخزن الطاقة ويكون سمكها كبير نسبيا لمقاومة التآكل وبالنتيجة زيادة عمر البطارية بأكبر عدد من دورات التشغيل.

يوضح هذا البحث أهم مواصفات ومكونات بطاريات تشغيل السيارات وأخرى لخزن الطاقة. ويبين أهم العوامل التي تؤثر في أداء البطاريات، منها سمك مشبك الخلايا ووزن المادة الفعالة وسرعة دورة الشحن والتفريغ وكثافة المحلول ألحامضي ودرجة حرارته وتأثير الفترة الزمنية التي تبقى فيها البطارية فارغة وعوامل تشغيلية أخرى.

بعد تعريف من أهم العوامل التي تطيل من عمر البطارية وتحسين قدرتها، تم أخذ كل هذا في الاعتبار عند تصميم وبناء العديد من خلايا البطارية (60A 2V)، حيث تم زيادة سماك الشبكة الحاملة من 1،5 إلى 2,5 ملم، وتم تقليل كثافة الحامض من 1،25 إلى 1،1غم/سم^3 وذلك للحد من تآكل الشبكة. وأخيرا تم تجميع 3 بطاريات، ثم إجراء الاختبارات الفعلية عليها لغرض تقييم الأداء، ثم تحقق من نسبة التآكل في اللوح الموجب لمدة ثلاث سنوات، وأخيرا تم بناء ثلاث بطاريات سعة (60A 12V) وهي تعمل بكفاءة مقبولة.

Introduction:

A battery is a device that converts the chemical energy contained in its active materials into electrical energy by means of an electrochemical reaction. While the term "battery" is often used, the basic electrochemical element being referred to is the cell. A battery consists of two or more cells electrically connected in series to form a unit.

In 1859, Gaston Planté's lead-acid battery was the first battery that could be recharged by passing a reverse current through it. Planté's first model consisted of two lead sheets separated by rubber strips and rolled into a spiral, [1]. His batteries were first used to power the lights in train carriages while stopped at a station. In 1881, Camille Alphonse Faure invented an improved version that consisted of a lead grid lattice into which a lead oxide paste was pressed, forming a plate. This design was easier to mass-produce.

The lead-acid battery is still used today in automobiles and other applications in which greater weight is acceptable. In the 1970s the valve-regulated lead acid battery often called "sealed" was developed; it used a gel electrolyte instead of a liquid, allowing the battery to be used in different positions without leakage.

Fig. (1) shows the construction of a lead-acid battery. First the container of the cells, most containers are hard rubber, plastic, or some other material that is resistant to the electrolyte and mechanical shock and will withstand extreme temperatures. The container or battery case is vented through vent plugs to allow the gases that form within the cells to escape.

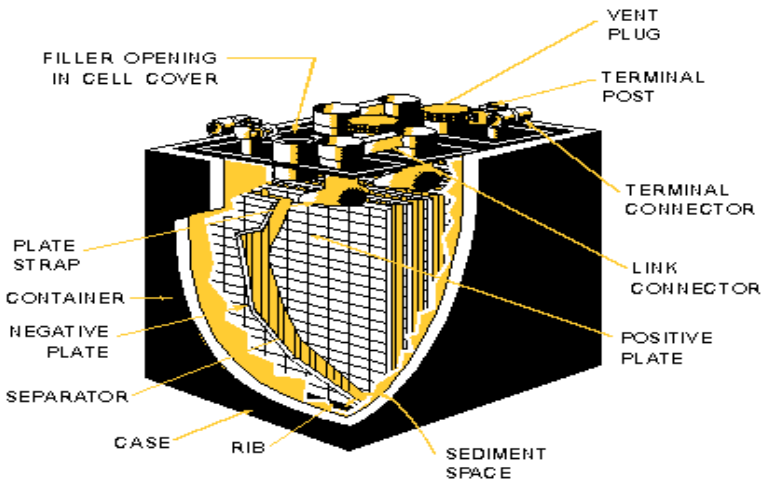

Fig. (1), The construction of Lead-acid battery,[2]

Second the plates in the battery are the cathodes and anodes, fig.(2) show the negative plate group is the cathode of the individual cells and the positive plate group is the anode, the plates are interlaced with a terminal attached to each plate group. The terminals of the individual cells are connected together by link connectors as shown below. The cells are connected in series in the battery and the positive terminal of one end cell becomes the positive terminal of the battery. The negative terminal of the opposite end cell becomes the negative terminal of the battery.

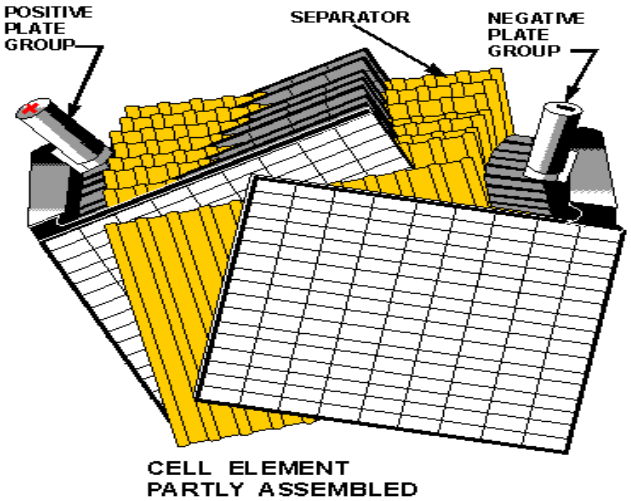

Fig. (2), Lead-acid battery plate arrangement in the cell.

Most of the world's lead–acid batteries are automobiles starting, lighting and ignition batteries, with an estimated 320 million units shipped in 1999. [1] In 1992 about 3 million tons of lead is used in the manufacture of batteries.

The starting batteries:

Lead acid batteries designed for starting automotive engines are not designed for deep discharge. They have a large number of thin plates designed for maximum surface area, and therefore maximum current output, but which can easily be damaged by deep discharge. Repeated deep discharges will result in capacity loss and ultimately in premature failure, as the electrodes disintegrate due to mechanical stresses that arise from cycling. Starting batteries kept on continuous float charge will have corrosion in the electrodes which will result in premature failure. Starting batteries should be kept open circuit but charged regularly (at least once every two weeks) to prevent sulfation.

Starting batteries are lighter weight than deep cycle batteries of the same battery dimensions, because the cell plates do not extend all the way to the bottom of the battery case. This allows loose disintegrated lead to fall off the plates and collect under the cells, to prolong the service life of the battery. If this loose debris rises high enough it can touch the plates and lead to failure of a cell, resulting in loss of battery voltage and capacity. [3]

The deep cycle batteries:

Specially designed deep-cycle cells are much less sensitive to frailer due to cycling, and are required for applications where the batteries are full discharged, such as photovoltaic and wind systems, electric cars and other. These batteries have thicker plates that can deliver less peak current, but can withstand frequent discharging.

Some batteries are designed as a compromise between starter (high-current) and deep cycle batteries. They are able to be discharged to a greater degree than automotive batteries, but less so than deep cycle batteries. Fig. (3) shows the construction of the deep cycle battery. [3]

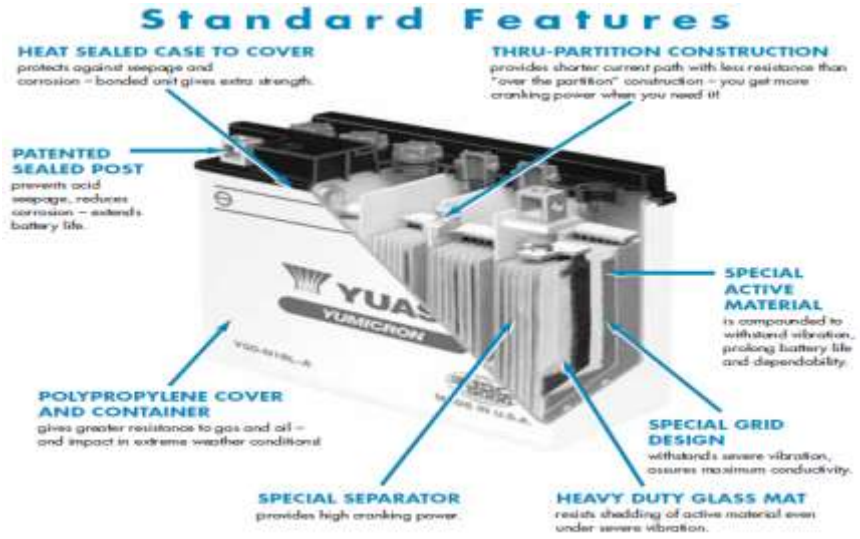

Fig(3) show the construction of deep cycle battery. [3]

Battery lack ability to recharging;

Lead–acid batteries lose the ability to accept a charge when discharged for too long due to sulfation, the crystallization of lead sulfate. They generate electricity through a double sulfate chemical reaction. Lead and lead dioxide, the active materials on the battery's plates, react with sulfuric acid in the electrolyte to form lead sulfate. The lead sulfate first forms in a finely divided, amorphous state, and easily reverts to lead, lead dioxide and sulfuric acid when the battery recharges. As batteries cycle through numerous discharges and charges, some lead sulfate is not recombined into electrolyte and slowly converts to a stable crystalline form that no longer dissolves on recharging. Thus, not all the lead is returned to the battery plates, and the amount of usable active material necessary for electricity generation declines over time fig(4) show the condition of the battery blades. Cathode plate (left) and sulfated anode plate (right) from 12V 5aH battery. [4]

Fig(4) show the condition of the battery plates.

Sulfation occurs in all lead–acid batteries during normal operation. It impedes recharging; sulfate deposits ultimately expand, cracking the plates and destroying the battery. Eventually so much of the battery plate area is unable to supply current that the battery capacity is greatly reduced. In addition, the sulfate portion (of the lead sulfate) is not returned to the electrolyte as sulfuric acid. The large crystals physically block the electrolyte from entering the pores of the plates. Sulfation can be avoided if the battery is fully recharged immediately after a discharge cycle. A white coating on the plates may be visible (in batteries with clear cases, or after dismantling the battery). Batteries that are sulfated show a high internal resistance and can deliver only a small fraction of normal discharge current.

Efficiency of the battery:

Battery efficiency is highly dependent on the way a battery is charged and discharged but is likely to be in the range of 50% to 75%, although efficiencies up to of 90% can be achieved. It is convenient to calculate the columbic or Amp hour (Ah) efficiency of a battery: [5]

$$\eta = \frac{\text{Charge_Out_(Ah)}}{\text{Charge_In_(Ah)}}\% \qquad \text{……(1)}$$

The energy or watt hour efficiency would be calculated by multiplying amp hours by battery voltage. However, although we consider battery voltage as a constant it is not. During discharge cell voltage drops from 2.048 volts to around 1.7 volts. During charge voltage at the terminals varies depending on the charger but may range from 2.2 volts to 2.5 volts or higher for a 2 volt (nominal) battery. Calculating energy in and out is therefore a function of time varying voltage. Current flow and time i.e. amp hours are a far easier and therefore more convenient parameter to work with. Battery efficiency varies with current flow as losses are converted to heat which is an exponential (I^2R) relationship. To obtain the overall efficiency other system losses must be accounted for such as battery charger losses and wiring losses.

Theory:

Lead-Acid Battery Active Materials;

The active materials in a battery are those that participate in the electrochemical charge/discharge reaction. These materials include the electrolyte and the positive and negative electrodes. As mentioned earlier, the electrolyte in a lead-acid battery is a dilute solution of sulfuric acid (HSO). The negative electrode of a fully charged battery is24 composed of sponge lead (Pb) and the positive electrode is composed of lead dioxide (PbO).2 [6]

Electrochemistry of the Lead-Acid Cell:

All lead-acid batteries operate on the same fundamental reactions. As the battery discharges, the active materials in the electrodes (lead dioxide in the positive electrode and sponge lead in the negative electrode) react with sulfuric acid in the electrolyte to form lead sulfate and water. On recharge, the lead sulfate on both electrodes converts back to lead dioxide

2-(positive) and sponge lead (negative), and the sulfate ions (SO) are driven back into the4 electrolyte solution to form sulfuric acid. The reactions involved in the cell follow.

Discharge:

Fig.(5) Fully Discharged: Two identical lead sulfate plates.

In the discharged state both the positive and negative plates become lead sulfate ($PbSO_4$) and the electrolyte loses much of its dissolved sulfuric acid and becomes primarily water, as show in fig(5). The discharge process is driven by the conduction of electrons from the negative plate back into the cell at the positive plate in the external circuit. [7]

At the positive electrode.

$$pbo_2 + 3H^+ + HSO_4^- + 2e \Leftrightarrow Pbso_4 + 2H_2O(1.685V) \text{ ……..(2)}$$

At the negative electrode

$$Pb + HSO^-{}_4 \Leftrightarrow PbSO_4 + H^+ + 2e^-(0.356V) \text{ ……(3)}$$

For the overall cell

$$PbO_2 + Pb + 2H_2SO_4 \Leftrightarrow 2PbSO_4 + 2H_2O(2.041) \text{ ……(4)}$$

Therefore the maximum open-circuit voltage that can be developed by a single lead-acid cell is. 2.041v.

The sum of the molecular weights of the reactants is 642.6, so theoretically a cell can produce two faradays of charge from 642.6 g of reactants, or 83.4 amp-hours per kg (or 13.9 amp-hours per kg for a 12-volt battery). At 2 volts per cell, this comes to 167 watt-hours per kg, but lead-acid batteries in fact give only 30 to 40 watt-hours per kg due to the weight of the water and other factors. [7]

Charging:

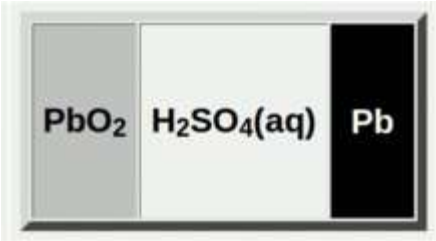

Fig.(6) Fully Charged: Lead and Lead Oxide plates

In the charged state as shown in fig(6), each cell contains negative plates of elemental lead (Pb) and positive plates of lead oxide (PbO_2) in an electrolyte of approximately 33.5% *v/v* (4.2 Molar) sulfuric acid (H_2SO_4). The charging process is driven by the forcible removal of electrons from the positive plate and the forcible introduction of them to the negative plate by the charging source.

Parameter effecting the battery performance:

Fast and slow charge and discharge:

Charge current needs to match the ability of the battery to absorb the energy. Using too large a charge current on a small battery can lead to boiling and venting of the electrolyte, battery case has ballooned due to the high gas pressure developed during overcharge.

The capacity of a lead–acid battery is not a fixed quantity but varies according to how quickly it is discharged. An empirical relationship exists between discharge rate and capacity, known as Peukert's law.

When a battery is charged or discharged, this initially affects only the reacting chemicals, which are at the interface between the electrodes and the electrolyte. With time, the charge stored in the chemicals at the interface, often called "interface charge", spreads by diffusion of these chemicals throughout the volume of the active material.

If a battery has been completely discharged (such as by leaving the car lights on overnight) and then is given a fast charge for only a few minutes, the battery plates charge only near the interface between plate and electrolyte. The battery voltage may rise to be close to the charger voltage so that the charging current decreases significantly. After a few hours this interface charge will spread to the volume of the electrode and electrolyte, leading to an interface charge so low that it may be insufficient to start the car, [8]

On the other hand, if the battery is given a slow charge, which takes longer, then the battery will become more fully charged. During a slow charge the interface charge has time to redistribute to the volume of the electrodes and electrolyte, while being replenished by the charger. The battery voltage remains below the charger voltage throughout this process allowing charge to flow into the battery.

Similarly, if a battery is subject to a fast discharge (such as starting a car, a current draw of more than 100 amps) for a few minutes, it will appear to go dead, exhibiting reduced voltage and power. However, it may have only lost its interface charge. If the discharge is halted for a few minutes the battery may resume normal operation at the appropriate voltage and power for its state of discharge. On the other hand, if a battery is subject to a slow, deep discharge (such as leaving the car lights on, a current draw of less than 7 amps) for hours, then any observed reduction in battery performance is likely permanent.

Gaston Planté found a way to provide a much larger effective surface area. In Planté's design, the positive and negative plates were formed of two spirals of lead foil, separated with a sheet of cloth and coiled up. The cells initially had low capacity, so a slow process of "forming" was required to corrode the lead foils, creating lead dioxide on the plates and roughening them to increase surface area. Initially this process used electricity from primary batteries; when generators became available after 1870, the cost of production of batteries greatly declined. Planté plates are still used in some stationary applications, where the plates are mechanically grooved to increase their surface area.

Faure pasted-plate construction is typical of automotive batteries. Each plate consists of a rectangular lead grid alloyed with antimony or calcium to improve the mechanical characteristics. The holes of the grid are filled with a paste of red lead and 33% dilute sulfuric acid. (Different manufacturers vary the mixture). The paste is pressed into the holes in the grid which are slightly tapered on both sides to better retain the paste. This porous paste allows the acid to react with the lead inside the plate, increasing the surface area many fold. Once dry, the plates are stacked with suitable separators and inserted in the battery container. An odd number of plates is usually used, with one more negative plate than positive. Each alternate plate is connected. The positive plates are the chocolate brown color of lead dioxide, and the negative are the slate gray of "spongy" lead at the time of manufacture. In this charged state the plates are called 'formed'.

One of the problems with the plates is that the plates increase in size as the active material absorbs sulfate from the acid during discharge, and decrease as they give up the sulfate during charging. This causes the plates to gradually shed the paste. It is important that there is room underneath the plates to catch this shed material. If it reaches the plates, the cell short-circuits.

Addition of the carbon:

The paste contains carbon black, blank fixe (barium sulfate) and lignosulfonate. The blank fixe acts as a seed crystal for the lead to lead sulfate reaction. The blank fixed must be fully dispersed in the paste in order for it to be effective. The lignosulfonate prevents the negative plate from forming a solid mass during the discharge cycle, instead enabling the formation of long needle like crystals. The long crystals have more surface area and are easily converted back to the original state on charging. Carbon black counteracts the effect of inhibiting formation caused by the lignosulfonates. Sulfonated naphthalene condensate dispersant is a more effective

expander than lignosulfonate and speeds up formation. This dispersant improves dispersion of barium sulfate in the paste, reduces hydroset time, produces a more breakage-resistant plate, reduces fine lead particles and thereby improves handling and pasting characteristics. It extends battery life by increasing end of charge voltage. Sulfonated naphthalene requires about one third to one half the amount of lignosulfonate and is stable to higher temperatures. [9]

Addition of alloying element :

Practical cells are usually not made with pure lead but have small amounts of antimony, tin, calcium or selenium alloyed in the plate material to add strength and simplify manufacture. The alloying element has a great effect on the life of the batteries, with calcium-alloyed plates preferred over antimony for longer life and less water consumption on each charge/discharge cycle.

Types of plate separators:

Separators between the positive and negative plates prevent short-circuit through physical contact, mostly through dendrites (‘treeing’), but also through shedding of the active material. Separators obstruct the flow of ions between the plates and increase the internal resistance of the cell. Wood, rubber, glass fiber mat, cellulose, and PVC or polyethylene plastic have been used to make separators. Wood was the original choice, but deteriorated in the acid electrolyte. Rubber separators were stable in the battery acid.

An effective separator must possess a number of mechanical properties; such as permeability, porosity, pore size distribution, specific surface area, mechanical design and strength, electrical resistance, ionic conductivity, and chemical compatibility with the electrolyte. In service, the separator must have good resistance to acid and oxidation. The area of the separator must be a little larger than the area of the plates to prevent material shorting between the plates. The separators must remain stable over the battery's operating temperature range.

Constructed of the deep cycle battery:

To construct the battery first we must produce the grid plate by casting process 4% antimony lead bass alloy is used for this process. Fig. (a-7) show the grid of lead antimony alloy and fig. (b-7) the grid covered by baste of lead oxide and sulfuric acid.

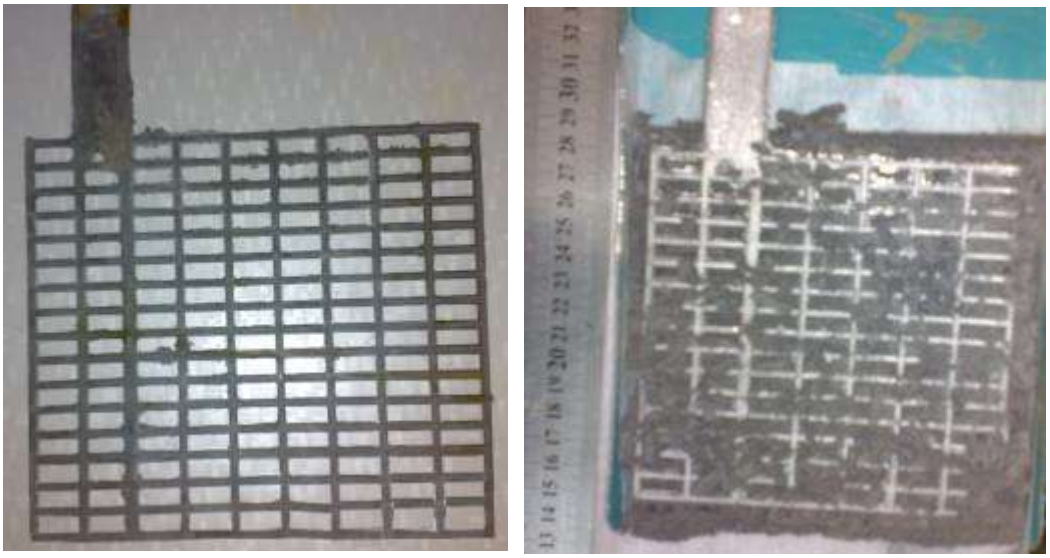

Fig(a-7) the grid of the cell and (b-7) the grid covered by the lead paste.

Second constructed the lead–acid cell using sheet lead plates for the two electrodes, separated by special insulator as polyethylene plastic, than all the cell compacted by binder as shown in fig.(8).

Fig(8) side and front view of the constructed battery cell.

Battery with teams of voltage 12v consist of 6 cells, and the total battery capacity is equal to the capacity of a each cell, so it was required to build a 6-cell and put it in a container of plastic material with 6 hole for the construction of the battery. As shown in Fig.(9).

Fig.(9) show how to build a 12-volt battery, composed of 6 cells.

3 batteries of this type was built, and these batteries submitted to load test. these batteries subjected to number of charging and full discharging operation, up to more than 500 times, during this process voltage and current of the battery was measure to find the amount of battery energy stored in each step of charging and discharging process. Figure (10) illustrates the method of measuring the energy stored in the battery.

Fig.(10) measuring the voltage and current values of the battery to calculate the amount of storage energy.

Voltages recommendation for common usages

These are general voltage ranges for *six-cell* lead-acid batteries: [10]

- Open-circuit (quiescent) at *full charge*: 12.6 V (2.1V per cell)
- Open-circuit at *full discharge*: 11.7 V
- Loaded at full discharge: 10.5 V.
- Continuous-preservation (float) charging: 13.4 V for gelled electrolyte; 13.5 V for absorbed glass mat and 13.9 V for flooded cells

- Typical (daily) charging: 14.2 V to 14.4 V (depending on temperature and manufacturer's recommendation)
- Equalization charging (for flooded lead acids): 15 V for no more than 2.205 hours. Battery temperature must be absolutely monitored.
- Gassing threshold: 14.4 V

Measuring the charge level:

Because the electrolyte takes part in the charge-discharge reaction, this battery has one major advantage over other chemistries. It is relatively simple to determine the state of charge by merely measuring the specific gravity (S.G.) of the electrolyte as shown in Fig.(11), the S.G. falling as the battery discharges. Some battery designs include a simple hydrometer using colored floating balls of differing density. When used in diesel-electric submarines, the S.G. was regularly measured and written on a blackboard in the control room to indicate how much longer the boat could remain submerged.[11]

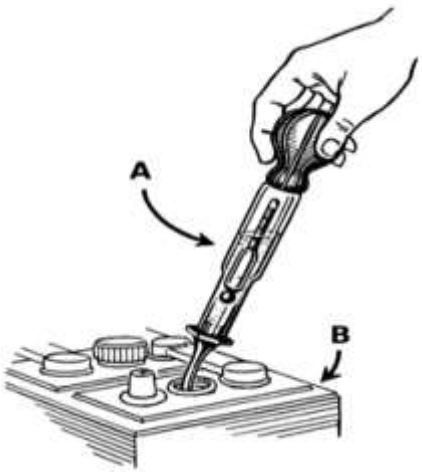

Fig.(11), A hydrometer can be used to test the specific gravity of each cell as a measure of its state of charge.

A battery's open-circuit voltage can be used to estimate the state of charge, in this case for a 12-volt battery.

The battery's open circuit voltage can also be used to gauge the state of charge. If the connections to the individual cells are accessible, then the state of charge of the each cell can be determined which can provide a guide as to the state of health of the battery as a whole.
Sulfation also affects the charging cycle, resulting in longer charging times, less efficient and incomplete charging, and higher battery temperatures.

Recovery of the dead battery:

Desulfation is the process of reversing the sulfation of a lead-acid battery. Desulfation is achieved by high current pulses produced between the terminals of the battery. This technique, also called *pulse conditioning*, breaks down the sulfate crystals that are formed on the battery plates.[16] Short high current pulses tend to work best. Electronic circuits are used to regulate the pulses of different widths and frequency of high current pulses. These can also be used to automate the process since it takes a long period of time to desulfate a battery fully. Battery chargers designed for desulfating lead-acid batteries are commercially available. A battery will be unrecoverable if the active material has been lost from the plates, or if the plates are bent due to over temperature or over charging. [12]

Batteries which have sat unused for long periods of time can be prime candidates for desulfation. A long period of self-discharge allows the sulfate crystals to form and become very large. Some typical cases where lead acid batteries are not used frequently enough are planes, boats (esp sail boats), old cars, and home power systems with battery banks that are under utilized.
Some charging techniques can aid in prevention such as equalization charging and cycles through discharging and charging regularly. It is recommended to follow battery manufacturer instructions for proper charging.
SLI batteries (starting, lighting, ignition; i.e. car batteries) have less deterioration because they are used more frequently vs deep cycle batteries. Deep cycle batteries tend to require more desulfation, can suffer from overcharging, and can be in a very large bank which leads to unequal charging and discharging.

Avoiding High Temperatures:

One of the most detrimental conditions for a battery is high temperature, particularly above 55oC, because the rates of corrosion, solubility of metal components, and self discharge increase with increasing temperature. High operating temperature during cycle service requires higher charge input to restore discharge capacity and self discharge losses. More of the charge input is consumed by the electrolysis reaction because of the reduction in the gassing voltage at the higher temperature. While 10% overcharge per cycle maintains the state of charge at 25 to 35oC, 35 to 40% overcharge may be required to maintain state of charge at the higher (60 to 70oC) operating temperatures. On float service, float currents increase at the higher temperatures, resulting in reduced life. Eleven days float at 75oC is equivalent in life to 365 days at 25oC. Batteries intended for high-temperature applications should use

a lower initial specific gravity electrolyte than those intended for use at normal temperatures. Manufacturers should be consulted on acceptable temperature ranges for operation of their batteries and on the associated effects of temperature. Nickel-cadmium batteries may be more suitable for higher-temperature applications.

Aced water separation:

A typical lead–acid battery contains a mixture with varying concentrations of water and acid. There is a slight difference in density between water and acid, and if the battery is allowed to sit idle for long periods of time, the mixture can separate into distinct layers with the water rising to the top and the acid sinking to the bottom. This results in a difference of acid concentration across the surface of the plates, and can lead to greater corrosion of the bottom half of the plates.

Frequent charging and discharging tends to stir up the mixture, since the electrolysis of water during charging forms hydrogen and oxygen bubbles that rise and displace the liquid as the bubbles move upward. Batteries in moving vehicles are also subject to sloshing and splashing in the cells, as the vehicle accelerates, brakes, and turns.

Risk of explosion;

Excessive charging electrolyzes some of the water, emitting hydrogen and oxygen. This process is known as "gassing". Wet cells have open vents to release any gas produced, and VRLA batteries rely on valves fitted to each cell. Wet cells come with catalytic caps to recombine any emitted hydrogen. A VRLA cell normally recombines any hydrogen and oxygen produced inside the cell, but malfunction or overheating may cause gas to build up. If this happens (for example, on overcharging) the valve vents the gas and normalizes the pressure, producing a characteristic acid smell. Valves can sometimes fail however, if dirt and debris accumulate, allowing pressure to build up fig.(12). [13]

Fig.(12) Car battery after explosion

If the accumulated hydrogen and oxygen within either a VRLA or wet cell is ignited, an explosion results. The force can burst the plastic casing or blow the top off the

battery, spraying acid and casing shrapnel. An explosion in one cell may ignite the combustible gas mixture in remaining cells. The cell walls of VRLA batteries typically swell when the internal pressure rises. The deformation varies from cell to cell, and is greater at the ends where the walls are unsupported by other cells. Such over-pressurized batteries should be carefully isolated and discarded. Personnel working near batteries at risk for explosion should protect their eyes and exposed skin from burns due to spraying acid and fire by wearing a face shield, overalls, and gloves. Using goggles instead of a face shield sacrifices safety by leaving one's face exposed to acid and heat from a potential explosion. [14]

A flat discharge curve simplifies the design of the application in which the battery is used since the supply voltage stays reasonably constant throughout the discharge cycle. A sloping curve facilitates the estimation of the State of Charge of the battery since the cell voltage can be used as a measure of the remaining charge in the cell. Modern Lithium Ion cells have a very flat discharge curve and other methods must be used to determine the State of Charge.

The X axis shows the cell characteristics normalized as a percentage of cell capacity so that the shape of the graph can be shown independent of the actual cell capacity. If the X axis was based on discharge time, the length of each discharge curve would be proportional to the nominal capacity of the cell.

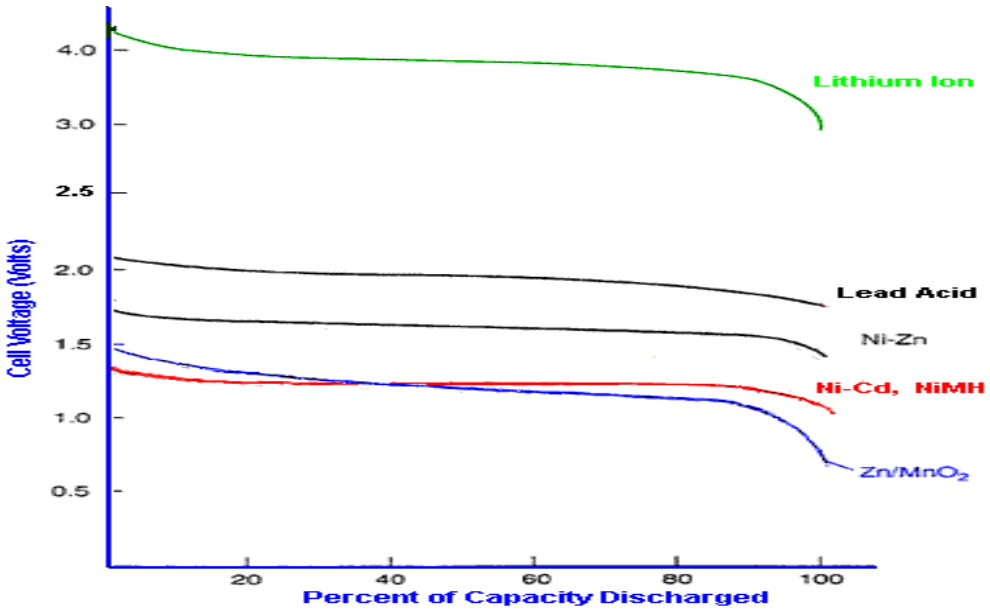

Fig. 13 The relation of the battery voltage with discharge current.

Temperature Characteristics

Cell performance can change dramatically with temperature. At the lower extreme, in batteries with aqueous electrolytes, the electrolyte itself may freeze setting a lower limit on the operating temperature. At low temperatures Lithium batteries suffer from Lithium plating of the anode causing a permanent reduction in capacity. At the upper extreme the active chemicals may break down destroying the battery. In between these limits the cell performance generally improves with temperature

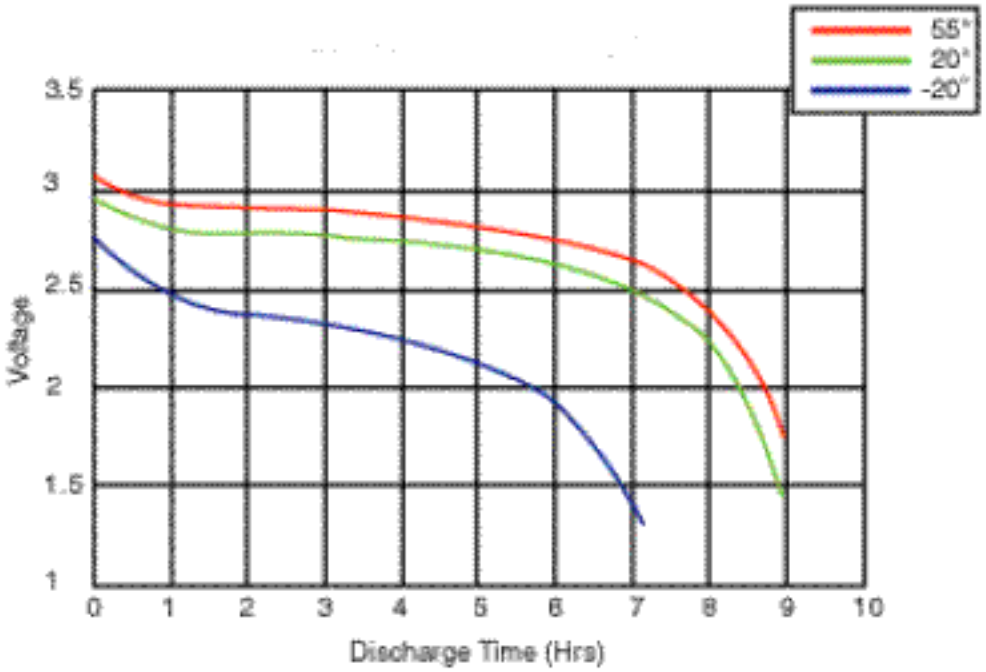

Fig. 14 relation of the battery voltage vs discharge time.

The above graph shows how the performance of Lithium Ion batteries deteriorates as the operating temperature decreases.

Probably more important is that, for both high and low temperatures, the further the operating temperature is from room temperature the more the cycle life is degraded

Discharge Rates

The discharge curves for a Lithium Ion cell below show that the effective capacity of the cell is reduced if the cell is discharged at very high rates (or conversely increased with low discharge rates). This is called the capacity offset and the effect is common to most cell chemistries.

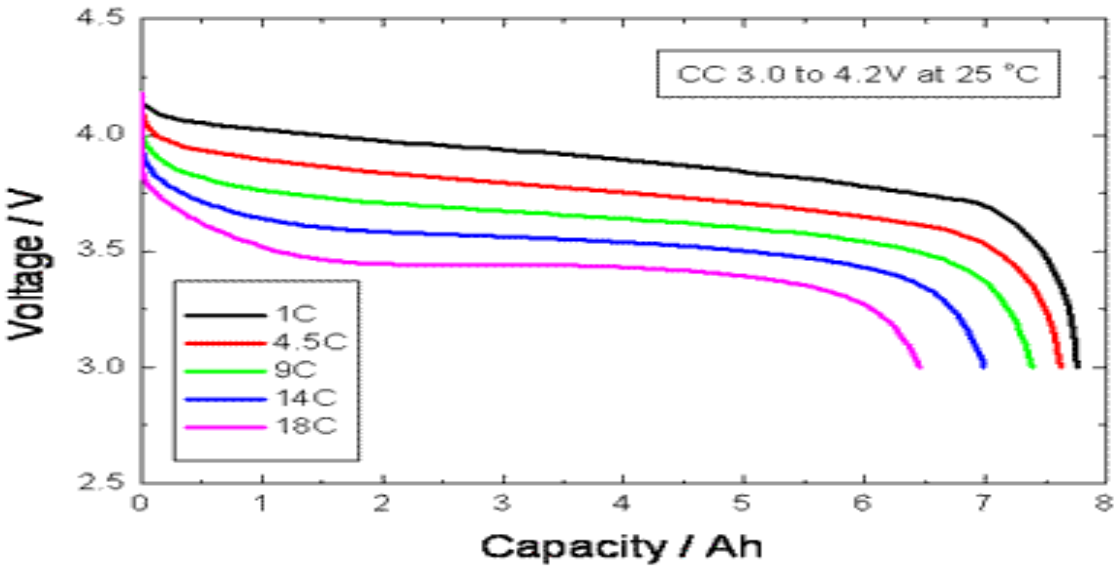

Fig. 15 relation of the battery voltage vs battery capacity.

Recommendation:

The most important technical specifications that you should take into account, when buying a battery that is used for the storage of energy, including:

The thickness of the lead alloy grid must be great to withstand the acid corrosion.

Preferred to use low concentration solution of sulfuric acid at in order to increase the battery life, but that will reduce the battery capacity.

It is better to store and sit the battery during operation in cold place, because the high temperature will damage the battery

It prefers not to discharge the battery completely during the work and keep at least 40% of the storage power to protect battery from corrosion

It is better to reduce the charging and discharging rate to minimum to maintain structure of the battery cells.

It is important to use the accurate charging control to prevent the over charge condition which it is the main cause of batter damage.

References:

[1] - Linden, David; Reddy, Thomas B., ed. (2002). Handbook Of Batteries (3rd ed.). New York: McGraw-Hill. p. 23.5. ISBN 0-07-135978-8.

[2]-J J A Wilkinson, "A new pulse charging methodology for lead acid batteries". IPENZ Transactions, Vol. 25, No.1/EMCh, 1998.

[3]-John A. Yoder, "Primer on lead-acid storage batteries". U.S. Department of Energy FSC-6910 Washington, D.C. 20585 September 1995.

[4]- Facilities instruction, standards, and techniques "Storage battery maintenance and principles", Internet version of The Manual Created. Volume 3-6 June, 1998.

[5]- CSIR- Central Electrochemical Research Institute, Karaikudi. Design and Development of Batteries For Solar Photovoltaic, MNRE-Solar Energy Centre, New Delhi. JUNE 2012

[6]- Troy C. Dayton, Dean B. Edwards, Improving the performance of a high power, lead–acid battery with paste additives, Department of Mechanical Engineering, Uniĺersity of Idaho, Moscow, ID, USA, Accepted 22 September 1999

[7]- Shen Guo, The Application of Genetic Algorithms to Parameter Estimation in Lead-Acid Battery Equivalent Circuit Models. University of Birmingham Research Archive, May 2010

[8]- Broussely, Michel; Pistoia, Gianfranco, ed, Equalize charging can prevent sulfation if performed prior to the lead sulfate forming crystals. Industrial applications of batteries: from cars to aerospace and energy storage. Elsevier. pp. 502–3. ISBN 0-444-52160-7.. (2007).

[9]- Improving the performance and reducing the cost of lead-acid batteries for large-scale energy storage. Energy Storage Program, Sandia National Laboratories October 2012.

[10]- M.P. Vinod), K. Vijayamohanan, Effect of gelling on the impedance parameters of PbrPbSO electrode in maintenance-free lead-acid batteries. Physical Chemistry Division, National Chemical Laboratory, Pune 411 008, India, 23 December 1999.

[11]- John B. Olson. "A High Power Spiral Wound Lead-Acid Battery for Hybrid Electric Vehicles" OPTIM Advanced Technologies, Inc. 17500 East 22nd Avenue Aurora, CO 80011, 1997.

[12]- John W. Stevens. A Study of Lead-Acid Battery Efficiency Near Top-of-Charge and the Impact on PV System Design. Sandia National Laboratories, Photovoltaic System Applications Department. Albuquerque, New Mexico 87185-0753.

[13]- Horst Bauer (ed.) Automotive Handbook 4th Edition, Robert Bosch GmBH, , ISBN 0-8376-0333-1, page 805. 1996.

[14]- Crown Battery Manufacturing Co. "Deep Cycle Battery Handling, Maintenance & Test Procedures", Crown Battery Mfg. Company 2010.

الجامعة التكنولوجية

مركز تكنولوجيا الطاقة والطاقات المتجددة

البحوث المقترحة لخطة عام 2015 / 2016

1. Power – Electronic and Control of Renewable Energies System.

Dr. Mahdi Ali Abdul Hussien & Roshan Tarek Ahmad

2. Performance of Hybrid Power System Consisting of wind Turbine , PV , Storage Battery and Diesel.

Dr. Mahdi Ali Abdul Hussien & Dr. Raed Saleh Jawad

Selecting of Renewable Effective Adsorbent for Treating Phosphate Contamination

Ahmed Hassoon Ali
Al- Mustansiryiah University, College of Engineering, Environmental Engineering Department, Iraq – Baghdad, Bab – Al – Muthem, P.O. Box 14150.
ahmedhassoon_2021@yahoo.com

Abstract:

Experimental researches on adsorptive capacity of: Granular Activated Carbon GAC, Phosphate Rock PR, Saw Dust SD and Rice Husk RH for phosphate from simulated wastewater were conducted. Results showed that removal efficiency of four adsorbents were in the consequence as: RR (82.6%) > SD (43.72%) > GAC (41.28%) > RH (34.4%). To understand the action of phosphate uptake, factors influencing the adsorption process using best adsorbent (PR) including pH, mixing speed, contact time, weight of the adsorbent, initial phosphate concentration and temperature were investigated. It was found that the equilibrium data fitted very well to the Langmuir model with high determination coefficient (R^2). The maximum loading capacity (q_{max}) was 24.716 mg/g. Adsorption data were modeled using the pseudo-first, pseudo-second-order Intraparticle diffusion and Elovich models. It was seen that the pseudo-second-order kinetic equation could best describe the adsorption kinetics. Thermodynamic parameters showed that the adsorption of investigated phosphate onto PR was endothermic, spontaneous in nature and the process is physiosorption. It was found that sodium hydroxide (0.1 M NaOH) was efficient desorbent solution in recovery of phosphate pollutant among different desorbents: HCl, H_2SO_4, NaOH, Na_2CO_3, EDTA and deionized distilled water (DDW) from PR. The breakthrough curves for the adsorption column test was obtained in a continuous adsorption fixed-bed experiment, The measured breakthrough times for RH, GAC, SD and PR were found to be 10, 30, 40 and 60 min, respectively.

KeyWords: Adsorption; Phosphate; GAC; PR, SD; RH.

1. Introduction

Wastewater containing phosphate should be treated before discharge to eliminate the possible. To protect aquatic quality, waste water containing phosphate must be treated to meet the discharge limit for phosphate (Puckett 1995; Zhao and Sengupta 1998; Ugurlu and Salman 1998). As this discharge limit is becoming more and more stringent, even further treatment of the effluent is required. When the input of phosphorus to waters is higher than it can be assimilated by a population of living organisms the problem of excess phosphorus content occurs. Regulatory control on phosphorus disposal is evident all over the world in recent years. Strict regulatory

requirements decreased the permissible level of phosphorus concentration in wastewater at the point of disposal (i.e. 1 mg/L). This has made it very important to find appropriate technological solution for treatment of wastewater prior to disposal.

Conventional phosphorus removal methods from wastewater include chemical precipitation (Donnert and Salecker, 1999), biological processes (De La Noueand de Pauw, 1988; L. De-Bashan and Bashan, 2004), reverse osmosis (Van Voorthuizen et al. 2005) and sorption processes (Morse et al. 1998; Kang et al. 2003). Among these techniques, adsorption is a promising method to treat waste water, especially at lower phosphate concentrations, which pose a challenge to the use of the traditional flocculation methods (Seida and Nakano, 2002). In recent decades, booming studies have been focused on the selection of ideal P adsorption materials (Agyei et al. 2000;; Khelifi et al. 2002; Tanada et al. 2003; Zeng et al. 2004).

In order to eliminate the possible dangers to receiving water sources, it is necessary to treat before discharge. Adsorption of phosphate from aqueous solution has been studied in the past few decades by several authors using different adsorbents, like activated alumina (Brattebo and Odegaard, 1986), half-burnt dolomite (Roques et al. 1991), activated carbon (Koh and Chung, 1998), coconut shell carbon (Palanivelu and Elangovan, 1994), clays (Fox, 1993), bentonite (Gonzalez-Pradas et al. 1992), ferrihydrite (Hawka et al. 1989), goethite (Parfitt, 1989), and hematite (Colomb et al. 1994).

The objective of this study was to select an effective adsorbent from conventional and nonconventional adsorbents for the removal of phosphate from simulated wastewater. The influences of different experimental parameters such as solution pH, dosage, contact time, temperature, initial concentration on phosphate removal as well as phosphate desorption were also investigated. Moreover, phosphate adsorption mechanism was elucidated in this paper.

2. 2. Materials and methods

2.1. Adsorbents preparation

Four different types of adsorbents are used: commercial granular activated carbon (GAC), rise husk (RH), phosphate rocks (PR) and sawdust (SD).

Commercial granulated activated carbon (GAC) was supplied by (Unicarbo, Italians) and was bought from the Iraqi markets.

The activated carbon was washed before being used with distilled water to remove fine powder and then dried in an oven at 110 ^{o}C for 24 hours, after which the GAC is kept in a desiccators for use.

The rice husk was collected from Al-Shamiyyah rice mill located in Al-Diwaniya where large amounts of residual rice husk were produced in production of rice. The rice husk was filtered and washed with excess distilled water and dried in an oven at 60°C.

The PR comes from the Akashat phosphate mines located in the western region of Iraq, about 110km west of the capital Baghdad. The choice of this material is based on its low cost, considering its abundance in the Iraqi ores. Iraq is one of the

major courtiers in phosphate production. The amount of phosphate production in Iraq was about 1,199,343 tons/year (Setatnia et al. 2004).

The Sawdust was collected from several furniture factories in Baghdad where large amount are produced as residuals from production of different furniture. This was washed with double distilled water to remove water-soluble impurities and surface-adhered particles. Then the adsorbent was oven-dried at 60°C to remove the moisture and other volatile impurities.

The GAC, RH, PR and SD samples was sieved into mesh 0.6, 1 mm using Germany sieves. For non-spherical particles, the particle diameter is defined as the equivalent diameter of a spherical particle with the same volume. As an approximation, the particle diameter may be calculated from the geometric mean of the two consecutive sieve openings without introducing serious errors. The geometric mean diameter is given by, $d_{gm} = (d_1 d_2)^{1/2}$, where d_1 is the diameter of the lower sieve on which the particles are retained and d_2 is the diameter of the upper sieve through which the particles pass (Alexander, 1989).

The physical and chemical properties of adsorbents are measured at the laboratories of the Ministry of Industry and Minerals (Ibn Sina State Company), Ministry of Oil (Petroleum Development and Research Center), Al-Mustansiriya University (College of Engineering, Environmental Department) and according to the data from the supplier and listed in Table 1. The specific surface area and total pore volume were measured using the multi-point-N2-Brunauer, Emmett and Teller (BET) method (Surface area analyzer, BET method, Quantachrome.com, USA). The functional groups of PR was detected by FT-IR analysis. The proportion of adsorbent/KBr is 1/100. The background is obtained from the scan of pure KBr. FT-IR spectrophotometer, IRPRESTIGE-21, SHIMADZU, Japan was used for analysis. Phases present in the samples (chemical analysis) were analyzed using an X-ray diffractometer (PAN analytical X-ray, Philips Analytical, Germany) and present in Table 2.

Table 1. Adsorbents specifications

Specifications	Adsorbents			
	GAC	RH	PR	SD
Source	Uncarbo company Italy form local markets	Local Iraqi mills	Akashat phosphate mines	Collected from a local furniture factory
Bulk density (real density) (kg/m^3)	641 (1544)	233.52 (1390)	674.56 (2500)	462.05 (1509)
Surface area (m^2/g)	351.965	136.69	607.53	10.1712
Porosity %	53.44	83.2	36	69.38
Pore volume (cm^3/g)	0.422	0.054	0.437	Nil
*CEC (meq/100g)	-	43.118	-	116.8
*Cation Exchange Capacity				

Table 2 Chemical analysis of GAC, RH, PR and SD samples

GAC		R.H		PR		S.D	
constituent	Wt.%	constituent	Wt.%	constituent	Wt.%	constituent	Wt.%
C	88.77	SiO_2	96.36	P_2O_5	25.47	SiO_2	86.1
O	10.51	MgO	0.4	CaO	52.29	$CaSiO_3$	2.9
Si	0.28	Al_2O_3	0.42	MgO	0.7	MgO	2.6
S	0.05	K_2O	2.30	Fe_2O_3	16.5	Al_2O_3	4.4
K	0.18	CaO	0.42	SiO_2	3.5	SO3	2.1
Ca	0.21	Fe_2O_3	0.1	L.O.I	1.54	L.O.I*	1.9
*Loss Of Ignition							

2.2. Preparation of phosphate solution

All chemicals are analytical grade and used without further purification. Reaction vessels (glass) were cleaned with 1 % HNO_3 and rinsed several times with deionized water before use. Phosphate stock solution was prepared by dissolving the anhydrous potassium dihydrogen orthophosphate (KH_2PO_4) in deionized water. Phosphate working solutions were freshly prepared by diluting phosphate stock solution with appropriate amounts of deionized water.

3 Results and discussion

3.1 Selection the best adsorbent

In order to select the best adsorbent from GAC, RH, PR and SD in removing of phosphate from simulated wastewater. Four glass bottles of 300 mL volume contains 100 mL solution of initial concentration C_o 50 mg/L, the pH was fixed at 4 using 0.1 M NaOH or HNO_3 solution. The dose of each adsorbent was 1 gm. The glass bottles were then placed on a shaker (HV-2 ORBTAL, Germany) and agitated continuously for 4 hr at 200 rpm and 30 ^oC. The samples filtered by 42 Whatman filter paper (APHA, 1995). The final equilibrium concentrations were measured by means of spectrophotometer device.

The removal efficiency (adsorption efficiency) is calculated by the difference in the initial and final concentration of each phosphate by the following relationship:

$$R(\%)=\frac{(C_o - C_e)}{C_o}\times 100 \quad (1)$$

Where C_o and C_e are the initial and final concentration respectively (mg/L). The experiments are repeated triple and the average concentration was taken.

The removal efficiency of phosphate ions using GAC, RH, PR and SD are shown in Fig. 1. As shown from this Figure that, the removal efficiency of phosphate onto tested adsorbents follows the sequence as: PR > SD > GAC > RH

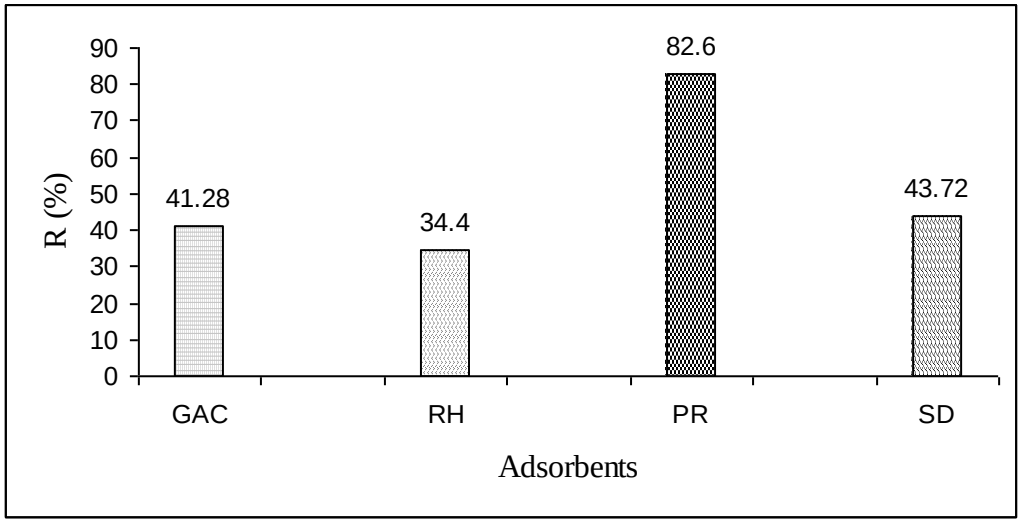

Figure 1. Removal efficiency of phosphate onto different adsorbents, C_o 50 mg/L, pH 4, adsorbent dose 1 g per 100mL and temperature 30 ^oC.

PR has more surface area than other adsorbents as determined in Table 1. Therefore, more adsorption sites are available for phosphate ions adsorption. However, cation exchange capacity (CEC) for SD represents the total amount of phosphate ions that can be replaced by positive ions (K^+,Na^+,Ca^{2+}, and Mg^{2+}) on SD. CEC for SD used in this study was 116.8 meq/100 g . Thus, adsorption capacity for SD exceeds that for GAC and RH. Therefore, PR will be used as adsorbent in next batch experiments.

3.2 FTIR analyses of PR

In order to find out which functions are responsible for the phosphate adsorption, FT-IR analysis of PR was carried out. Figure 2 shows the spectra of raw and treated phosphate samples. The sharp bands near 435.91, 921.97, and 1145.72 define the Si–OH stretches. The peak at 875.68 cm^{-1} is associated with the PO_4^{-3} group. The bands between 1000 and 1095.57 cm^{-1} are Si-O and those at 1427.32, 1454.33, and 1635.64 are C=O, and at 1998.25–2357.01 are P-H. The sharp peaks at 3641.60 and 3448.72 are O-H stretching. All peaks defined above are related to the mineralogical composition of the sorbent (PO_4, SiO_2, and CO_3) (Ma et al., 1995; Soejoko and Tjia, 2002).

Peak displacement decrease defines the change in the structure with phosphate, implying that the related functional groups are responsible for the adsorption process. Table 3 shows the main functional groups before and after phosphate rocks were loaded with phosphate ions. The results show that the bands of carboxylic (C=O) groups shifted to lower frequency. The bands of functional groups shifted to lower frequency with a total amount of 78.89.

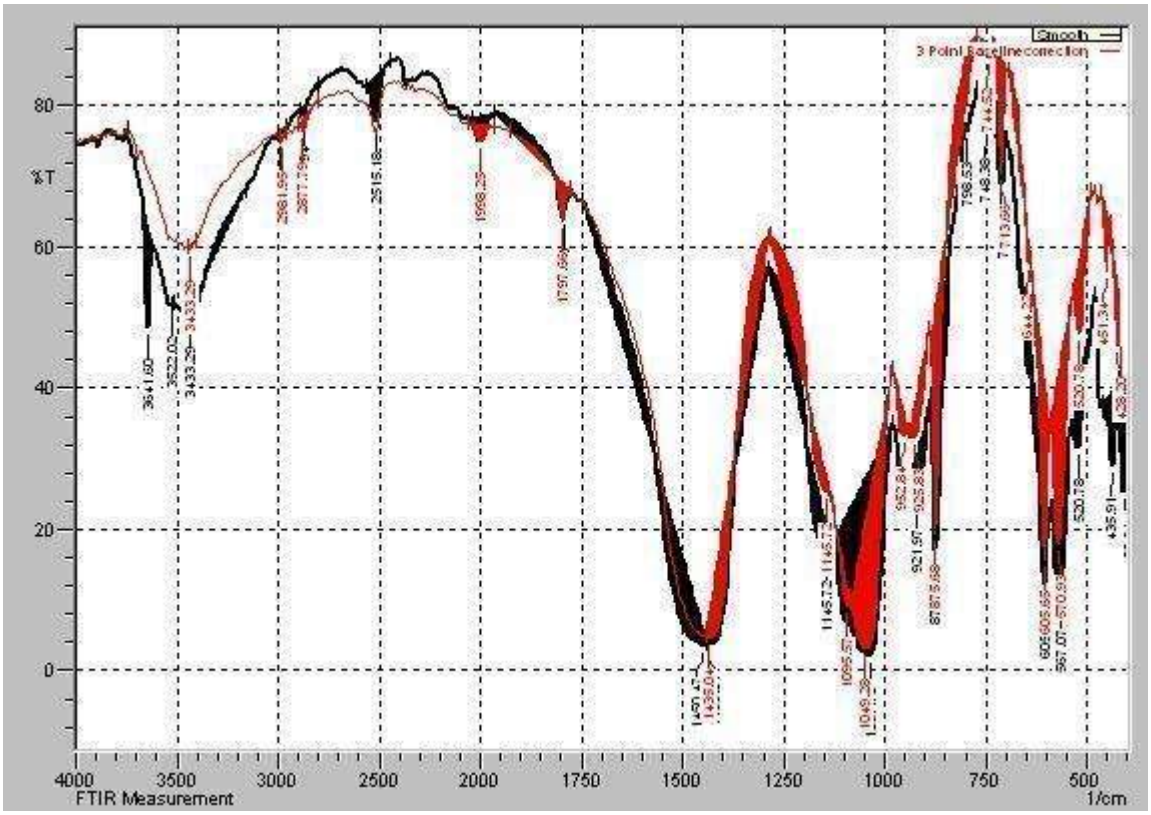

Figure 2. FT-IR spectra of PR (1) before, (2) after phosphate adsorption.

Table 3. Functional groups before and after PR was loaded with phosphate ions.

Assignment groups	Unloaded, cm^{-1}	Loaded with phosphate, cm^{-1}	Δ
Hydroxyl ($^{-}$OH)	3641.60	3634.35	7.25
	3448.72	3443.21	5.51
Summation			12.76
Phosphine (p-H)	2357.01	2353.85	3.16
	2017.54	2012.78	4.76
	1998.25	1996.21	2.04
Summation			9.96
Carboxylic (C=O)	1635.64	1619.34	16.3
	1454.33	1443.54	10.79
	1427.32	1417.9	9.42
Summation			36.51
Silanol (Si–OH)	1157.29	1153.97	3.32
	929.69	923.75	5.94
	493.78	488.86	4.92
Summation			14.18
Siloxane (Si-O)	1095.57	106.42	3.15
Phosphate (PO_4^{-3})	876.78	873.45	3.33
Total summation			78.89

3.3 Determination of optimum conditions for PR performance

3.3.1 Effect of pH

The influence of pH on the removal efficiency for phosphate is shown in Figure 3. As cleared from Fig. 3, the phosphate uptake was evidently dependent on pH with the greatest adsorption occurring under acidic conditions and decreased with increase in solution pH. For example, the phosphate PO_4^{3-} removal rate decreased from 88.65 % around pH 3 to about 34.62 % at pH 9. Similar pH effect on phosphate ions adsorption by iron or iron-based oxides has been reported by a number of authors (Zhang et al. 2009). Such phenomenon could be explained as follows: negative charged $H_2PO_4^-$ and HPO_4^{2-} are dominant phosphate species in the solution under the tested pH range (3–9). Lower pH is favoring the protonation of PR surface and increased protonation is thought to increase the positively charged sites, enlarge the attraction force existing between the PR surface and phosphate ions and therefore increase the amount of adsorption in the lower pH region. As solution pH increase, the negatively charged sorptive sites dominate gradually and more negatively charged phosphate species are also becoming dominant, which enhances the repulsion effect between the PR and the phosphate ions. Therefore, the amount of phosphate uptake is consequently dropped.

The point of zero charge pH (pH_{PZC}) study also confirms the increase of phosphate elimination with a pH of round 3. The pH at point zero charge (pH_{PZC}) of the prepared PR was determined by the solid addition method (Rivera-Utrilla et al., 2001). The pH_{PZC} of a material in a solution is the pH value at which the net surface charge of this material is equal to zero. Below this pH (pH=4 in the present study) the adsorbent functional group is protonated and the adsorbent surface is positively charged; however, adsorption of negatively charged ions is favorable. In the simplest interpretation, hydrogen ions become winners in this competition. Above this pH, these groups deprotonate and the adsorbent surface becomes negatively charged, so in this region of pH phosphate ions cannot be attracted effectively onto the PR surface (Iqbal et al., 2009).

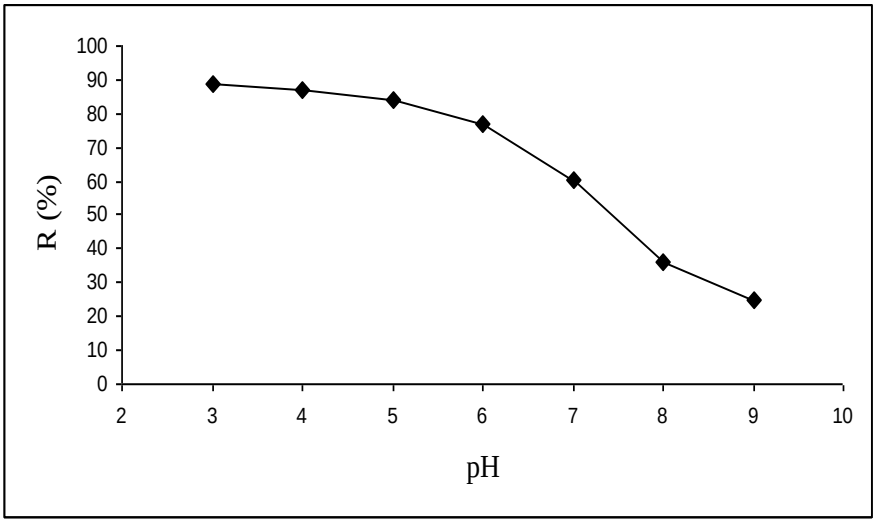

Figure 3. Effect of pH on the adsorption of phosphate onto PR at C_o= 50 mg/L, mixing speed=200 rpm, contact time = 4 h, PR dose=0.5 g/100mL and temperature= 30 ^oC.

3.3.2 Effect of mixing speed

The effect of the mixing speed on the removal efficiency of phosphate using PR is shown in Figure 4. The efficiency value increase from: 45.32 to 90.34 % as the agitation speed increased from 50 to 250 rpm. It can be clearly seen that mixing speed increases the removal efficiency until it reaches a certain value and further increase is then of no benefit (i.e., above 250 rpm). The increase in efficiency is due to the increase in turbulence and as a consequence, the decrease in the external mass transfer resistance thickness around the adsorbent particles with increase in mixing speed (Yasemin and Tez, 2007). Moreover these results clearly indicate that a mixing speed of 250 rpm is sufficient to obtain maximum removal efficiency by reducing the boundary layer thickness to a minimum value.

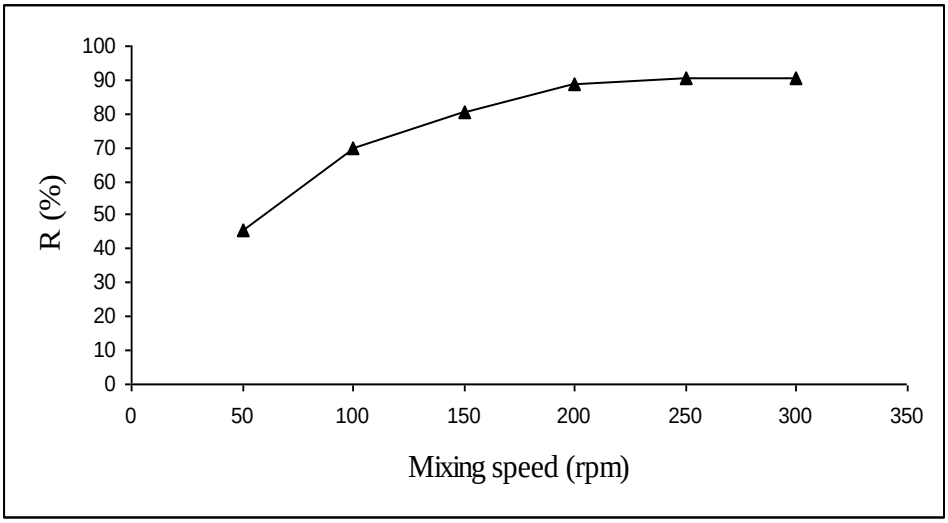

Figure 4. Effect of mixing speed on the adsorption of phosphate at C_o= 50 mg/L, pH= 3, contact time = 4 h, adsorbent dose=1g/100mL and temperature= 30 ^oC.

3.3.3 Effect of PR dose

The effect of varying the adsorbent dose (mass) on the adsorption of various metal ions is shown in Figure 5. It is clearly seen that the removal efficiency increases as the PR mass increases. As the PR mass increases the number of binding sites for the phosphate ions also increases. After some point (2.5 g), adsorption capacity was steady due to a screen effect between adsorbent, this produced a block of the adsorbent active sites by an increase of adsorbent (PR) in the system (Ali, 2013). Similar observations were also made by other investigators (Hammaini et al., 2006; Kumar et al., 2009). Removal efficiency increases from: 79.45 to 96.78%. Thus in next experiments, the optimum dosage was fixed at 2.5 g.

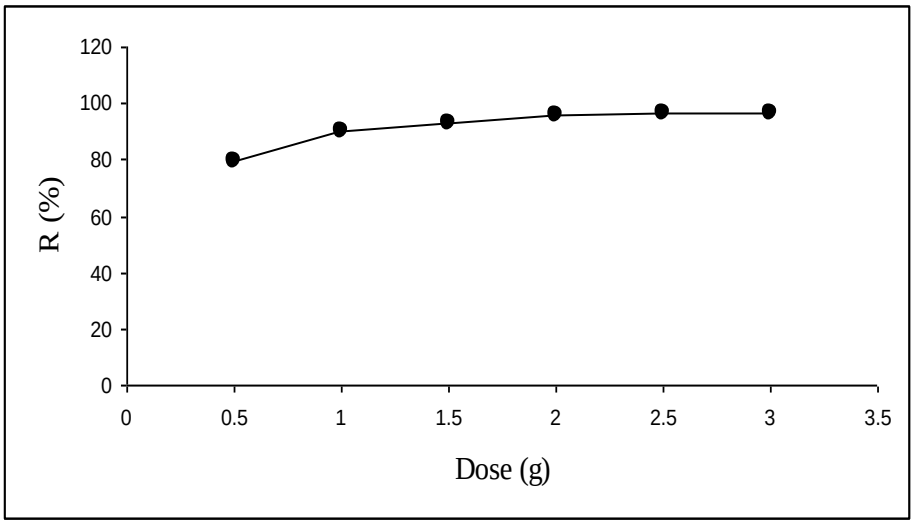

Figure 5. Effect of adsorbent on the adsorption of phosphate onto PR at C_o= 50 mg/L, pH= 3, contact time = 4 h, mixing speed=250 rpm and temperature = 30 ^oC.

3.3.4 Effect of contact time

Contact time plays an important role in the efficient removal of phosphate using PR. Therefore, the adsorption of phosphate at constant temperature, initial concentration, best mixing speed, best adsorbent dose and best pH was studied as a function of contact time to determine the equilibrium time. The influence of contact time on the adsorption capacity is shown in Figure 6. Removal efficiency increases from 15.35 to 97.88% as the contact time increases from 30 to 270 min. The results revealed that rate of adsorption is higher at the beginning and this is due to availability of a large number of active sites on the adsorbent. As these sites are exhausted, the uptake rate is controlled by the rate at which the adsorbate is transported from the exterior to the interior sites of the adsorbent particles (Dorris et al., 2000). Maximum removals were attained with in the first 240 min of stirring time. There must not be seemed to be much benefit after 270 min. Therefore the equilibrium time was set to be 270 min in further experiments.

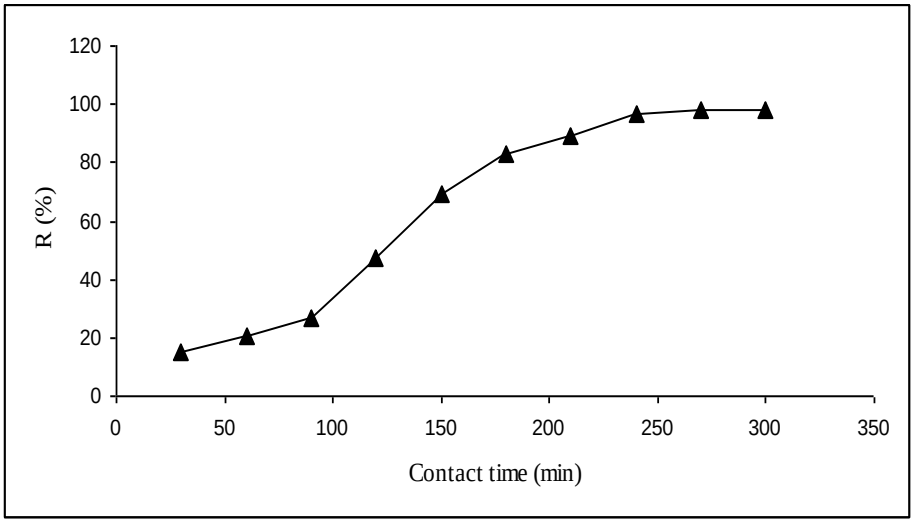

Figure 6. Effect of contact time on the adsorption of phosphate onto PR at C_o= 50 mg/L, pH= 3, dose = 2.5 g/100 mL, mixing speed=250 rpm and temperature= 30 ^oC.

3.3.5 Effect of initial concentration

The experiments were performed at distinct initial concentrations ranging from 25 to 100 mg/L. As shown in Figure 7, the efficiency values decreases from: 98.65 to 80.75 % as the initial concentration increased from 25 to 100 mg/L. This is due to the lack of binding sites in the PR sample for the adsorption of metal ions at higher concentrations. The effect of initial metal concentration could be explained as follow: at low metal ion/adsorbent ratio, metal ion adsorption involves higher energy binding sites. As the metal ion/adsorbent ratio increase (i.e., at higher initial concentration), the higher energy binding sites are saturated and adsorption begins on lower energy binding sites, resulting in decrease in the adsorption efficiency (Al-Qodah, 2006).

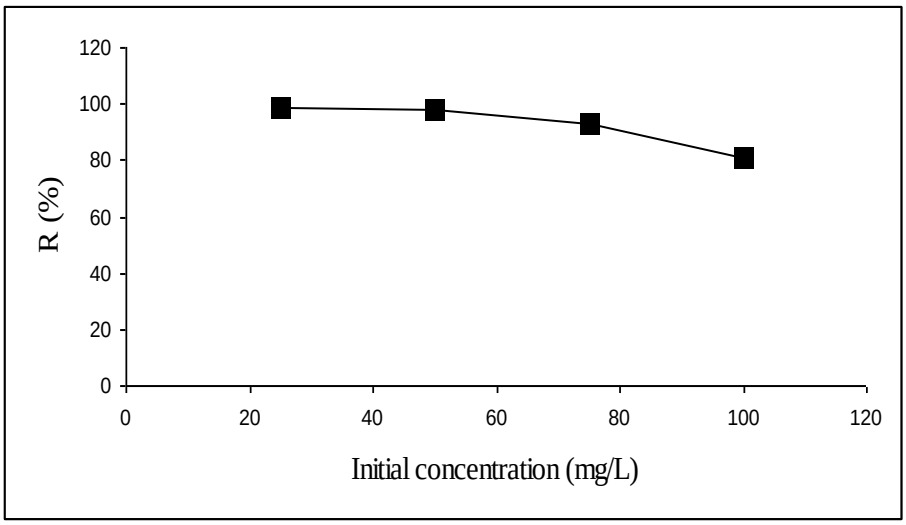

Figure 7 Effect of initial concentration on the adsorption phosphate onto PR at pH= 3, mixing speed=250 rpm, dose= 2.5g/100 mL, contact time = 4.5h and temperature= 30 ^oC.

3.3.6 Effect of temperature

Figure 8 shows the adsorption efficiency of phosphate onto PR at six different temperatures of 10, 20, 30, 40, 50 and 60 ^{o}C. It can be seen that as the temperature increases, the adsorption capacity decreased. For instance, for an initial concentration 50 mg/L the adsorption efficiency of the adsorbent decreases from 99.43 to 88.98 % as the temperature increase from 10 to 60 ^{o}C. This means that, as the temperature increased the rate of desorption was more significant than the rate of adsorption, which implies that adsorption is an exothermic reaction, a well-known scientific fact (Sag and Kutsal, 2000).

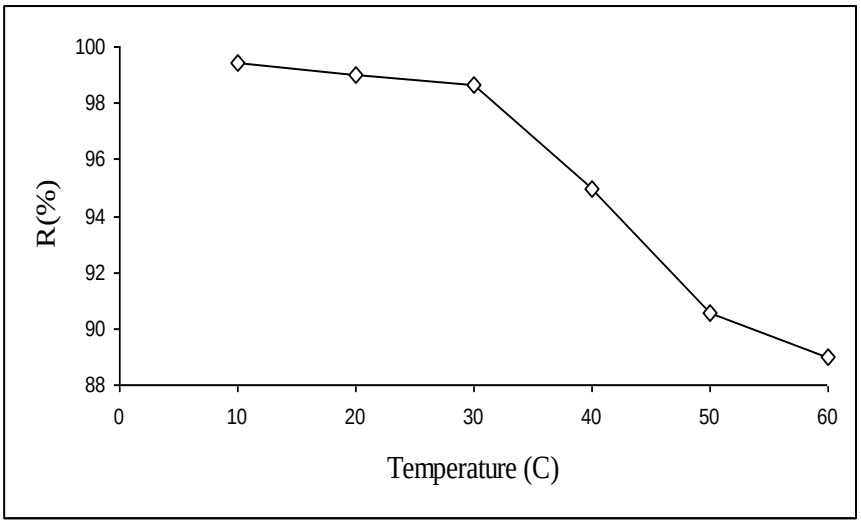

Figure 8 Effect of temperature on the adsorption of phosphate onto PR at C_o= 50 mg/L, pH= 3, mixing speed=250 rpm, t adsorbent dose= 2.5g/100mL, contact time = 4.5h.

3.4 Adsorption isotherm

The adsorption isotherm for phosphate onto PR is shown in Figure 9. The obtained data have been correlated with five models. The parameters for each model which obtained from non-linear statistical fit of the equation to the experimental data (Statistica-v6) are summarized in Table 2.

From Fig. 9 and Table 4, the following conclusions can be drawn: Langmuir model gave the best fit for the experimental data for phosphate adsorption with correlation coefficients of 0.994. This indicates that the adsorption process occurs as a mono layer. The maximum adsorbed amount (q_m) is 24.716 mg/g. A comparison of the maximum adsorption capacity (q_m) of the PR sample with that of some other adsorbents reported in the literature is given in Table 5. The adsorption capacity of the PR samples was relatively high when compared with other adsorbents.

Table 4. Parameters of adsorption isotherm for phosphate ions onto PR

Model	Equation	Parameters	Values	Reference
Freundlich	$q_e = KC_e^{1/n}$	K, $(mg/g)(L/mg)^{(1/n)}$	1.231	Gupta and Rastogi, 2008
		n	1.249	
		R^2	0.995	
Langmuir	$q_e = \frac{q_m b C_e}{1+bC_e}$	q_m, (mg/g)	24.716	Sulaymon et al. 2009
		b, (L/mg)	0.046	
		R^2	0.994	
Reddlich–Peterson	$q_e = \frac{A_R C_e}{1+B_R C_e^{m_R}}$	A_R, mg/g L/mg	0.1336	Quintelas et al. 2008
		B_R, $(L/mg)^{mR}$	-0.897	
		m_R	-0.034	
		R^2	0.995	
Sips	$q_e = \frac{bq_m C_e^{1/n}}{1+bC_e^{1/n}}$	q_m, (mg/g)	140.820	Özer, 2003
		b, (L/mg)	0.008	
		n	1.208	
		R^2	0.995	
Khan	$q_e = \frac{Q_{max} b_k C_e}{(1+b_k C_e)^{a_k}}$	Q_{max}, (mg/g)	0.044	Vijayaraghavan and Yun 2008
		b_K, (L/mg)	65.231	
		a_K	0.200	
		R^2	0.995	

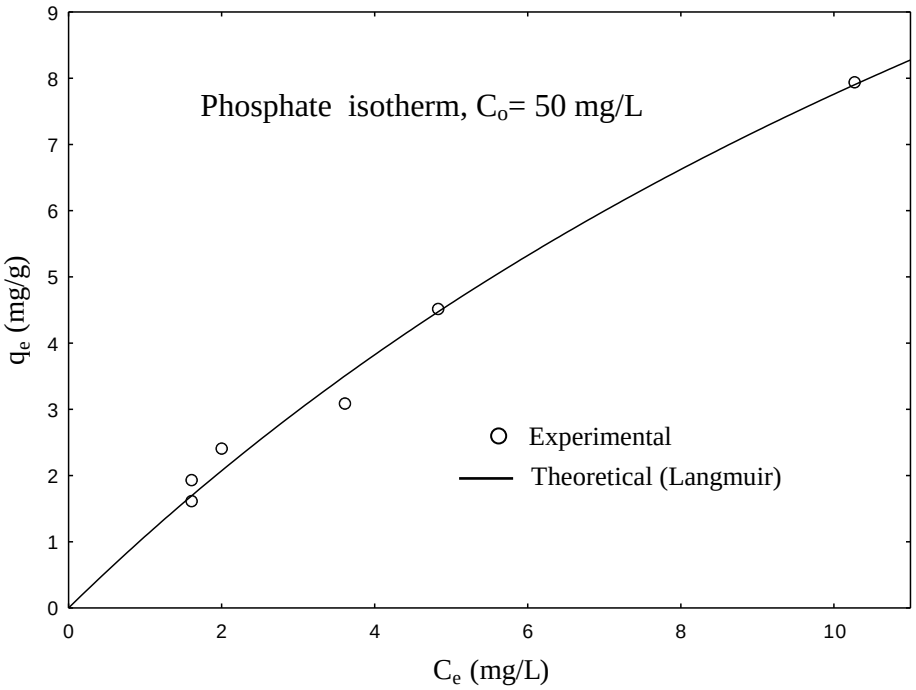

Figure 9 Adsorption isotherm for cadmium onto PC

Table 5. Adsorption capacities (q_m, mg/g) for phosphate ions of various adsorbents

Adsorbent	q_m, mg/g	References
Mesoporous ZrO2	29.7	Liu et al. 2008
Red mud	0.23	Huang et al. 2008
Hydrous niobium oxide	4	Ye et al. 2006
Magnetic Fe–Zr binary oxide	13.6	Long et al. 2011
Hydrous niobium oxide	13	Rodrigues and Silva 2009
Akaganéite	49	Deliyanni et al. 2007
PR	24.716	Present study

3.5 Kinetic model

The kinetics of phosphate adsorption onto PR was analyzed using pseudo-first-order, pseudo-second-order, intra-particle diffusion, and Elovich kinetics models. Table 6 and Figure 10 demonstrate the results of these models. From the application of various kinetic models, the following conclusion can be achieved:

- Pseudo-second order was the most fitted model to experimental data. The adsorption uptake equal to 7.758 mg/g, this is closed to the experimental uptake of 7.025 for phosphate ions, respectively with R^2 of 0.986.
- The value of constant (C) in the intra-particle diffusion model is not equal to zero, suggesting that adsorption proceeds from boundary layers mass transfer across the interfaces to the intra-particle diffusion within the pores of adsorbent. This indicates the mechanisms of metal ions adsorption is complex and both the surface adsorption as well as intra-particle diffusion contribute to the rate determining step (Ali, 2011).

Table 6. Kinetic model parameters for phosphate adsorption onto PR.

Model	Equation	Parameters	Value
Pseudo-first-order	$\log(q_{eq}-q_t)=\log q_{eq}-(\frac{k_L t}{2.303})$	q_{eq}(mg/g)	33.014
		K_L(1/min)	0.030
		R^2	0.826
Pseudo-second-order	$\frac{t}{q_t}=\frac{1}{k_s q^2_{eq}}+\frac{t}{q_{eq}}$	q_{eq} (mg/g)	7.758
		K_s(g/mg.min)	3.44×10^{-3}
		R^2	0.986
Intraparticle diffusion	$q_t=k_{id}t^{1/2}+C$	C	1.864
		K_{id}(mg/g.min$^{0.5}$)	0.358
		R^2	0.934
Elovich	$q_t=\frac{1}{b}\ln a\bar{b}+\frac{1}{b}\ln t$	a(mg/g.min)	0.88
		b^- (g/mg)	0.784
		R^2	0.912

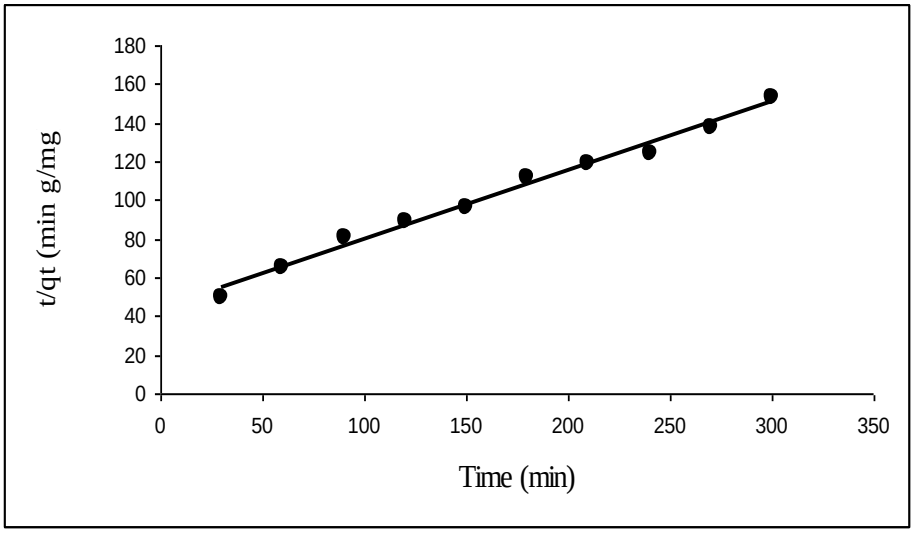

Figure 10 Pseudo-second order model for adsorption of phosphate ions onto PR.

3.6 Adsorption Thermodynamics

Based on fundamental thermodynamic concepts, it is assumed that in an isolated system, energy cannot be gained or lost and the entropy change is the only driving force. The apparent equilibrium constant for the process has been shown to be (Tang et al., 2012):

$$\Delta G^{o} = -RT \ln Kc \tag{14}$$

$$K_c = \frac{C_o - C_{eq}}{C_{eq}} \tag{15}$$

Also, enthalpy changes (ΔH^o) and entropy changes (ΔS^o) can be estimated by the following equation:

$$\Delta G^{o} = \Delta H^{o} - \Delta S^{o} T \tag{16}$$

where ΔG° is standard Gibbs free energy change in kJ/mol; ΔH° is change in enthalpy (heat of adsorption, kJ/mole), ΔS° is change in entropy in kJ/mol, R is the universal gas constant (=0.8314 kJ/mol.K) and T is the temperature in K.

Table 7 and Fig. 11 show the thermodynamic constants of adsorption for phosphate onto PR. The value of enthalpy ΔH° was −34.765 kJ/mol, suggested the physiosorption and exothermic nature of adsorption. This is also supported by the decrease in the values of uptake capacity of adsorbent with the rise in temperature. The value of entropy ΔS was -0.0872 J/mol K, reflect the affinity of phosphate ions to be adsorbed onto PR. The negative values of G° confirm the feasibility of the process and the spontaneous nature of adsorption (Zubeyde et al. 2009).

Table 7 Thermodynamic parameters for the adsorption of phosphate onto PR.

Temperature, K	$-\Delta G^o$, kJ/mol	$-\Delta H^o$, kJ/mol	$-\Delta S^o$, J/mol.K	R^2
383	9.828	34.768	0.0872	0.975
393	9.485			
303	8.234			
313	7.875			
323	6.447			
333	5.622			

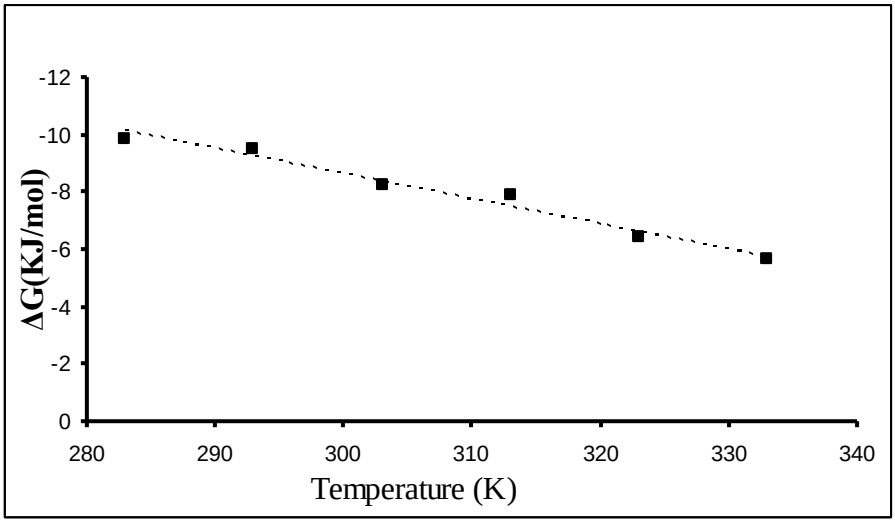

Figure 11 Free energy change for phosphate adsorption.

3.7 Desorption and regeneration

Desorption experiments were performed in order to demonstrate the ability of spent selected adsorbent for regeneration and reuse. Desorption of phosphate ions from loaded PR was carried out by solvent elution, using 0.1M of HCl, H_2SO_4, NaOH, Na_2CO_3, EDTA and deionized distilled water (DDW) as an eluents. The desorption of phosphate ions were carried out from each 1 g of loaded adsorbent which had previously adsorbed phosphate in experiments of effect of adsorbent dosage and dried, with initial concentration of 50 mg/L. It was carried out by 50 mL of elute for 4.5 h shaking in a batch system at 250 rpm. Volume of elutant solution was selected to achieve complete immersing and good mixing of solid particles.

Thereafter, the desorbed ions was analyzed and the eluting efficiencies of the desorbents $E_{d.}$ are calculated according to Eq. (17). The most efficient elutant was then used in consecutive adsorption–desorption–regeneration cycle.

The desorption efficiencies using the different desorbing elutants from PR are calculated from Eq. below:

$$E_{d.}(\%) = \frac{m_{d.}}{m_{ad.}} = \frac{C_{d.} \times V_e}{C_{ads.} \times V_L} \quad (17)$$

The results are listed in Table 8 and shown in Figure 12. It is clear from the previous Figure and Table that, the elution tendency as a percentage recovery of metal ions followed the sequence as:

NaOH > Na_2CO_3 > EDTA > H_2SO_4 > HCl > DDW

NaOH and Na_2CO_3 found to be the most efficient elutants in desorbing of phosphate ions. This observed trend may be due to affinity between negative ions present in phosphate and NaOH. Sodium hydroxide is considered one of the chelating agents which interact with phosphate through molecular attraction through covalent bond, which is stronger than that responsible to bind phoshate to functional groups onto PR surface. A similar conclusion was given by Qadeer and Rehan, 1998.

Table 8 Desorption efficiency of the different elutants.

Elutant (0.1 M)	Desorption of Phosphate from PR; V_e=50 mL, V_L= 100 mL $C_{ads.}$= 48.638 mg/L	
	$C_{d.}$ (mg/L)	$E_{d.}$(%)
HCl	7.724	7.940
H_2SO_4	10.068	10.349
NaOH	94.698	97.350
Na_2CO_3	93.608	96.229
EDTA	86.534	88.957
DDW	7.192	7.393

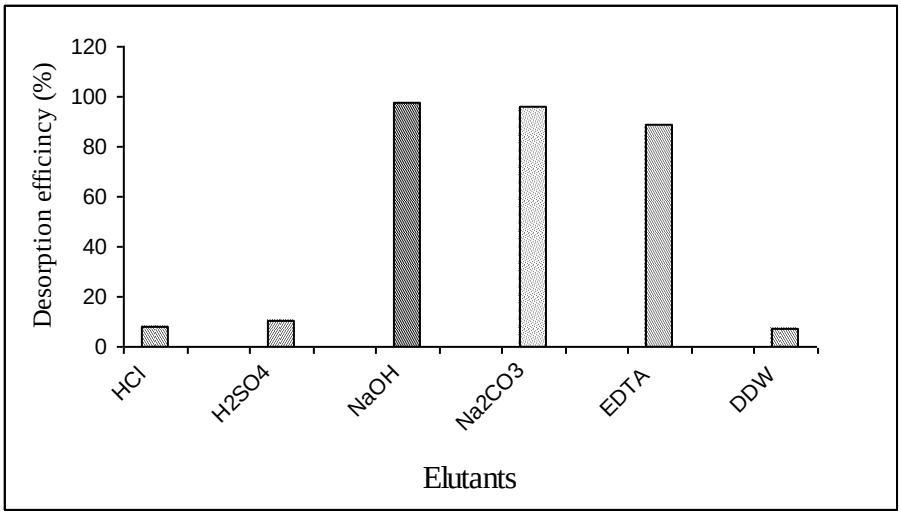

Figure 12. Phosphate recovery from PR

4. Column Experiments (Continuous Process)

The fixed-bed breakthrough curve was measured by a continuous adsorption experiment. An acrylic column of (50 mm) inner diameter and (0.5 m) height was packed with 100 g adsorbent as shown in Fig. 13. There was a distributor on the top of the column in order to allow a homogeneous flow distribution. Porous organic plastic supports were used to hold the carbons in the column. Phosphate initial concentration solution of 50 mg/L was pumped through the carbon bed at the rate of 2.78×10^{-6} m^3/s using a peristaltic pump (BT-100, China). Effluent samples were taken at various times for phosphate concentration analysis.

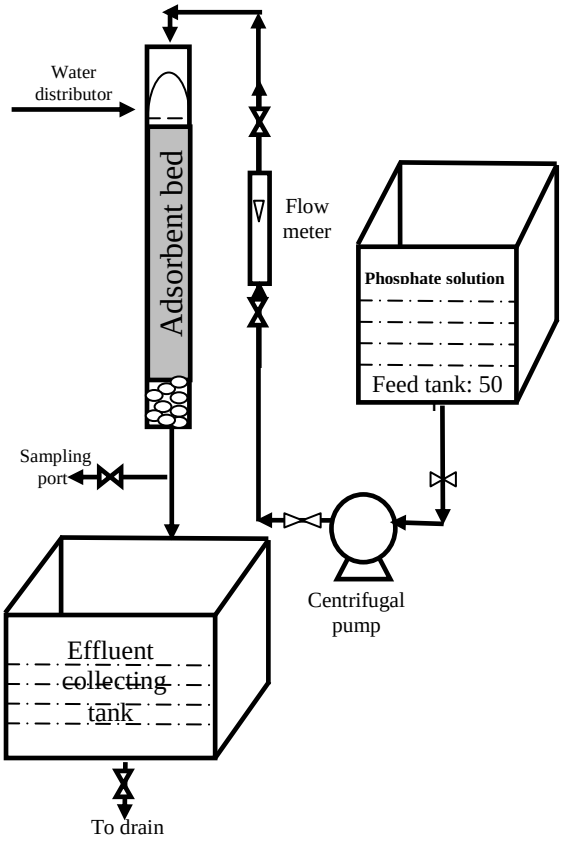

Fig. 13 Schematic diagram of the experimental set up for a continues process.

The fixed-bed breakthrough curve was obtained by a continuous adsorption experiment. It can be seen from Fig. 14 that all phosphate were initially retained in the fixed- bed because of full adsorption (no phosphate in the effluent). With greater phosphate solution flow through the bed, the phosphate concentration in the effluent increases steadily until it reaches the same value as its inlet concentration (C_o), the so-called breakthrough point, when the fixed-bed is saturated. The measured breakthrough times for RH, GAC, SD and PR are 10, 30, 40 and 60 min, respectively. These results proved that those obtained in batch system where (PR) is adsorbed phosphate ions more strongly than other types of adsorbents.

The bed-depth service-time model is used to estimate the required bed depth for a given service-time. The BDST model can be expressed as below[29]:

$$t_b = \frac{N_o}{C_i u} Z - \frac{1}{C_i K} \ln\left(\frac{C_i}{C_b} - 1\right) \quad (18)$$

where C_b is the solute concentration in the effluent of the column at breakthrough (at 10% breakthrough point , i.e. t_b at C_b=5 mg/L), C_i is the solute concentration in the effluent to the column (50 mg/L), N_o is the adsorption capacity, Z is the bed height (0.05 m), u is the superficial velocity (3.37×10^{-7} m/sec) and K is the rate constant which represents the solute transfer from the liquid phase to the solid phase. The parameters N_o and K for BDST model were obtained from nonlinear statistical fit of the equation to the experimental data (Statistica, v6) which are summarized in Table 9. The R^2 value mostly close to unity indicating the suitability of the BDST model to represent the adsorption of phosphate in a fixed-bed of PR, SD, GAC and RH. The adsorption capacity N_o as shown in Table 9 for PR is higher than that for other adsorbents. This result proved the results obtained in batch system for maximum adsorption capacity (q_m). This models has been used successfully by other researchers to estimate the required depth for a specific adsorption time (Muhamad et al., 2012; Al-Degs, 2009).

Table 9 parameters predicted from the BDST model for adsorption of phosphate on tested adsorbents.

Type of carbon	N_o, mg/L	K, L/mg.min	R^2
PR	153.5	0.00023	0.982
SD	156	0.00044	0.990
GAC	164	0.00083	0.979
RH	190	0.00101	0.979

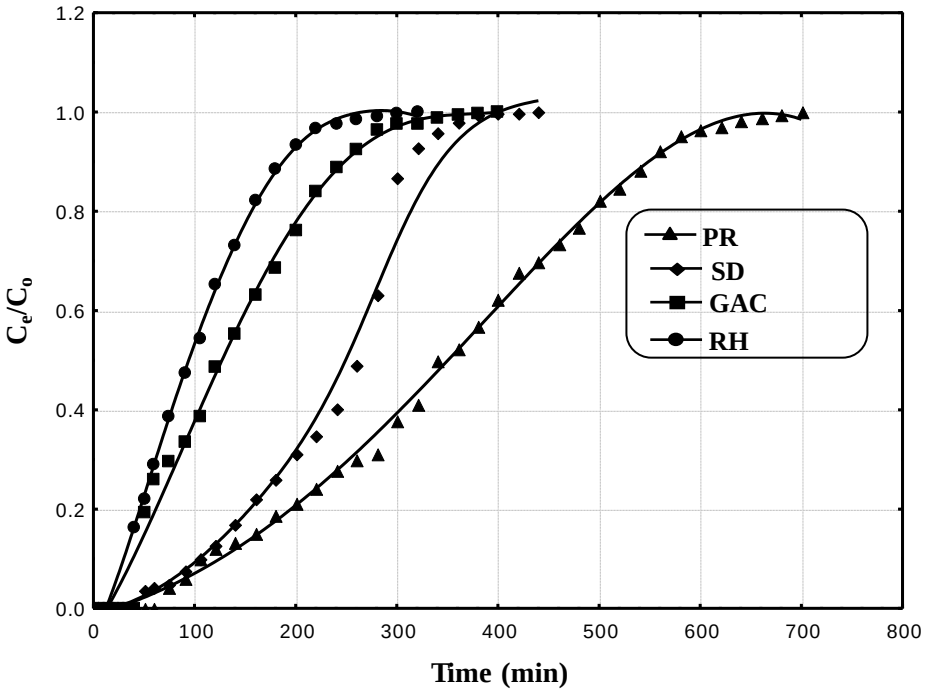

Fig. 14 Fixed- bed breakthrough curve for GAC and MGAC**.**

5. Conclusions

The study showed numbers of conclusions during batch and continuous experiments for adsorption of phosphate ions solutions.

1. Removal efficiency by PR greater than that of SD, GAC and RH for the phosphate ions removal.
2. Optimum pH, mixing speed, adsorbent dosage and contact time were 3, 250 rpm, 2.5 g and 270 min respectively.
3. Removal efficiency decreased with increasing initial concentration and temperature this is due to the lack of binding sites in the PR sample for the adsorption of phosphate ions at higher concentrations and increased the rate of desorption at high temperature.

4. Langmuir isotherm gives the best fit model for representing the experimental data for this system.

5. Pseudo-second-order was best model to predict the kinetic process for the phosphate adsorption.

6. Adsorption of phosphate ions was exothermic and physical in nature.

7. Alkaline solution such as NaOH and Na_2CO_3 seem to be successful for phosphate desorption with high desorption efficiency.
8. Experimental data, after adsorption column study, fits well to linear form of BDST model. The equation can be modified to make suitable for a different flow rate and effluent phosphate concentration.

References

Agyei, N., Strydom, C., Potgieter, J., 2000. An investigation of phosphate ion adsorption from aqueous solution by fly ash and slag. Cement and Concrete Research, 30, 823–826.

Al-Degs, Y.S., Khraisheh, M.A.M., Allen, S.J. Ahmad, M.N., 2009. Adsorption characteristics of reactive dyes in columns of activated carbon, Journal of Hazardous Materials, Vol. 165, pp. 944–949.

Al-Qodah, Z., 2006. Biosorption of heavy metal ions from aqueous solutions by activated sludge. Desalination, 196, 164-176.

Alexander, P. M., Zayas, I., 1989. Particle size and shape effects on adsorption rate parameters", Environ. Eng., 115, 41–55.

APHA, 1995. Standard methods for the examination of water & wastewater", 19th Edition, American Public Health Association, Washington, DC.

Ali, A.H., 2013. Comparative study on removal of cadmium(II) from simulated wastewater by adsorption onto GAC, DB, and PR. Desalination and Water Treatment J., (2013) 1–12.

Ali, A.H., 2011. Performance of Adsorption/Biosorption for Removal of Organic and Inorganic Pollutants, Thesis, University of Baghdad, college of engineering.

Brattebo, H., Odegaard, K. 1986. The influence of different substrates on enhanced chemical phosphorus removal in a sequencing batch reactor, J. Water Res.,20, 977-981.

Colombo, C., Barren, V., Torrent, J., 1994. Using hematite in phosphate removal from its waste streams, Geochim. Cosmochim. Acta, 58, 1261-1266.

De La Noue, J., de Pauw, N., 1988. The potential of microalgal biotechnology: a review of production and uses of microalgae. Biotechnology Advances, 6, 725–770.

De-Bashan, L., Bashan, Y., 2004. Recent advances in removing phosphorus from wastewater and its future use as fertilizer (1997–2003). Water Research, 38, 4222–4246.

Donnert, D., Salecker, M., 1999. Elimination of phosphorus from waste water by crystallization. Environmental Technology, 20, 735–742.

Fox, I., 1993. Using different caly types in phosphate removal processes, J. Chem. Technol. Biotechnol., 57, 97-101.

Gonzalez-Pradas, E., Sanchez, M.V. and Allego Campo, G.A. 1992. Removal of Phosphorus from aqueous solutions using bentonite as an adsorbent, J. Chem. Technol. Biochenol. 54, 291-297.

Gupta, VK., Rastogi A., 2008b. Equilibrium and kinetic modeling of cadmium (II) biosorption by nonliving algal biomass Oedogonium sp. from aqueous phase. J Hazard Mater, 153(1-2), 759–766.

Hawka, D., Carpenter, P. D., Hunter, K. A., 1989. Synthetic routes for preparation of good adsorbents for phosphorus removal. Environ. Sci. Technol., 23, 187-191.

Hammaini, A., Ballester, F. A., Blazquez, M.L., Munoz, J.A., 2006. Biosorption of heavy metals by activated sludge and their desorption characteristics, J. Environ. Manage., 84(4) 419-426.

Kumar, S.D., Subbaiah, V. M., Reddy, A. S., Krishnaiah, A., 2009. Biosorption of phenolic compounds from aqueous solutions onto chitosan-abrus precatorius blended beads. J Chem Technol Biotechnol., 84, 972-981.

Kang, S., Choo, K., Lim, K., 2003. Use of iron oxide particles as adsorbents to enhance phosphorus removal from secondary wastewater effluent. Separation Science and Technology, 38, 3853–3874.

Khelifi, O., Kozuki, Y., Murakami, H., Kurata, K., Nishioka, M., 2002. Nutrients adsorption from seawater by new porous carrier made from zeolitized fly ash and slag. Marine Pollution Bulletin, 45, 311–315.

Koh, K.J., Chung, G. J., 1998. Phosphorus removal and recovery technologies, Hwahok Kanghok, 23, 303-308.

Morse, G. K., Brett, S. W., Guy, J. A., Lester, J. N., 1998. Review: phosphorus removal and recovery technologies. Science of the Total Environment, 212, 69–81.

Martin-Lara, M.A., Herninz, F., Calero,M., Blzquez, G. and Tenorio, G., 2009. Surface chemistry evaluation of some solid wastes from olive-oil industry used for lead removal from aqueous solutions, Biochem. Eng. J., 44, 151-159.

Ma, QY., Traina, SJ., Logan, TJ., Ryan, JA., 1995. Lead immobilisation from aqueous solutions and contaminated soils using phosphate rocks. Environ. Sci. Technol. 29, 1118–1126.

Muhamad, H., Doan, H., Lohi, A., 2012. Batch and fixed bed column biosorption of Cd^{+2} and Cu^{2+}, chemical engineering journal, 158, 369-377.

Özer, A., 2003. Comparative study of the biosorption of Pb(II), Ni(II) and Cr(VI) ions onto S. cerevisiae: determination of biosorption heats. J Hazard Mater, 100, 219–229.

Puckett, L., 1995. Identifying the major sources of nutrient water pollution. Environmental Science Technology, 29, 408–414.

Palanivelu, K., Elangovan, N., 1994. Removal of Phosphorus from solutions using coconut shell carbon, Indian J. Environ. Prot., 14, 688-695.

Parfitt, R. L., 1989. Studying the adsorption properties of goethite towards phosphorus and nitrogen removal, J. Soil Sci., 40, 359.

Qadeer, R., Rehan, A., 2002. A Study of the Adsorption of Phenol by Activated Carbon from Aqueous Solutions. Turk J Chem., 26, 357 – 361.

Quintelas, C., Fernandes, B., Castro J, Figueiredo H, Tavares, T.,2008. Biosorption of Cr(VI) by three different bacterial species supported on granular activated carbon—a comparative study. J Hazard Mater 153, 799–809.

Roques, H., Jeddy, N., Libuglf, A., 1991. Phosphorus removal from wastewater by half-burned dolomite, Water Res., 25,959-965.

Soejoko, DS., Tjia, MO., 2002. Infrared spectroscopy and X-ray diffraction study on the morphological variations of carbonate and phosphate compounds in giant prawn (Macrobrachium rosenbergii) skeletons during its moulting period, J. Mater. Sci. 38, 2087–2093.

Seida, Y., Nakano, Y., 2002. Removal of phosphate by layered double hydroxides containing iron. Water Research, 36, 1306–1312.

Setatnia, A., Madami, A., Bakhti, M.Z., Keryous, L., Mansouri, Y., Yous, R., 2004. Biosorption of Ni^{2+} from aqueous solution by a NaOH treated bacterial dead Streptomices rimosus biomass, Miner. Eng., 17, 903–911.

Sag, Y. and T. Kutsal,2000. Determination of the biosorption heats of heavy metal ions on Zoogloea and Rhizopus arrhizus. Biochem. Eng. J., 6, 145-151.

Sulaymon, HA., Abidb AB., Al-Najar AJ., 2009. Removal of lead copper chromium and cobalt ions onto granular activated carbon in batch and fixed-bed adsorbers. Chem Eng J., 155(3), 647–653.

Tang, H., Zhou, W. and Zhang, L., 2012. Adsorption isotherms and kinetics studies of malachite green on chitin hydrogels, J. Hazard. Mater., 218– 225.

Tanada, S., Kabayama,M., Kawasaki, N., Sakiyama, T., Nakamura, T., Araki, M., Tamura, T., 2003. Removal of phosphate by aluminum oxide hydroxide. Journal of Colloid and Interface Science, 257, 135–140.

Ugurlu, A., Salman, B., 1998. Phosphorus removal by fly ash. Environment International, 24, 911–918.

Vijayaraghavan, K., Yun, Y-S., 2008. Bacterial biosorbents and biosorption. Biotechnol Adv 26:266–291.

Van Voorthuizen, E., Zwijnenburg, A., Wessling, M., 2005. Nutrient removal by NF and RO membranes in a decentralized sanitation system. Water Research, 39, 3657–3667.

Yasemin, B., Tez, Z., 2007. Adsorption studies on ground shells of hazelnut and almond, J. Hazazrdous Materials, 149(1) 35-41.

Zeng, L., Li, X., Liu, J., 2004. Adsorptive removal of phosphate from aqueous solutions using iron oxide tailings. Water Research, 38, 1318–1326.

Zhao, D., Sengupta, A., 1998. Ultimate removal of phosphate from wastewater using a new class of polymeric ion exchangers. Water Research, 32, 1613–1625.

Zhang, G. S., Liu, H. J., Liu, R. P., Qu, J. H., 2009. Removalof phosphate from water by a Fe–Mn binary oxide adsorbent. Journal of Colloid and Interface Science, 335, 168– 174.

Zubeyde, B., Ercan, C., Mehmet, D., 2009. Equilibrium and thermodynamic studies on biosorption of Pb(II) onto Candida albicans biomass. J Hazard Mater 161, 62–67.